SU(N) gauge theories in 2+1 dimensions

Michael J. Teper

Theoretical Physics, University of Oxford, 1 Keble Road, Oxford, OX1 3NP, United Kingdom

We calculate the mass spectra and string tensions of SU(2), SU(3), SU(4) and SU(5) gauge theories in 2+1 dimensions. We do so by simulating the corresponding lattice theories and then extrapolating dimensionless mass ratios to the continuum limit. We find that such mass ratios are, to a first approximation, independent of the number of colors, N_c, and that the remaining dependence can be accurately reproduced by a simple $O(1/N_c^2)$ correction. This provides us with a prediction of these mass ratios for all SU(N_c) theories in 2+1 dimensions and demonstrates that these theories are already "close" to $N_c = \infty$ for $N_c \geq 2$. We find that the theory retains a non-zero confining string tension as $N_c \to \infty$ and that the dimensionful coupling g^2 is proportional to $1/N_c$ at large N_c, when expressed in units of the dynamical length scale of the theory. During the course of these calculations we study in detail the effects of including over-relaxation in the Monte Carlo calculation, of using a mean-field improved coupling to extrapolate to the continuum limit, and the use of space-time asymmetric lattice actions to resolve heavy glueball correlators. [S0556-2821(98)04423-3]

PACS number(s): 11.15.Ha, 11.10.Kk, 11.15.Pg, 12.39.Mk

I. INTRODUCTION

The non-perturbative physics of QCD continues to be largely impervious to analytic attack. Thus 't Hooft's proposal to consider SU(N_c) gauge theories (with quarks) as perturbations in powers of $1/N_c$ around $N_c = \infty$ [1] remains of great interest. In many ways the $N_c = \infty$ theory is much simpler than the physically interesting $N_c = 3$ theory, and the fact that the phenomenology of the SU(∞) quark-gluon theory appears to be strikingly similar to that of (the non-baryonic sector of) QCD [1,2] motivates the suggestion that the physically interesting SU(3) theory might be largely understood if we could solve the much simpler SU(∞) theory. Unfortunately an analytic solution of the latter still eludes us, even if much progress has been made in understanding aspects of its structure [3–6].

This situation has motivated a number of computational explorations [7]. Almost all of these have used the fact that the lattice SU(∞) theory can be re-expressed as a single plaquette theory [5]. Although these calculations have produced interesting results, the approach suffers from a basic problem: it tells us nothing about the corrections to the $N_c = \infty$ limit and so cannot address the critical question of how close SU(3) is, in fact, to SU(∞). The twisted Eguchi-Kawai approach also suffers from the fact that the space-time volume described by the theory is finite and related to N_c.

In this paper we take a more direct approach to the problem. We calculate the continuum properties of SU(2), SU(3), SU(4), . . . theories by simulating the corresponding lattice theories. We then compare these properties and see how well they can be described by simple corrections to a common $N_c = \infty$ limit. This approach has the advantage that it will tell us just how close the physically interesting SU(3) theory is to the simpler SU(∞) theory. It has, of course, a potential disadvantage: if the theories we consider are far from the $N_c = \infty$ limit, then we will have learned nothing about the physics of that limit. Fortunately, as we shall see, this turns out not to be the case.

Ultimately we would like to consider SU(N_c) gauge theories coupled to light quarks (in the fundamental representation) in 3+1 dimensions. But this is beyond our current computational resources. So our first restriction is to disregard the quarks and focus instead on the pure gauge theory. Since the non-perturbative physics of QCD is largely driven by the self-coupling of the gauge fields, this is certainly a physically relevent problem. Moreover, one expects the pure gauge theory to have leading corrections that are $O(1/N_c^2)$ rather than the $O(1/N_c)$ that one expects with quarks. Thus the onset of large-N_c physics should be easier to spot.

Our second restriction is to consider the pure gauge theory in 2+1 rather than in 3+1 dimensions. Although it is less obvious that this leaves us with a physically relevant problem, we shall argue in the next section that gauge theories in 3 and 4 dimensions are sufficiently similar that this is likely to be so. Moreover, it turns out that in $D = 2+1$ we can calculate the continuum properties of gauge theories with such accuracy that there is little ambiguity in our final conclusions. This is not the case in $D = 3+1$ where the preliminary calculations of this kind [8] are very inaccurate in comparison.

Motivating our calculations are several questions of particular interest. What we know about the large-N_c limit of gauge theories essentially comes from considering Feynman diagrams to all orders. Such considerations indicate that SU(N_c) gauge theories possess a smooth $N_c \to \infty$ limit if one varies the coupling so as to keep $g^2 N_c$ fixed. Moreover, the leading correction to this limit should be $O(1/N_c^2)$. It is obviously of interest to check these expectations in a fully non-perturbative calculation. In addition, the phenomenology of large-N_c theories assumes that the theory remains confining in that limit. It is important to check that this is really the case. Finally we wish to see how large the corrections are at, say, $N_c = 3$. Is it really the case that SU(3) is close to SU(∞)?

In addition we aim to calculate the detailed mass spectrum of the SU(∞) theory. We note that models and theoret-

ical approaches are usually simpler in that limit. For example, the flux tube model of glueballs [9–11] would naively appear to be identical for $N_c > 2$. However, because the model does not incorporate the effects of glueball decay, it should really be tested against the $N_c \to \infty$ spectrum since it is only in that limit that there are no decays. A second example is provided by the recent progress in calculating the large-N_c mass spectrum using light-front quantization techniques [12]. Thus our large-N_c spectrum can serve as a useful testing ground for models and attempts at analytic solutions of the theory [12,13]. Of course in the process we shall also calculate the spectra of the theories at finite N_c and these too can be used as a testing ground for models and analytic approaches. We remark that the most recent examples of the latter [14–16] are intriguingly successful. For example, in [15] the SU(2) and SU(3) 0^{++} glueball masses are within 15% of our values and the 0^{--} is even closer. In [16] the string tension is calculated for all N_c and is within 2% of the values in this paper.

We now briefly outline the contents of this paper. In the next section we discuss some general properties of SU(N_c) theories in 2+1 dimensions. The aim is not only to set the framework for the subsequent calculations, but also to convince the reader that these theories are sufficiently similar to their $D=3+1$ counterparts that what we learn in this paper about the former probably tells us something about the latter. We then move on to discuss the technical details of how we carry out our calculations. This includes details of our operators and of the variational principle that underlies our extraction of excited states from the matrix of correlation functions. We also discuss the problem of identifying the continuum spin of a particle on a lattice with only cubic symmetry, and provide a simple criterion for doing so. In the following section we present our calculations of the string tension. It is here that we aim to demonstrate that the theory remains confining as $N_c \to \infty$, thus providing the crucial ingredient for extracting the phenomenology of those theories. It turns out that the string tension is the physical quantity that we calculate the most accurately. So it is in this section that we shall test most precisely the expectation that there is a smooth limit reached by keeping $g^2 N_c$ constant, and that the leading corrections to that limit are $O(1/N_c^2)$. The next section contains our calculations of the glueball spectrum. (Since we have only gluons in our theories, all the physical particles are color singlet composites of gluons i.e. glueballs.) We shall briefly comment on the features of this spectrum, in particular upon how it compares to what we know about the $D=3+1$ spectrum. It would of course be nice to be able to spot some striking regularities in the mass spectrum of the SU(∞) theory. However, one can only read significance into the details of the spectrum if one has some framework that relates those details to the underlying dynamics. For such an analysis, within the context of a model in which glueballs are composed of closed loops of chromoelectric flux, we refer the reader to [10,11]. We shall find that the glueball spectra are in fact very similar to each other for all $N_c \geq 2$. To provide a contrast it is amusing to compare this to the spectrum that one obtains in the $D=2+1$ U(1) theory—the theory that is farthest from U(∞) in the se-

quence of U(N_c) theories. This we do in Appendix E. We conclude with a brief discussion of our results.

We have relegated to the Appendixes details of some self-contained aspects of our calculations which should be of general interest. Appendix A contains a detailed evaluation of the effects of the over-relaxation in the Monte Carlo update. This is done by directly comparing the statistical errors on the masses that one obtains in (realistically large) calculations that contain various ratios of over-relaxation to heat bath. We are not aware of any previous comparison of this kind. We find that over-relaxation brings a modest but worthwhile improvement, particularly for the smaller values of the lattice spacing. Appendix B contains some analyses relevant to our choice of operators. In particular we study how sensitive our operator basis is to variations in the parameter governing the ''blocking,'' whether anything is gained by the inclusion of operators incorporating ''baryonic'' vertices (for $N_c \geq 3$), and we give more details about our variational calculations of the excited states. These are no doubt known to some experts, but we hope they will be of use to others in the field. In Appendix C we compare continuum extrapolations of the string tension in the bare and mean-field improved couplings. We show that using the latter considerably improves the accuracy of the final results. This is of some interest because we are not aware of any such previous comparison. Appendix D contains details of the calculations we have performed with asymmetric lattices which have timelike lattice spacings that are much smaller than the spacelike spacings. The primary purpose of this calculation is to check that our procedure for estimating the masses of the heavier states is in fact reliable. However, our methods for determining the ratio of the lattice spacings are likely to be of more general interest and so we develop this calculation in some detail. This enables us to calculate the SU(2) spectrum of the theory close to its ''Hamiltonian'' limit, and to compare it with the symmetric case as a test of universality. Finally, in Appendix E we summarize some properties of the U(1) mass spectrum. This is to provide a contrast to the SU(N_c) spectra that are the subject of this paper.

During the course of this work, we have published some preliminary summaries of some of the topics in this paper, as well as on related topics not covered herein. Our early results on the SU(2) spectrum appeared in [17]. (See [18] for an interesting comparison with the spectrum of the gauge Ising model.) The preliminary SU(2) string tension was discussed in [19]. That paper also contained a study of the width and vibrational properties of the corresponding flux tube, which is not repeated here. Also not covered in this paper are the SU(2) and SU(3) deconfining temperatures [20]. (See [21] for a more extensive discussion.) Some preliminary results on the N_c dependence in 2+1 dimensions have appeared in [8]. This paper also contains some *very* preliminary calculations for gauge theories in 3+1 dimensions.

II. SOME FEATURES OF $D=2+1$ GAUGE THEORIES

In the first part of this section we discuss some of the fundamental dynamical properties of SU(N_c) gauge theories

in 2+1 dimensions. Since we are much more familiar with the corresponding properties of the same theories in 3+1 dimensions, it will be illuminating to compare the two theories as we go along.

The second part of the section focuses on the consequences of the fact that in $D=2+1$ parity and angular momentum do not commute. We show that this leads to some parity doubling in the spectrum, but that precisely what gets doubled is sensitive to the ultraviolet and infrared cutoffs that we impose in our calculations.

A. $D=2+1 \sim D=3+1$?

Gauge theories in 2+1 dimensions possess a dimensionful coupling: g^2 has dimensions of mass and so provides a scale even for the classical theory. By contrast, in $D=3+1$, g^2 is dimensionless; the theory is classically scale-invariant. In addition the Coulomb interaction in $D=2+1$ is $\propto g^2 \log r$; so the theory is already confining at the "classical" level—albeit only logarithmically. Nonetheless, these apparently quite striking differences are misleading: the $D=2+1$ theory shares with its $D=3+1$ counterpart its most important dynamical properties, as we now remind the reader.

Ultraviolet freedom. Both theories become free at short distances. In 3 dimensions the coupling, g^2, has dimensions of mass so that the effective dimensionless expansion parameter on a scale l will be

$$g_3^2(l) \equiv l g^2 \overset{l \to 0}{\to} 0. \tag{1}$$

In 4 dimensions the coupling is dimensionless and runs in a way we are all familar with:

$$g_4^2(l) \simeq \frac{c}{\ln(l\Lambda)} \overset{l \to 0}{\to} 0. \tag{2}$$

In both cases the interactions vanish as $l \to 0$, although they do so much faster in the super-renormalizable $D=2+1$ case than in the merely asymptotically free $D=3+1$ case.

Infrared slavery. The counterpart of the couplings becoming weak at short distances is that they become strong at large distances—"infrared slavery." This is immediate if we let $l\uparrow$ in Eqs. (1),(2). Thus in both 3 and 4 dimensions the interesting physics is nonperturbative.

The coupling and the mass scale. In 3 dimensions the coupling has dimensions of mass and so explicitly sets the mass scale for the theory

$$m_i = c_i g^2 \tag{3}$$

where m_i is any dynamically generated mass in the theory (for example, a glueball mass). In 4 dimensions the coupling is dimensionless and so, naively, things appear quite different. However, in fact here too the coupling sets the overall mass scale. It does so through the phenomenon of dimensional transmutation: the classical scale invariance is anomalous, the coupling runs and this introduces a mass scale through the rate at which it runs:

$$m_i = c_i \Lambda \tag{4}$$

where Λ is as in Eq. (2). So in both 3 and 4 dimensions the value of the coupling determines the overall mass scale.

Confinement. Both theories confine with a linear potential. This is not something that we can prove of course. However, lattice simulations provide convincing evidence that this is indeed the case. Note that although the $D=2+1$ Coulomb potential is already confining, this is a weak logarithmic confinement, $V_C(r) \sim g^2 \ln(r)$, which has nothing to do with the nonperturbative linear potential, $V(r) \simeq \sigma r$, that one finds at large r.

In addition to these theoretical similarities, we shall see that the calculated mass spectra also show some striking similarities. For example, the lightest glueball is the scalar 0^{++} with a similar mass, $m_{0^{++}} \sim 4\sqrt{\sigma}$, in both cases.

While the above comparisons provide some support for the argument that what we learn about $D=2+1$ gauge theories might have something to teach us about the more interesting $D=3+1$ theories as well, it is important to emphasize that the theories do differ in important respects and are certainly not the same. For example, there are no instantons in $D=2+1$ non-Abelian gauge theories. This would surely matter a great deal if we were to include quarks. Another difference is the fact that the rotation group in two space dimensions is Abelian. This has some important consequences to which we now turn.

B. Spin and parity doubling

In two space dimensions rotations commute: the group is Abelian. So states of spin J do not come in multiplets in the way that they do in 3+1 dimensions where the rotation group is non-Abelian. We shall use (x,y) for the spatial coordinates and θ for the angle of rotation. We can then define a parity transformation, P, by $(x,y) \to (x,-y)$. We note that the angular momentum operator, $x\partial_y - y\partial_x$, flips sign under parity. That is to say, if some state $|\phi\rangle$ has angular momentum j, then the state $P|\phi\rangle$ will have angular momentum $-j$.

This last fact has an important consequence for the spectrum. Suppose $|j\rangle$ is some state of angular momentum j and energy E_j. Consider the two linear combinations

$$|j,\pm\rangle = |j\rangle \pm P|j\rangle. \tag{5}$$

If they are both non-null, they will form a pair of states that have opposite parity, since we easily see that $P|j,\pm\rangle = \pm|j,\pm\rangle$. Moreover, these two states will be degenerate, since P commutes with the Hamiltonian H, and so we have the phenomenon of parity-doubling. Of course, so far the argument could be equally applied to the case of $D=3+1$. The crucial question is whether both combinations are indeed non-null. Now as long as $j \neq 0$ the states $|j\rangle$ and $P|j\rangle$ are orthogonal because they have eigenvalues $\pm j$ respectively with respect to J. In that case it immediately follows that neither of the linear combinations in Eq. (5) can be null. This argument clearly fails for $j=0$ just as it fails for any j in 4 dimensions. Thus we conclude that the $j \neq 0$ states come in

degenerate pairs of opposite parity, while for the $j=0$ states there is no reason to expect parity doubling.

The above argument assumes the continuum rotation group. Our calculations, on the other hand, will be performed upon a square spatial lattice whose explicit symmetries are rotations under $\pi/2$. Does this make any difference? Indeed it does. States of angular momenta $\pm j$ are distinguished by the phases $\exp\{\pm ij\theta\}$ that they acquire under a rotation of θ. We note that for $j=2$ in particular, these phases are identical if we restrict ourselves to rotations of $\theta=n\pi/2$. Thus on a square lattice there is no reason to expect parity-doubling for $j=2$, any more than for $j=0$. Of course as we reduce the lattice spacing, a, we expect to increasingly recover continuum rotational invariance on physical length scales. The extent to which we do will be reflected in the extent to which we recover $j=2$ parity doubling in our mass spectrum.

The rotational invariance is not only broken by the square lattice: it is also broken by the fact that our space-time is a finite hypertorus. If the lattice is symmetric in the two spatial directions (as it usually will be), this once again leaves us with rotations of $\pi/2$. As the volume becomes large compared to the physical length scale of the theory, we expect to recover full rotational invariance, and re-obtain $j=2$ parity-doubling.

We thus expect to find parity doubling for $j\neq0$ states in the $D=2+1$ theory. However, some of this parity doubling may be lost to the extent that either the lattice spacing or the periodic boundary conditions affect physical length scales. Thus the restoration of parity doubling, in particular for $j=2$ states, will provide us with direct evidence for the separation of the physical length scale from both the ultraviolet and infrared cutoffs.

III. METHODOLOGY

We work on a cubic lattice with periodic boundary conditions. The lattice spacing is labelled a and the length of the lattice in the μ-direction is L_μ in lattice units. The field variables are $SU(N_c)$ matrices. They reside on the links of the lattice and are represented by U_l or by $U_\mu(n)$, using an obvious notation. The ordered product of the matrices around a plaquette of the lattice is represented by U_p or by $U_{\mu\nu}(n)$. We use the standard plaquette action

$$S=\beta\sum_p \left\{1-\frac{1}{N_c}\mathrm{ReTr}U_p\right\} \tag{6}$$

and this appears as a weighting factor e^{-S} in the Euclidean path integral. In the continuum limit this becomes the usual Yang-Mills action with

$$\beta=\frac{2N_c}{ag^2}. \tag{7}$$

Note the factor of a that is there because g^2 has dimensions of mass; the dimensionless bare coupling, being a coupling on the scale a, is just ag^2.

We shall perform a few calculations on lattices with different spatial and temporal lattice spacings: a_s and a_t, respectively. In that case we use an action

$$S=\beta_s\sum_{p_s} \left\{1-\frac{1}{N_c}\mathrm{ReTr}U_{p_s}\right\}+\beta_t\sum_{p_t} \left\{1-\frac{1}{N_c}\mathrm{ReTr}U_{p_t}\right\} \tag{8}$$

where the spatial and temporal plaquette matrices, U_{p_s} and U_{p_t}, are multiplied by different couplings whose values are chosen to reproduce the desired ratio of lattice spacings, a_s/a_t. How this choice is made is described in detail in Appendix D.

The main technicalities involve the Monte Carlo calculation and the calculation of masses. We treat these in turn.

A. Monte Carlo calculation

The Monte Carlo calculation consists of a mixture of heat bath and over-relaxation sweeps. We discuss these in turn.

1. Heat bath

For SU(2) we use the standard Kennedy-Pendleton [22] heat bath algorithm. This is extended to higher groups using the Cabibbo-Marinari [23] algorithm where effectively one updates some of the SU(2) subgroups of the SU(N) matrices.

An important practical question here is how many of these subgroups to update. Clearly the more subgroups one updates the faster we will explore phase space. However, one does not want to carry this past the point of diminishing returns. To determine an appropriate number of these subgroups we have chosen a criterion which involves monitoring how efficiently the action of the $SU(N_c)$ fields is reduced by cooling the fields [24,25], when the cooling is applied through different numbers of SU(2) subgroups. We recall that to cool an SU(2) lattice link we simply replace the matrix that is on that link by the matrix which minimizes the action. This matrix is easy to determine [24,25]. A link appears in 4 plaquettes and hence its contribution to the action can be written as

$$\delta S_l=-\frac{\beta}{2}\mathrm{Tr}\{U_l\Sigma\} \tag{9}$$

where the matrix Σ is the sum of the "staples" enclosing the link l. Each staple is an SU(2) matrix and hence Σ is proportional to an SU(2) matrix. Then it is easy to see that the matrix that minimizes δS_l is given by

$$U_l=\frac{\Sigma^\dagger}{|\Sigma|}. \tag{10}$$

We note that this is just the choice of matrix that the heat bath algorithm makes if we set $\beta=\infty$. Once we have applied this procedure to every link of the lattice we have performed a cooling sweep. And we can systematically reduce the action by performing a sequence of such cooling sweeps. We can extend this to $SU(N_c)$ fields by using the Cabibbo-Marinari algorithm and cooling within the chosen SU(2) sub-

TABLE I. Average action per plaquette when a thermalized SU(5) field is cooled using n_G SU(2) subgroups.

Cools	$n_G=4$	$n_G=5$	$n_G=6$	$n_G=8$
0	0.2010	0.2085	0.2072	0.2088
1	0.1272	0.1199	0.1067	0.0874
2	0.0813	0.0662	0.0494	0.0266
5	0.0596	0.0417	0.0254	0.0073
10	0.0516	0.0328	0.0168	0.0028
15	0.0483	0.0291	0.0132	0.0015
20	0.0463	0.0269	0.0111	0.0010

groups. In this case the algorithm no longer exactly minimizes the action. Instead the rate at which it reduces the action is a measure of how rapidly it moves through phase space. So our procedure is to generate some (plausibly) thermalized SU(N_c) fields, and then to cool these fields using various numbers of SU(2) subgroups. An example of this, for the case of SU(5), is shown in Table I. We see that if we use very few subgroups, the decrease in the action is very slow [compared, for example, to what happens in the SU(2) theory]. As we increase the number of subgroups the action decreases more rapidly, indicating that the algorithm explores phase space more efficiently. If we were to increase the number further, then clearly at some point we would find that it led to little further change in the rate of decrease in the action. At this point we would certainly be into diminishing returns. We thus try to choose the smallest number of subgroups that will reduce the action reasonably fast. We then use these same subgroups in the Monte Carlo calculation. In practice we have used 3, 4 and 8 subgroups in the case of SU(3), SU(4) and SU(5) respectively. (There is obviously some ambiguity in the precise choice.)

2. Over-relaxation

In addition to heat-bath sweeps one can also use over-relaxation sweeps [26–28]. In SU(2) this corresponds to replacing our old link matrix, U_{old}, by a new link matrix, U_{new}, defined by

$$U_{new} = \frac{\Sigma^\dagger}{|\Sigma|} U_{old}^\dagger \frac{\Sigma^\dagger}{|\Sigma|}, \qquad (11)$$

where the notation is as in Eq. (9). It is easy to see that this change does not alter the action. Moreover, it can be extended to SU(N_c) using the Cabibbo-Marinari algorithm.

An over-relaxation step involves a large change in the link matrix and so it is plausible that it will increase the rate at which we traverse our phase space [26–28]. Indeed, in 4 dimensions, there is evidence that this is so for large Wilson loops [29]. However, what we are interested in is the calculation of the low-lying mass spectrum and so what we want to know is how over-relaxation affects such a calculation. In Appendix A we present a rather detailed study of this both in SU(2) and in SU(3). (This is, we believe, the only study of this kind for gauge theories in 3 or 4 dimensions.) We find that for physical quantities, such as masses, a suitable mix of

over-relaxation and heat bath sweeps decorrelates field configurations significantly, although not dramatically, faster than a pure heat bath. There is an additional gain that arises from the fact that an over-relaxation step is faster than a heat bath step, which in any case involves the calculation of all the staples. (This gain is greater in 3 than in 4 dimensions since there are fewer staples to calculate in the former case.)

Thus in the calculations of this paper we shall typically choose to make 4 or 5 over-relaxation sweeps for each heat bath sweep.

B. Calculating masses

Our mass calculations are entirely conventional. The starting point is the observation that

$$\langle \phi^\dagger(t)\phi(0)\rangle = \sum_n |\langle \text{vac}|\phi|n\rangle|^2 \exp\{-E_n t\}$$

$$\overset{t\to\infty}{\longrightarrow} |\langle \text{vac}|\phi|0\rangle|^2 \exp\{-E_0 t\} \qquad (12)$$

where $|0\rangle$ is the lightest state that couples to the operator ϕ and E_0 is its energy. (We use operators that are localized within a single time-slice.) So if we want the mass of the lightest color singlet state with quantum numbers J,P,C we simply construct a $\vec{p}=0$ operator with those quantum numbers, calculate its correlation function and then obtain the mass ($=E_0$) using Eq. (12). If the quantum numbers are trivial, the lightest state might be the vacuum, in which case we use vacuum subtracted operators. Of course it might be that for some quantum numbers the lightest state is a multi-glueball state. We shall come back to this possibility later on, but shall, for convenience, ignore it for now.

On the lattice $t=na$ and so what we obtain, not surprisingly, is aE_n, the energy in lattice units. Note that if we are on a lattice with a finite periodic temporal extent, then the expression in Eq. (12) needs to have an additional term for the propagation around the ''back'' of the torus. Such a term will always be included in the numerical calculations of this paper, although we shall, for simplicity, persist in writing all our expressions as though the temporal extent were infinite. We also note that the temporal extent of our lattice, $T \equiv aL_t$, will always be chosen large enough for the partition function, Z, to be accurately given by its vacuum contribution: $Z \simeq \exp\{-E_{vac}T\}$. Thus the energies we calculate will always be with respect to the energy of the vacuum.

In principle we can obtain from Eq. (12) any number of excited states as well. In practice, however, fitting sums of exponentials to a function is a badly conditioned problem. So one needs to develop a more sophisticated strategy, as described later on in this section.

Again in principle, one can use in Eq. (12) any operator with the desired quantum numbers. However, a numerical calculation has finite statistical errors, and because the function $\langle \phi^\dagger(t)\phi(0)\rangle$ is decreasing roughly exponentially in t, it will, at large enough t, disappear into the statistical noise. Thus in practice we need to be able to extract E_0 from Eq. (12) at small values of t. This requires the coefficient

$|\langle \text{vac}|\phi|0\rangle|^2$ to be large. That is to say, we need to use operators that are close to the wave-functional of the state in question.

If we want to use good operators, we obviously need some simple way to decide which operator is in fact better. We shall use a variational criterion. However, before coming to that we say something more about the operators we actually use. This splits naturally into a discussion of glueball operators and those from which we extract the string tension.

1. Operators for glueballs

We are interested in color singlet operators because, as we shall see, our theories are confining. Now, the trace of an ordered product of link matrices around any closed path of the lattice is a color singlet. So we can build our operators out of such loops. Moreover, under charge conjugation the trace will go to its complex conjugate: so the real part is $C = +$ and the imaginary part is $C = -$. For $N_c \neq 2$ we can also construct color singlet operators containing ''baryonic'' vertices. We shall not use such operators in the calculations of this paper, but include a discussion of their properties in Appendix B.

As a simple example, consider the set of spatial plaquettes $U_{xy}(\vec{x},t)$ and form the operator

$$\phi(t) = \sum_{\vec{x}} \text{ReTr} U_{xy}(\vec{x},t). \quad (13)$$

It is a color singlet. Moreover, it is translation invariant and so has $\vec{p} = 0$. (To obtain a non-zero momentum we would include a factor of $\exp\{i\vec{p}\cdot\vec{x}\}$.) It is $C = +$ because we take the real part of the trace. It is obviously invariant under parity and so is $P = +$. Finally it is obviously invariant under the $n\pi/2$ rotational symmetry of our lattice: so it has $J = 0$. This operator will therefore project onto states that have $J^{PC} = 0^{++}$ and $\vec{p} = 0$. So from its correlation function we can, using Eq. (12), extract the lightest 0^{++} glueball mass.

Suppose we now consider the ordered product of link matrices around an arbitrary closed curve C that starts and ends at the point $(\vec{x},t)$. Call it $U_C(\vec{x},t)$. Then the linear combination

$$\phi(t) = \sum_{\vec{x}} \sum_{n} e^{ij\theta_n} \text{ReTr} \{ U_{R(\theta_n)C} \pm U^{\dagger}_{PR(\theta_n)C} \} \quad (14)$$

will have $J = j$, $C = +$, and $P = \pm$. Here the angles being summed over are $\theta_n = n\pi/2$. $R(\theta)$ is a rotation operator, so that $R(\theta)C$ is the contour obtained when we rotate C by an angle θ. Similarly PC is the parity transform of C. In the second term U is conjugated because the order around the curve is reversed under parity. If we replace ReTr by ImTr, we get $C = -$. Symmetries of the curve C will be reflected in the operator in Eq. (14), being null for some values of J^{PC}.

There is obviously an ambiguity in our assignment of J. We use the continuum notation because we are interested in the continuum spectrum and we expect that the lattice will recover continuum rotational invariance as $a \to 0$, at least on

physical length scales $\xi/a \to \infty$. If in constructing our operators we limit ourselves to rotations of $n\pi/2$, then any continuum spin J that gives the same value of $\exp\{ijn\pi/2\}$ will couple to this operator. That is to say, the state that we label by $J = 0$ actually contains states with $J = 0,4,8,12,\ldots$ and similarly for the states we label by $J = 1$ and $J = 2$ (which is all we have with rotations of $\pi/2$). A similar ambiguity occurs in 4 dimensions. It is usually assumed that in this tower of states it is the state with the smallest value of J that has the smallest mass. Thus, in our case, we shall claim to calculate the lightest $J = 0$, 1 and 2 states. We shall return to this point later.

It might be useful to indicate the operators U_C that we actually use. Clearly we need only specify the curves C. The first set consists of square and rectangular curves, in particular the 1×1, 2×2, 3×3 squares and the 1×2, 1×3, 2×3 rectangles. These curves are obviously symmetric under parity reflection. Taking into account that parity also conjugates the matrix, it is easy to see from Eq. (14) that we can only get J^{++} and J^{--} states. Moreover, the square loops can give us only $J = 0$ while linear combinations of the rectangular loops can give both $J = 0$ and $J = 2$. However, all the loops are symmetric under rotations of π and so cannot give $J = 1$. To obtain $J = 1$ and $P = -C$ states we need other operators; in particular we need curves that are not symmetric under P. To describe such curves it is convenient to use an obvious shorthand notation in which the plaquette in the x,y plane would be written as $xyx^{\dagger}y^{\dagger}$. In this notation the curves we use are a path ordered product of 2 plaquettes i.e., $xyx^{\dagger}y^{\dagger}x^{\dagger}y^{\dagger}xy$, and the ''twisted'' version of this $xyx^{\dagger}y^{\dagger}y^{\dagger}x^{\dagger}yx$; the path ordered product of the 1×2 loop and a plaquette i.e., $xyyx^{\dagger}y^{\dagger}y^{\dagger}x^{\dagger}y^{\dagger}xy$, and the twisted version of this $xyyx^{\dagger}y^{\dagger}y^{\dagger}y^{\dagger}x^{\dagger}yx$; and finally the path ordered product of two 1×2 loops i.e., $xyyx^{\dagger}y^{\dagger}y^{\dagger}xxy^{\dagger}x^{\dagger}x^{\dagger}y$ and the twisted version of this, $xyyx^{\dagger}y^{\dagger}y^{\dagger}y^{\dagger}xxyx^{\dagger}x^{\dagger}$. From suitable linear combinations of rotations, parity inversions and real or imaginary parts of these loops we can construct operators with $J = 0,1,2$, $P = \pm$, and $C = \pm$.

At this point we have described in some detail the symmetry properties that the operators need to have. However, all the operators we have described so far are ultraviolet: they are based on loops of size $O(a)$. Such operators will have an approximately equal projection onto all states of the specified quantum numbers. The number of excited states increases rapidly as $a \to 0$. Thus the normalized projection onto the ground state decreases rapidly. This means that as $a \to 0$ we have to go to much larger t in Eq. (12) to see the ground state dominating the correlation function. But we cannot do so because of the statistical noise in our Monte Carlo calculation. This means that we rapidly lose the ability to calculate ground states as we approach the continuum limit.

An efficient remedy for this has been known for a long time [30–32]. What one needs are operators that extend over physical length scales and are smooth on such scales. Only such an operator has a chance of looking like the ground state wave-functional if, as one expects, the latter is smooth on physical length scales. Guided by an intuition developed

in the context of $q\bar{q}$ wave-functions, one would expect the first excited state to have a node. This could be approximated by a linear combination of large smooth operators. Higher excited states would be characterized by more nodes, hence by more complicated linear combinations. While this argument is by itself no more than plausible, it turns out that this strategy works remarkably well.

We use the iterative "blocking" or "fuzzing" algorithm that has been used extensively in $D=3+1$ spectrum calculations [30,32]. We shall not repeat the details here; for a recent detailed account [in the context of SU(2) gauge fields coupled to fundamental scalars in $D=2+1$] see [33]. Briefly, at the first "blocking" level one has the usual link matrices: $U_\mu^1(\vec{x},t)\equiv U_\mu(\vec{x},t)$. At the second level we construct a "blocked" link matrix, e.g., $U_x^2(\vec{x},t)$, by summing the paths xx, $yxxy^\dagger$, and $y^\dagger xxy$ and projecting back to the "nearest" SU(N_c) matrix. All the paths start from the point $(\vec{x},t)$ and end at the point $2a$ away in the x direction. But these blocked links are not just longer; they are fatter (in the spatial directions) as well. One iterates this procedure: the blocked link matrices U_μ^N are formed in exactly this way from the U_μ^{N-1} (all this for spatial μ only). Thus these operators join sites that are $2^{N-1}a$ apart, and are correspondingly fat as well. We can form path ordered products of these blocked links: for example around a super-plaquette, $C\equiv xyx^\dagger y^\dagger$, where now each step is of length $2^{N-1}a$. The trace of this will be a color singlet. [After taking expectation values, there may be small non-gauge invariant pieces that depend on how we projected from the sum of paths back into SU(N_c). See Appendix B for a brief discussion.] Clearly the blocking algorithm is far from unique. In Appendix B we compare a particular subset of such algorithms in order to motivate the particular version we have used.

Thus we can form large smooth operators on any size-scale we like. When we reduce a by a factor of 2, we need only iterate the blocking procedure one extra time. We form operators, using a sufficient range of blockings (as determined by preliminary test calculations), on all the paths described earlier in this subsection. Thus we often have $O(50)$ different operators for any given quantum numbers. Of course we do not need to consider all of these; many are dominated by uninteresting ultraviolet excitations. How to choose the "best" is the question we shall return to, after a brief detour describing the slightly different problem of extracting the string tension.

2. Operators for the string tension

We can calculate the string tension by calculating the energy of the lightest state composed of a static q and $\bar{q}$ a distance R apart. (Any fundamental charges will do; we use q for quarks because they are so familiar.) If we have linear confinement, then this energy, $E_{min}(R)$, provides our definition of the string tension, σ, as well as providing us with a definition of the static quark "potential," $V_{q\bar{q}}(R)$:

$$E_{min}(R)\equiv V_{q\bar{q}}(R)\underset{R\to\infty}{\simeq}\sigma R. \qquad (15)$$

For large R one thinks of this state as being composed of the dressed static quarks with a confining flux tube of length $\simeq R$ joining them.

We note that the usual potential that enters phenomenological discussions of the string tension [34] is essentially based on the Schrödinger equation and the relationship with our definition is not a simple one; this is apparent if one considers, for example, the case of QCD. Vacuum quark fluctuations break the string; so the potential as defined in Eq. (15) will flatten off for larger R. The phenomenological potential, on the other hand, continues to rise, although it may acquire a modest imaginary part to incorporate the decay of the confining flux tube. Effectively it incorporates information about the time-scales associated with the different dynamical processes that contribute. The two definitions differ most dramatically in the large-N_c, narrow-width limit of QCD (less so in the pure gauge theories of interest here, unless, for example, one considers the potential between adjoint sources).

To project onto this $q\bar{q}$ state we define the gauge-invariant operator

$$\phi(t)=\bar{q}(0)\prod U_l q(R) \qquad (16)$$

where we can suppose that the quarks are separated along the x-direction and the product of link matrices is along the shortest path joining them. The correlation function of this operator, taken from $t=0$ to $t=T$, will, for large enough T, be $\propto\exp\{-E_{min}(R)T\}$. This correlation function involves two quark propagators, one from $(x=R,t=0)$ to $(x=R,t=T)$ and the other from $(x=0,t=T)$ to $(x=0,t=0)$. In the $m_q\to\infty$ limit (which is how one implements static quarks dynamically) the quark hops along the shortest available route: that is to say its propagator is equal to the product of links along the straight line joining its end-points. Thus the correlation function is equal (up to some irrelevant factor) to the expectation value of the Wilson loop, $\langle W(R,T)\rangle$. If we have linear confinement, as in Eq. (15), then $\langle W(R,T)\rangle\propto\exp\{-E_{min}(R)T\}\propto\exp\{\sigma RT\}$, the usual confining area decay of Wilson loops. We can improve this calculation, just as we have improved the glueball calculation, using the smeared link matrices in Eq. (16). The timelike link matrices will, of course, not be smeared; they arise from the quark propagator calculation.

We shall use a modified version of the above that employs Polyakov loops rather than Wilson loops. Construct a product of link matrices that closes on itself through a spatial boundary, for example

$$\phi_P(x,t)=\text{Tr}\prod_{n=1}^{L} U_y(x,y+n\hat{y},t), \qquad (17)$$

on a $L\times L$ spatial lattice. This non-contractible loop is what one gets if one stretches our operator in Eq. (16) until the q and $\bar{q}$ meet and annihilate. It couples to the corresponding state: a flux tube of length L that encircles the torus. Such an operator has zero overlap onto any contractible loop. One can readily prove this using the symmetry of the action and

measure under the transformation $U_y(x,y_0,t)$ $\rightarrow z_N U_y(x,y_0,t), \forall t$ where y_0 is an arbitrarily chosen value of y and z_N is a non-trivial element of the center. A contractible loop is obviously invariant under this symmetry while the Polyakov loop is not. This argument breaks down if the symmetry is spontaneously broken, which occurs, for example, in the high temperature deconfining phase.

If we sum over x to make ϕ translation invariant ($\vec{p}=0$) and form the correlation function, we obtain at large t the mass, $m_P(L)$, of the lightest state containing a periodic flux loop of length aL:

$$\langle \phi_P^\dagger(t)\phi_P(0)\rangle \overset{t\to\infty}{\propto} e^{-m_P(L)t} = e^{-\{\sigma aL - \pi/6aL + \cdots\}t}. \quad (18)$$

Here we have explicitly included the first correction term which is the translation to Polyakov loops [36] of the usual Luscher correction [37] for Wilson loops. This correction is ''universal,'' but obviously one needs to test whether the physical flux tube does indeed fall into this particular universality class.

As we have seen above, using Wilson loops produces a heavy-quark potential. This contains a Coulomb term which is long range, $\propto g^2 \log r$, in $D=2+1$. This term will of course be screened, but having to disentangle it from the linear piece, at the intermediate values of r where the calculations are accurate, can decrease the accuracy of the estimate of σ. In $D=3+1$ the Coulomb term is $\propto 1/r$ and its presence makes it difficult to identify the $\pi/12r$ universal string correction. By contrast, in using as we do correlators of $\vec{p}=0$ sums of *spatial* Polyakov loops, we have completely dispensed with any charges and have transformed the problem into a standard mass calculation. Because there are no charges, there is no longer a Coulomb contribution. This benefit has of course been achieved at a price: we no longer have a calculation of the heavy quark potential, but only of the string tension.

Just as for glueballs, the simplest operator is too ultraviolet to be useful as $a\to 0$. To remedy this we replace the product of elementary links in Eq. (17) with a product of blocked link matrices, as defined earlier in this section. As we shall see, there is always a blocking level for which this smeared Polyakov loop is very close to the wave-functional of the ground state of a flux tube that winds around the torus.

Two technical asides: when using link matrices at a blocking level N_B, the sites are spaced a distance $2^{N_B-1}a$ apart. A given product of blocked links, which starts at say $y=1$, is not quite invariant under translations in the y-direction because the blocked links themselves are not completely invariant. One can remedy this by summing products that start at $y=1,2,\ldots,2^{N_B-1}-1$, respectively, and this does in fact improve the operator overlap slightly. A second point is that L need not be divisible by the length of the blocked link. In that case we include links of a lower blocking level, averaged with staples that include transverse links blocked to the level of interest. (In practice this extra smearing with staples is of marginal utility in getting a good overlap.)

3. Variational criterion and excited states

Our lattice action possesses the positivity properties that allow our lattice correlation functions to be decomposed as in Eq. (12). Let us define an effective mass by

$$am_{eff}(t) = -\ln\left\{\frac{\langle \phi^\dagger(t)\phi(0)\rangle}{\langle \phi^\dagger(t-a)\phi(0)\rangle}\right\}. \quad (19)$$

Then it is easy to see from the fact that all the coefficients in Eq. (12) are positive that

$$am_{eff}(t) \geq am_{eff}(t+a) \forall t. \quad (20)$$

This is a very useful property; it tells us that $m_{eff}(t)$ provides an upper bound for the mass, m_G, of the lightest state with the quantum numbers of the operator ϕ, whatever the value of t and whatever the actual operator used. Since the statistical errors on $am_{eff}(t)$ increase with t, we can assume that any apparent increase of the effective mass with t is in fact a statistical fluctuation.

Now we know from Eq. (12) that

$$am_{eff}(t) \overset{t\to\infty}{\longrightarrow} am_G. \quad (21)$$

When is t large enough for this limit to have been effectively reached? Since we know that $m_{eff}(t)$ decreases with increasing t, we can estimate m_G by the value of the effective mass

$$am_G \simeq am_{eff}(t_0) \quad (22)$$

where t_0 is the lowest value of t for which

$$m_{eff}(t_0) \lesssim m_{eff}(t>t_0) \quad (23)$$

within errors.

Obviously this criterion becomes convincing only if the errors are small enough for the relation in Eq. (23) to represent a significant constraint. In practice that will only be the case if t_0 is small, which will only happen if we have a ''good'' operator, i.e. one which mainly projects onto the lightest state. Thus it would be useful to have a simple practical criterion to decide, early on in a calculation, which operator is the best. Such a criterion is immediately suggested by considering the normalized correlation function

$$C(t) \equiv \frac{\langle \phi^\dagger(t)\phi(0)\rangle}{\langle \phi^\dagger(0)\phi(0)\rangle} = \frac{\langle \phi^\dagger e^{-Ht}\phi\rangle}{\langle \phi^\dagger \phi\rangle}. \quad (24)$$

Clearly if we were using a complete basis of operators, then the best operator would be the one that maximized $C(t)$: it would be the wave-functional of the lightest state and we would have $C(t)=\exp\{-m_G t\}$. If the basis is not complete, this suggests a variational criterion: the ''best'' operator, ϕ, is the one which maximizes $C(t)$. In practice we shall use $t=a$. The reason is that one obtains an accurate value of $C(a)$ in even a small calculation, and so can determine early on which are the operators that one needs to calculate with. The value of $C(a)$ provides us with an estimate of $\exp\{-am_G\}$ and hence am_G, which we know to be an upper bound on the true mass. In practice we improve upon this

estimate by calculating the correlation function of this best operator and getting our mass estimate using the first effective mass that satisfies Eq. (23).

Our general strategy for obtaining estimates of the ground state and excited state masses is an extension of the procedure we have just described. We start with some set of, say, N lattice operators, ϕ_i, $i=1,\ldots,N$, which we normalize so that $\langle\phi_i^\dagger\phi_i\rangle=1$. (These are chosen from the operators discussed earlier in this section.) We then find the normalized linear combination of the ϕ_i that maximizes $C(a)$ $=\langle\phi^\dagger(a)\phi(0)\rangle$. Call this operator Φ_1. This is our best estimate for the ground state wave-functional within the space $\{\phi_i\}$, and the associated value of $C(a)$ provides us with a lower bound estimate for $\exp\{-am_1\}$ where m_1 is the ground state mass. We can find higher excited states just as simply. First we construct a basis of operators, ϕ_i', $i=1,\ldots,N$ -1, that spans the $(N-1)$-dimensional subspace of the space $\{\phi_i\}$ which is orthogonal to Φ_1. We now find the linear combination of these ϕ_i' that maximizes $C(a)$ $=\langle\phi'^\dagger(a)\phi'(0)\rangle$. Call this operator Φ_2. This is our best estimate for the wave-functional of the first excited state. The associated value of $C(a)$ provides us with an estimate for $\exp\{-am_2\}$ where m_2 is the mass of the excited state. We can continue this procedure obtaining operators $\Phi_3,\Phi_4,\ldots$ from which we can obtain the energies of higher excited states.

Because our basis is finite, the above mass estimates need not be very good. To improve upon them we calculate correlations of our approximate wave-functionals, $\langle\Phi_i^\dagger(t)\Phi_i(0)\rangle$, and from these obtain effective masses for as large a range of t as our statistical errors (which grow with t) will allow. For each correlation function we look for a ''plateau'' in the effective masses and use the first mass along that plateau. For the lightest state we are, in principle, looking for a plateau that extends to $t=\infty$. For the excited states we expect, with our incomplete basis, to have some admixture of lighter eigenstates, and so the initial plateau should be finite and will eventually drop to the masses of the lighter states. That is to say, for excited states the mass estimate can be lower than the mass of the state whose mass is being estimated. This undoubtedly means that there is a larger systematic error on our estimate of the mass of an excited state than on that of a ground state. We do not know how to estimate this error (for either type of state) but the reader should be aware of its existence.

We have not yet said how we calculate the Φ_i. We use the following standard procedure [35]. Define the $N\times N$ correlation matrix $C(t)$ by

$$C_{ij}(t)=\langle\phi_i^\dagger(t)\phi_j(0)\rangle. \tag{25}$$

Let the eigenvectors of the matrix $C^{-1}(0)C(a)$ be $\vec{v}^i, i$ $=1,\ldots,N$. Then

$$\Phi_i=c_i\sum_{k=1}^N v_k^i\phi_k\equiv\sum_{k=1}^N a_{ik}\phi_k \tag{26}$$

where the constant c_i is chosen so that Φ_i is normalized to unity. There are of course many variations possible on the above procedure.

We return now to the choice of our original basis of N operators, $\phi_i, I=1,\ldots,N$. What we do is to carry out a short preliminary calculation with typically 5 blocking levels of perhaps 6–12 different operators. We calculate only the diagonal correlation functions. Comparing the values at t $=a$ we identify the best operator and a few which are almost as good. We also take a number which are significantly worse, since, after all, we want our basis to contain a reasonable overlap onto some excited states. The sort of basis that we were easily able to accommodate (in terms of memory) had ~15 operators. In those cases where we had more we split the basis into two and worked with both bases separately. Ideally of course one wants to work with a single basis. The smallest basis was for the string tension, but here we were only interested in the ground state because by using operators that are translation invariant along the Polyakov loop, we automatically exclude any significant overlap onto the interesting string excitations of the basic flux loop.

4. Lattice and continuum J

Suppose we have an operator ϕ obtained by multiplying the (blocked) link matrices around some closed curve C. The rotation of this curve by an angle θ gives the operator ϕ_θ. We can then form an operator of spin J,

$$\phi(J)=\int d\theta e^{iJ\theta}\phi_\theta, \tag{27}$$

in the usual way. This assumes we are in the continuum of course. On our square lattice we only use rotations of $\pi/2$:

$$\phi_L(J)=\sum_n e^{iJn\pi/2}\phi_{n\pi/2}. \tag{28}$$

As we remarked earlier, $\phi_L(J)$ is not just spin J but will obviously contain all spins $J\pm4N,\forall N$, since all these spins provide identical phases at $\theta=n\pi/2$. It is nonetheless customary to label the lowest energy state by the lowest possible spin, in the expectation that higher spin states will naturally be more massive. This is quite unsatisfactory: for example it is really not at all obvious that a $J=3$ glueball must be heavier than a $J=1$ glueball [these are ambiguous since J $=-1$ and $J=1$ are degenerate parity transforms and 3 $-(-1)=4$]. Which one is heavier can be an important issue in any given dynamical model (as, for example, in [11]).

In fact the situation is significantly better than this [10] in the case where one uses smeared operators with large overlaps onto the ground state. We shall now show this.

We note that the smeared operators that we construct and, which we then insert into Eq. (28), spread substantially in all spatial directions. We are here only interested in the fact that this also involves an angular spread. We might imagine modelling this qualitative feature using some function like $\sim\exp\{-\theta^2/\alpha^2\}$, with the value of α determining the angular spread of the operator. This would be the amplitude to find $|\theta\rangle$ in $\phi|\text{vac}\rangle$. The amplitude would change to $\sim\exp\{-(\theta$

$-\theta_0)^2/\alpha^2\}$ if we rotate ϕ through an angle θ_0. Of course, we cannot use precisely this form because it does not reflect the periodic nature of the angular variable. However, we can modify it slightly so that it does,

$$\phi = \sum_n e^{-(\theta-2\pi n)^2/\alpha^2}, \qquad (29)$$

and in that case it possesses the Fourier expansion

$$\phi = \frac{1}{2\alpha\sqrt{\pi}} \sum_{m=-\infty}^{m=+\infty} e^{-\alpha^2 m^2/4} e^{im\theta}. \qquad (30)$$

Suppose we now insert this in Eq. (28) with, for example, $J=0$. We obtain

$$\phi_L(J=0) = \frac{1}{2\alpha\sqrt{\pi}} \sum_{m=-\infty}^{m=+\infty} e^{-\alpha^2 m^2/4}$$

$$\times e^{im\theta}\{1+i^m+(-1)^m+(-i)^m\}$$

$$= \frac{2}{\alpha\sqrt{\pi}} \sum_{N=-\infty}^{N=+\infty} e^{-4\alpha^2 N^2} e^{i4N\theta}. \qquad (31)$$

We see, as expected, that we not only have $J=0$, but that states with $J=4N, \forall N$ also contribute. However, what is interesting is their overlap, which is $\propto \exp\{-4\alpha^2 N^2\}$. We see from this that if α is not small, then these higher spin contributions are severely suppressed. This should be no surprise: in the extreme limit where our operator is smeared uniformly over all angles it is obvious that only $J=0$ can contribute.

We see from this argument that smeared operators will generically have the largest overlap onto the lowest $|J|$. The argument relies on the operator being smooth over some finite angular region. This is true of our elementary smeared operators, but is not necessarily true of linear combinations of these. Since our variational calculation produces such linear combinations, we need to continue the argument a little further.

What Eq. (31) tells us is that states of larger than minimal J will have a suppressed coupling to an elementary smeared operator. Thus while it is certainly possible that the lightest state with ''$J=0$'' actually possesses $J=4$ and that it has a large overlap onto the variationally selected linear combination of elementary smeared operators, its overlap onto any individual smeared operator should be visibly suppressed. In practice we have found this not to be the case in any of the channels: typically we can find a smeared operator for which the overlap is $\geq 80\%$. Thus we can confidently state that the lightest states with $J=0,1,2$ do indeed have those spins, for all values of P,C. We have not attempted to perform a similar check for the excited states in these channels.

Clearly one should use the approximate rotational invariance on scales $\xi \gg a$ to construct operators that, to a good approximation, have any value of J that one desires. Such a calculation is in progress [38].

IV. CONFINEMENT AND THE STRING TENSION

In the previous section we described how to calculate the mass, $m_P(L)$, of a flux tube that winds around our $L \times L$ spatial torus. Whether such a flux tube actually exists, that is to say whether we have linear confinement, will be revealed by how $m_P(L)$ varies with L. This is the first question we address.

Having shown that we do have linear confinement, we turn to the problem of extracting continuum values of the string tension in units of the mass scale provided by g^2. This turns out to be much less ambiguous than the corresponding $D=3+1$ calculations where the scale is provided by, say, Λ_{mom}. Nonetheless, we shall see that using ''improved'' couplings does indeed enable us to produce more accurate extrapolations. An explicit demonstration of the extent of the improvement is provided in Appendix C.

Having obtained the continuum values of $\sqrt{\sigma}/g^2$ for the SU(2), SU(3), SU(4), SU(5) gauge theories, we then test certain expectations concerning the large-N_c limit:
  (i) is SU(∞) confining?
  (ii) is the $N_c \to \infty$ limit reached by varying $g^2 \propto 1/N_c$?
  (iii) is the leading correction $O(1/N_c^2)$?
We also get our first indication of how small we can make N_c and still be close to the $N_c = \infty$ limit.

A. Testing for linear confinement

When we are using Eq. (18) to extract $m_P(L)$, it is not t that we know but n_t where $t = a n_t$: so what we actually extract is $a m_P(L)$. If we have linear confinement with a string tension σ, then we should find

$$a m_P(L) = a^2 \sigma L - \frac{\pi}{6L} + \cdots \qquad (32)$$

for large enough L. Here we have also included the ''universal'' string correction. Its presence is also something we would like to test.

Since the numerical calculations are fastest in SU(2), that is where we have performed our most detailed tests. In Figs. 1 and 2 we show how $a m_P(L)$ varies with L for $\beta=6.0$ and $\beta=9.0$, respectively. The first thing we note is that there is indeed an approximate linear dependence of $a m_P(L)$ on L, with an apparent trend towards exact linearity at large L. Ideally we would like to see this rise continue to $L=\infty$. This is not possible to test in a numerical calculation, but what we can ask is whether the linear rise extends to physically large values of the string length, aL, or not. Now a convenient physical length scale is given by $\xi_s \equiv 1/\sqrt{\sigma}$ where we can get $a^2\sigma$ from the asymptotic linear rise. Doing so we find that our largest lengths correspond to $aL \sim 8\xi_s$ and $aL \sim 5\xi_s$ at $\beta=6$ and $\beta=9$ respectively. These, we claim, are large distances. For example, they would correspond to $\simeq 4$ fm and 2.5 fm respectively in the real world where $\xi_s \equiv 1/\sqrt{\sigma} \simeq 0.5$ fm.

We can see from Fig. 1 and Fig. 2 that the dependence of the mass on L is not exactly linear; indeed in the latter figure we plot the ratio $a m_P(L)/L$ precisely in order to expose the
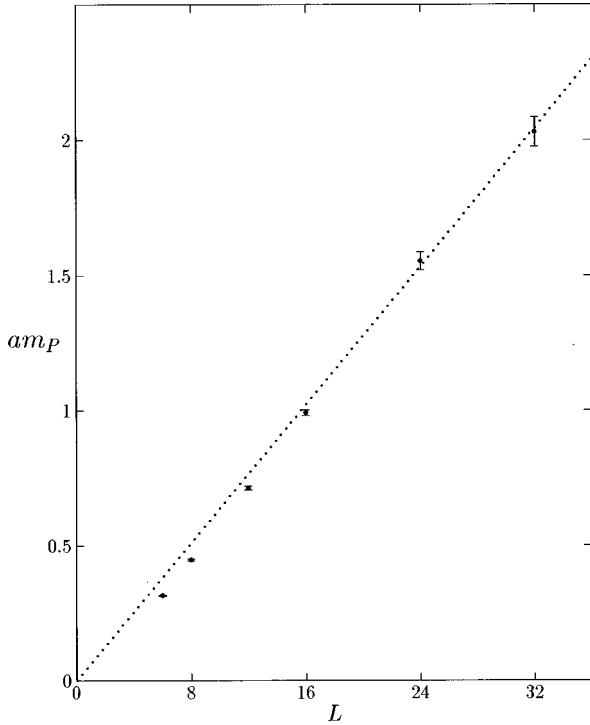
FIG. 1. Mass of periodic flux loop, am_P, against its length, L, at $\beta=6$. The straight line is to guide the eye.

deviations from linearity. We note that the approach is from below; i.e., the leading correction must have a negative sign, just as it does in Eq. (32). We have plotted a fit of this form in Fig. 2 and we see that it appears to be compatible with the observed variation. Can we test the correction term in Eq. (32) more precisely? Suppose the lattice sizes L_i are ordered so that $L_{i+1} > L_i$. Let us parametrize the corresponding loop masses by $am_P(L_i) = a^2 \sigma L_i - c_{eff}/L_i$ and the same for $am_P(L_{i+1})$. Then we obtain
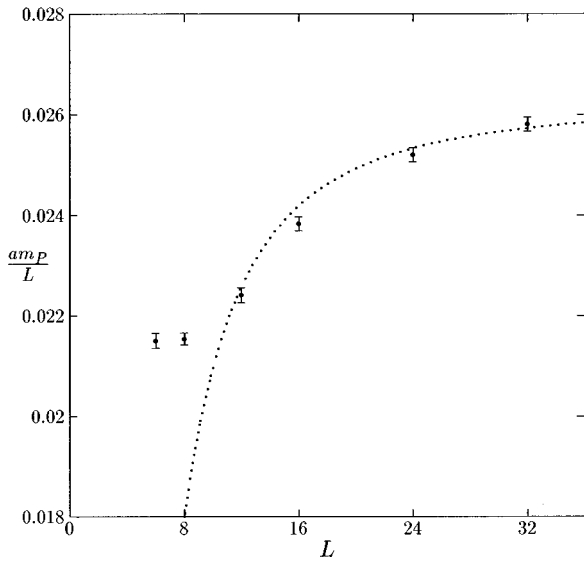

FIG. 2. Mass of periodic flux loop of length, L, at $\beta=9$, divided by L to expose the correction to the linear rise. Curve is fit using Eq. (32).

TABLE II. Coefficient of effective leading $1/L$ correction in the flux loop mass: as extracted from loops of length L and L' using Eq. (33).

β	L,L'	c_{eff}
12	32,48	0.66(20)
9	24,32	0.79(26)
	16,24	0.63(9)
	12,16	0.47(7)
	8,12	0.10(2)
	6,8	0.00(2)
6	24,32	-1.7(2.9)
	16,24	1.26(70)
	12,16	0.87(27)
	8,12	0.41(8)
	6,8	0.28(5)

$$c_{eff} = \frac{\dfrac{am_P(L_{i+1})}{L_{i+1}} - \dfrac{am_P(L_i)}{L_i}}{\dfrac{1}{L_i^2} - \dfrac{1}{L_{i+1}^2}}. \tag{33}$$

What are we looking for? At small L higher order corrections in $1/L$ will be important and so c_{eff} will vary as we increase L. If however $c_{eff} \to c$ as $L \to \infty$, then this tells us that the functional form of the leading correction is indeed c/L. If the value of c is compatible with $\pi/6 \simeq 0.52$, then we have some evidence that the correction is of the universal form. How much evidence depends on the precision of the comparison of course.

In Table II we list the values of c_{eff} for various ranges of L_i, L_{i+1}. We also show a single value obtained at $\beta=12$. In comparing the distances at various values of β, we can use the fact that $\lim_{a \to 0} \beta = 4/ag^2$ which tells us that, roughly, $a \propto 1/\beta$. So $L=32$–48 at $\beta=12$ corresponds roughly to $L=24$–36 at $\beta=9$ and to $L=16$–24 at $\beta=6$. As expected we see a strong variation of c_{eff} at the small values of L where our calculations are most accurate. As the length, L, of the flux loop increases its mass also increases and so the relative error on c_{eff} increases quite rapidly. So while there is good evidence that, for larger L, c_{eff} grows to be at least as large as the theoretical value of $\pi/6 \simeq 0.52$, there is only a little direct evidence, from the $\beta=9$ values, that this is indeed the asymptotic $L \to \infty$ value. Taken as a whole, we read the results in Table II as providing significant support for the applicability of the Luscher universal string correction to the confining flux tube. We remark that in contrast to $D=3+1$ studies using Wilson loops, the present analysis has the advantage of there being no confusion with a Coulomb term of the same functional form as the Luscher term.

Since this is our first serious mass calculation in this paper, it might be worth discussing the extraction of those masses in a little more detail. By way of example we list in Table III the effective masses, as defined in Eq. (19), for the $\beta=9$, 12, and 14.5 calculations. (The last corresponds to our smallest lattice spacing.) We show not only the masses ob-

tained using $\vec{p}=0$ operators, but also those obtained using operators with the lowest non-zero momentum, $ap=2\pi/L$ on an $L\times L$ spatial lattice. From the latter we obtain effective energies, $aE(p)$, which we have translated into effective masses using the continuum dispersion relation $m^2=E^2-p^2$. As L decreases, $ap=2\pi/L$ becomes larger and at some point it should become sensitive to the cutoff at which point this relation will break down. Comparing the two sets of masses in Table III, we observe that they are compatible, within small errors, thus demonstrating the restoration of continuum Lorentz invariance. The dispersion relation does break down on the $L=6$ lattice, but at this point $p=2\pi/3a \sim 2/a$ which is certainly an ultraviolet momentum.

It might seem remarkable how small we can make L while still retaining all the string-like properties of the flux tube, which after all will have a width of the order of $\sim 1/a\sqrt{\sigma}$. In fact, as we have argued elsewhere [19], this is not surprising if the fluctuations of the tube are not too rough, and the transverse volume is periodic.

We return to the masses. Our criterion is that we choose $m(t_0)$ as our mass estimate if, within errors, $m(t_0)=m(t)\forall t\geq t_0$. In most of the cases shown in Table III that is straightforward; the choice of $m(t=2a)$ seems appropriate. In some cases there is a downward drift in the value of $m(t)$ at larger t, for example on the $L=48$ lattice at $\beta=12$. In this case however the mass from the $\vec{p}\neq0$ operator shows no such effect: indeed it shows a slight upward drift. This suggests that this drift is a statistical fluctuation. Indeed the large drop seen in going from $m(3a)$ to $m(4a)$ cannot be accommodated in any realistic decomposition of the correlator that respects positivity. In the case of the $L=32$ masses at the same β there is a marginal hint that $m(2a)$ is not asymptotic, but it is difficult to see why it should not be if $t=2a$ is asymptotic at $\beta=9$ and at $\beta=14.5$ (as it appears to be). The fact that correlators can drift [32] and indeed oscillate [39] outside their apparent errors introduces some subjective bias into our analysis. But, as we have seen, it can often be resolved either by performing simultaneous $\vec{p}\neq0$ calculations or by considering other calculations at nearby values of β and L. This renders the problem a minor one in practice, although it may well induce a systematic bias at the level of the statistical errors. For this reason we do not take seriously the fact that the mean values of c_{eff} at larger L tend to be above $\pi/6$, albeit within statistical errors.

We turn now to the SU(3), SU(4) and SU(5) theories. In each case we have performed an explicit test of linear confinement at one value of β at least. These are listed in Table IV. We see that in every case there is an approximately linear increase of the mass with the length of the loop. That is to say, we have linear confinement. We also extract and list the values of c_{eff} as defined in Eq. (33). We see that we have some evidence for the validity of the string correction in Eq. (32) for all our values of N_c.

On the basis of this evidence we shall assume that we have linear confinement at all other values of β so that we need calculate $m_P(L)$ for only one value of L and can then use Eq. (32) to extract $a^2\sigma$. Of course aL has to be chosen large enough for the leading correction to be the dominant one. We shall use lattices that are about as large as $L=24$ at $\beta=9.0$ in SU(2). As we see from Table II, this should certainly be large enough.

B. Extrapolating to the continuum limit

In Tables V, VI, and VII we list the values of the string tension that we shall use. These have been obtained from the calculated flux loop masses using Eq. (32). The lengths of these loops are also shown in the tables.

The flux loop masses have been obtained from the cross-correlation matrix, as described earlier. The exceptions are all in SU(2): the $\beta=6.56$ and $L=16$, $\beta=6.0$ calculations and those at such strong coupling, $\beta\leq3.47$, that the eigenvalue calculation becomes error-driven and breaks down. In these cases we applied the simplified variational calculation where one chooses, from the original basis of operators, the single smeared Polyakov loop that maximizes $am_{eff}(t=a)$. By comparing how such a procedure differs from the full one at neighboring values of L and β we believe that any bias induced is within the statistical errors. Once we have chosen the ''best'' operator, we extract σ from $am_{eff}(t=2a)$. There are a few cases where the naive application of our ''effective mass plateau'' criterion would lead us to use $am_{eff}(t=3a)$ (or larger t). However, these are typically two standard deviation effects that occur infrequently enough that they can be fluctuations. And in practice if we were to use them, it would make no material difference to the calculations we now describe.

We now wish to use these values to obtain the continuum string tension. Since the only explicit mass scale is provided by g^2, we expect that $\sqrt{\sigma}$ should be some multiple of it. We can obtain this ratio from our tabulated values of $a\sqrt{\sigma}$:

$$\lim_{\beta\to\infty}\beta a\sqrt{\sigma}=2N_c\frac{\sqrt{\sigma}}{g^2} \qquad (34)$$

using Eq. (7).

To perform the limit in Eq. (34) we can add a correction term

$$\beta a\sqrt{\sigma}=c_0+\frac{c_1}{\beta} \qquad (35)$$

and fit the unknown constants, $c_0=2N_c\sqrt{\sigma}/g^2$ and c_1, to the values of $\beta a\sqrt{\sigma}$ that we obtain from our tables. In practice higher order corrections will be important at small β and so we will need to systematically drop off the lowest-β points until we get a fit with an acceptable χ^2. Although this is a workable approach, we recall, from the $D=3+1$ case, that the lattice bare coupling provides a poor definition of a running coupling. The basic problems are similar in $2+1$ and $3+1$ dimensions and so we might expect that the higher order corrections to Eq. (35) will be much larger than if we were to use a physically motivated coupling. A very simple such coupling [40] is the mean field improved coupling

$$\beta_I=\beta\left\langle\frac{1}{N_c}\operatorname{Tr}U_p\right\rangle. \qquad (36)$$

TABLE III. Effective loop masses for various loop lengths L and from the lowest 2 momenta, $p = 2\pi n_{mom}/L$, in SU(2) at the values of β shown.

β	L	n_{mom}	$am(a)$	$am(2a)$	$am(3a)$	$am(4a)$	$am(5a)$
14.5	40	0	0.373(1)	0.364(2)	0.364(2)	0.364(3)	0.363(5)
		1	0.375(1)	0.365(2)	0.363(2)	0.361(3)	0.358(4)
12.0	48	0	0.685(2)	0.668(5)	0.656(9)	0.628(16)	0.632(36)
		1	0.690(2)	0.670(4)	0.671(7)	0.677(13)	0.677(25)
	32	0	0.443(2)	0.434(2)	0.429(3)	0.426(4)	0.426(7)
		1	0.447(1)	0.434(2)	0.430(3)	0.425(4)	0.425(6)
9.0	32	0	0.846(3)	0.826(5)	0.832(10)	0.837(21)	
		1	0.846(2)	0.823(4)	0.821(7)	0.832(17)	
	24	0	0.617(2)	0.605(4)	0.601(6)	0.590(9)	0.593(17)
		1	0.622(1)	0.609(2)	0.600(5)	0.599(10)	0.597(17)
	16	0	0.389(2)	0.381(2)	0.378(4)	0.378(5)	0.379(7)
		1	0.398(2)	0.383(2)	0.378(4)	0.370(5)	0.364(9)
	12	0	0.274(2)	0.269(2)	0.268(3)	0.271(3)	0.272(4)
		1	0.291(3)	0.274(6)	0.261(10)	0.268(14)	
	8	0	0.174(1)	0.172(1)	0.172(1)	0.172(2)	0.173(2)
		1	0.215(6)	0.182(10)	0.163(25)		
	6	0	0.130(1)	0.129(1)	0.129(1)	0.128(2)	0.128(2)
		1	0.093(16)				

To define β_I we need the values of the average plaquettes, $\langle(1/N_c)\mathrm{Tr}U_p\rangle$. These are provided in Tables VIII, IX, and X. In Appendix C we compare extrapolations in β and β_I in the cases of SU(2) and SU(3), where we have calculations over a wide range of β values. We are able to demonstrate that the mean field improved coupling does indeed provide a much better expansion parameter. Thus we shall extrapolate to the continuum limit using

$$\beta_I a \sqrt{\sigma} = c_0 + \frac{c_1}{\beta_I} \qquad (37)$$

in all cases.

The results of these extrapolations are listed in Table XI together with the confidence levels of the fits and the fitted range. Having obtained the continuum string tensions

$$\frac{\sqrt{\sigma}}{g^2} = \begin{cases} 0.3353(18), & \mathrm{SU}(2), \\ 0.5530(20), & \mathrm{SU}(3), \\ 0.7581(40), & \mathrm{SU}(4), \\ 0.9657(54), & \mathrm{SU}(5), \end{cases} \qquad (38)$$

we turn now to an analysis of their N_c dependence.

C. Confinement at large N

In Fig. 3 we plot our calculated values of $\sqrt{\sigma}/g^2$ against N_c. We immediately observe that the variation approaches a linear form for larger N_c,

$$\frac{\sqrt{\sigma}}{g^2} \propto N_c, \qquad (39)$$

and indeed is nearly linear even down to $N_c = 2$. Now, if our SU(N_c) gauge theories are to have a smooth $N_c \rightarrow \infty$ limit, then in that limit they will have some fixed physical mass scale that we shall call μ. If this limit is to be confining, we must have

$$\frac{\sqrt{\sigma}}{\mu} \rightarrow \mathrm{const}, \quad N_c \rightarrow \infty. \qquad (40)$$

From Eq. (39) and Eq. (40) we immediately infer that

$$g^2 \propto \frac{\mu}{N_c}. \qquad (41)$$

TABLE IV. Flux loop masses as a function of the loop length, L, for SU(3), SU(4) and SU(5). Also shown is c_{eff}, the coefficient of the $1/L$ correction in Eqs. (32),(33).

N_c	β	L	am_P	c_{eff}
5	44	8	0.4490(33)	
		12	0.7314(71)	0.55(8)
		16	1.0110(56)	0.75(23)
	33	8	0.997(8)	
		12	1.551(25)	0.53(26)
4	28	8	0.4257(45)	
		12	0.7139(66)	0.72(9)
		16	0.9857(66)	0.70(23)
3	15	8	0.4425(27)	
		12	0.7391(46)	0.72(6)
		16	1.0103(92)	0.51(23)
		24	1.5636(180)	0.92(44)

TABLE V. SU(2) string tensions as extracted from flux loop masses of length L using Eq. (32).

β	L	$a\sqrt{\sigma}$	β	L	$a\sqrt{\sigma}$
14.5	40	0.09713(20)	6.0	16	0.2538(10)
12.0	48	0.1179(8)	5.0	16	0.3129(20)
12.0	32	0.1179(5)	4.5	12	0.3527(30)
9.0	32	0.1622(4)	3.75	8	0.4487(33)
9.0	24	0.1616(6)	3.47	8	0.4889(56)
6.56	24	0.2297(10)	3.0	6	0.584(16)
6.0	32	0.2529(33)	2.5	4	0.709(11)
6.0	24	0.2562(26)	2.083	4	0.852(50)

We recall that the usual all-order diagrammatic analysis demands that $g^2 \propto 1/N_c$ for a smooth large-N_c limit. Equation (41) embodies precisely that requirement and so provides a fully non-perturbative confirmation of those arguments.

To complete our demonstration that the theory is confining in the $N_c \rightarrow \infty$ limit we need to show that $\lim_{N_c \rightarrow \infty} m_G/\sqrt{\sigma}$ is finite and non-zero for the lightest glueball masses. That this is in fact the case is something that we shall demonstrate in the next section; for now we shall assume it to be so.

In addition to predicting that $g^2 \propto 1/N_c$, the usual diagrammatic analysis also predicts that the leading correction should be $O(1/N_c^2)$. To test this we fit our string tensions with the functional form

$$\frac{\sqrt{\sigma}}{g^2 N_c} = c_0 + \frac{c_1}{N_c^\alpha}. \tag{42}$$

In Fig. 4 we show how the goodness of fit varies with the power α. From this we can infer that

$$\alpha = 1.96 \pm 0.45. \tag{43}$$

If we assume, in addition, that the power should be an integer, then only one value is allowed: $\alpha = 2$. Thus we conclude that we have rather strong evidence that the leading correction is also in agreement with the usual diagrammatic expectations.

Fitting our calculated values, we obtain

TABLE VI. SU(3) string tensions as extracted from flux loop masses of length L using Eq. (32).

β	L	$a\sqrt{\sigma}$	β	L	$a\sqrt{\sigma}$
34.0	40	0.10379(26)	8.175	6	0.5598(31)
28.0	32	0.12753(20)	7.5	6	0.591(23)
21.0	24	0.17479(38)	7.5	4	0.633(3)
15.0	24	0.2570(15)	7.0	4	0.698(5)
15.0	16	0.2553(12)	6.5	4	0.782(26)
11.0	12	0.3748(23)	6.0	4	0.835(41)

TABLE VII. SU(4) and SU(5) string tensions as extracted from flux loop masses of length L using Eq. (32).

	SU(4)			SU(5)	
β	L	$a\sqrt{\sigma}$	β	L	$a\sqrt{\sigma}$
51.0	32	0.12859(23)	82.0	32	0.12715(27)
40.0	24	0.16804(30)	64.0	24	0.1664(4)
28.0	16	0.2523(8)	44.0	16	0.2554(7)
21.0	12	0.3597(24)	33.0	12	0.3645(29)

$$\frac{\sqrt{\sigma}}{g^2 N_c} = 0.1975(10) - \frac{0.119(8)}{N_c^2}. \tag{44}$$

This fit has a good confidence level, $\sim 80\%$. We note that this tells us something interesting: we can describe the physics of SU(N_c) gauge theories, all the way down to SU(2), by that of the SU(∞) theory supplemented by the leading correction with a modest coefficient. Of course, so far we have only shown this for the string tension: in the next section we shall see that this is also the case for the mass spectrum.

Before moving on from our result for the string tension, it is interesting to ask whether it is possible to quantify the potential error associated with keeping only the leading correction in Eq. (44). There is no unique way to do this, of course, but a first step would be to include a higher order correction and see what difference it makes. When we do so we obtain the following range of fits:

$$\frac{\sqrt{\sigma}}{g^2 N_c} = 0.1976(22) - \frac{0.121(43)}{N_c^2} - \frac{0.01(14)}{N_c^4}. \tag{45}$$

We observe that our result for $\lim_{N_c \rightarrow \infty} \sqrt{\sigma}/g^2 N_c$ is robust under the inclusion of the higher order correction. Our calculations constrain the coefficient of this higher-order correction to be small, and the only significant effect from including it is to double the error on the extrapolated value of the string tension.

The discussion so far has concerned the continuum limit, which is of course what we are mainly interested in. However, the large-N_c expectations will also apply to lattice cor-

TABLE VIII. Average SU(2) plaquette values.

β	L	Plaquette	β	L	Plaquette
14.5	40	0.929803(3)	6.0	16	0.824744(33)
12.0	48	0.914824(3)	5.0	16	0.786850(20)
12.0	32	0.914823(3)	4.5	12	0.760841(45)
9.0	32	0.885445(5)	3.75	8	0.706986(48)
9.0	24	0.885438(7)	3.47	8	0.680058(59)
6.56	24	0.840548(22)	3.0	6	0.624023(62)
6.0	32	0.824772(10)	2.5	4	0.54737(20)
6.0	24	0.824782(16)	2.083	4	0.47100(13)

TABLE IX. Average SU(3) plaquette values.

β	L	Plaquette	β	L	Plaquette
34.0	40	0.919680(2)	8.175	6	0.620730(45)
28.0	32	0.901903(2)	7.5	6	0.57810(19)
21.0	24	0.867671(5)	7.5	4	0.57801(8)
15.0	24	0.810773(9)	7.0	4	0.54118(11)
15.0	16	0.810767(11)	6.5	4	0.50060(13)
11.0	12	0.733401(18)	6.0	4	0.45736(19)

TABLE XI. Continuum extrapolations of $\beta_I a \sqrt{\sigma} \to 2 N_c \sqrt{\sigma}/g^2$ as in Eq. (37), with confidence level of best fit, and range of β fitted.

Group	c_0	c_1	C.L. (%)	$\beta \geqslant$
SU(2)	1.341(7)	-0.421(51)	60	3.0
SU(3)	3.318(12)	-2.43(22)	90	8.175
SU(4)	6.065(32)	-7.74(1.10)	90	21.0
SU(5)	9.657(54)	-21.4(2.7)	70	33.0

rections, and we can ask if they are fulfilled. What we would expect is that the $O(ag^2)$ correction should also be a function of $g^2 N_c$, i.e.,

$$\frac{a\sqrt{\sigma}}{ag^2 N_c} = b_0 + b_1 a g^2 N_c, \quad N_c \to \infty. \qquad (46)$$

In terms of our fit in Eq. (37) this implies that the lattice correction, c_1, should be given by

$$c_1 = 4 N_c^4 b_1, \quad N_c \to \infty. \qquad (47)$$

We note that our calculated values of c_1, as listed in Table XI, are entirely consistent with this being the leading large-N_c behavior. Indeed, if we fit these values with a functional form $c_1 = c N^\alpha$, we find a good fit with $\alpha = 4.2 \pm 0.6$.

V. MASS SPECTRUM

Having seen that all our gauge theories are linearly confining, we infer that the asymptotic states are color singlet and so we can calculate the mass spectrum using the operators described earlier on in this paper.

We shall first indicate the quality of the lattice mass calculations. We then investigate the finite volume dependence of these masses so as to establish control over this potential source of systematic error. We shall then carry out the extrapolation to the continuum limit. Finally we turn to a study of the dependence of the mass spectrum on N_c. We finish with a discussion of some features of the calculated mass spectrum.

A. Calculating the masses

We shall focus on the lightest states because the correlations mediated by heavier states decrease so rapidly with t that it becomes hard to know whether we have indeed isolated the asymptotic exponential decay. Moreover, glueballs

TABLE X. Average SU(4) and SU(5) plaquette values.

|	SU(4)			SU(5)	
β	L	Plaquette	β	L	Plaquette
51.0	32	0.898791(1)	82.0	32	0.899245(1)
40.0	24	0.869608(3)	64.0	24	0.869510(3)
28.0	16	0.809339(9)	44.0	16	0.805322(6)
21.0	12	0.737628(18)	33.0	12	0.731640(17)

that are heavy enough will decay into lighter glueballs and this may require more careful analysis.

Clearly we want to obtain the ground state in each J^{PC} channel, and in those cases where the ground state is light enough we can estimate one or two excited masses as well. So the states whose masses we shall calculate are those of the 0^{++}, 0^{++*}, 0^{++**}, 0^{--}, 0^{--*}, 0^{--**}, 0^{-+}, 0^{+-}, 2^{++}, 2^{++*}, 2^{-+}, 2^{-+*}, 2^{--}, 2^{--*}, 2^{+-}, 2^{+-*}, 1^{++}, 1^{-+}, 1^{--}, and 1^{+-} glueballs.

We shall calculate the masses, as described earlier, for SU(2), SU(3), SU(4) and SU(5) gauge groups and, in each case, for a range of β values sufficient to allow a continuum extrapolation. In practice this means for most, but not all, of the values of β at which we calculated the string tension.

For any state, the first question must be, how confident are we that we have indeed calculated the mass? That is to say, do we have evidence for an effective mass plateau?

To address this question we analyze, by way of an example, our SU(5) calculation at the highest value of β. We show in Table XII the effective masses we obtain there.
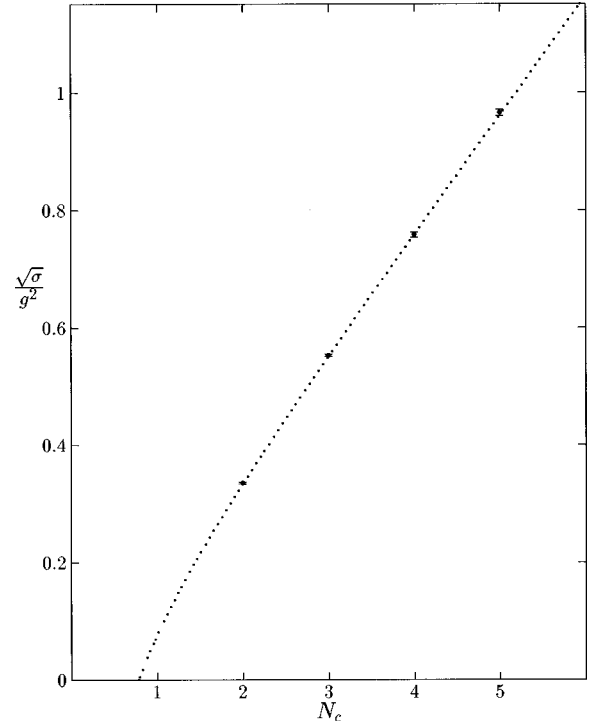
FIG. 3. The value of $\sqrt{\sigma}/g^2$ as a function of N_c. The line shows the fit in Eq. (44).
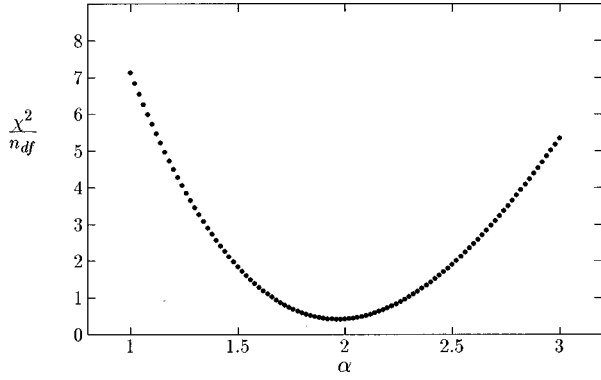
FIG. 4. The χ^2 per degree of freedom against the power, α, of the leading large-N_c correction when fitting $\sqrt{\sigma}/g^2 N_c$.

Since the highest β corresponds to the smallest a, these calculations are the closest to the continuum limit (and the closest to $N_c = \infty$) and so are the ones which are the most interesting. We note that it is when the value of a is smallest that the correlation functions drop most slowly and we can extract effective masses to larger t. At smaller β, farther away from the continuum limit, it will be harder to confirm that we are seeing mass plateaux.

From this table we infer that a good estimate of the mass is provided by $m_{eff}(2a)$ in each case. That is to say, within errors the effective mass is on a plateau for $t \gtrsim 2a$. This is self-evident in most cases. In some cases, e.g. for the 0^{--*}, one sees a drop in m_{eff} of over one standard deviation when going from $t = 2a$ to $t = 3a$. However, that is to be expected, just statistically, given the large number of correlation functions that we consider. Positivity can be useful in such cases.

TABLE XII. Effective masses for the states shown, on a 32^3 lattice at $\beta = 82$ in SU(5).

State	$am(a)$	$am(2a)$	$am(3a)$	$am(4a)$	$am(5a)$
0^{++}	0.541(3)	0.533(5)	0.539(7)	0.523(11)	0.533(14)
0^{++*}	0.821(3)	0.798(7)	0.796(14)	0.799(29)	0.795(65)
0^{++**}	1.033(4)	1.009(10)	1.028(28)	1.013(66)	1.18(22)
0^{--}	0.793(3)	0.779(7)	0.765(10)	0.750(30)	0.71(5)
0^{--*}	1.016(4)	1.002(8)	0.969(26)	1.054(62)	1.09(17)
0^{--**}	1.202(5)	1.193(14)	1.14(4)	1.20(18)	
0^{-+}	1.208(5)	1.155(11)	1.146(43)	1.02(11)	
0^{+-}	1.326(6)	1.256(14)	1.256(59)	1.59(26)	
2^{++}	0.913(3)	0.891(7)	0.905(19)	0.911(40)	
2^{++*}	1.103(4)	1.072(9)	1.074(31)	1.00(10)	
2^{-+}	0.906(3)	0.879(7)	0.853(14)	0.847(43)	
2^{-+*}	1.094(4)	1.076(9)	1.069(32)	1.04(10)	
2^{--}	1.081(4)	1.054(10)	1.051(28)	1.10(10)	
2^{--*}	1.271(5)	1.225(16)	1.218(46)	1.17(11)	
2^{+-}	1.075(4)	1.043(9)	1.049(30)	1.10(11)	
2^{+-*}	1.276(4)	1.230(17)	1.218(49)	1.36(17)	
1^{++}	1.344(4)	1.294(14)	1.284(48)	1.14(18)	
1^{-+}	1.355(5)	1.300(10)	1.327(46)	1.33(16)	
1^{--}	1.255(3)	1.212(9)	1.176(34)	1.18(10)	
1^{+-}	1.286(5)	1.255(14)	1.231(44)	1.15(19)	

If $m_{eff}(a)$ and $m_{eff}(2a)$ are sufficiently close, then one can argue that it is not possible for $m_{eff}(3a)$ to be very much lower. At the margins, this allows us to make choices about what is, or is not, likely to be a statistical fluctuation. At this level there is some subjective element in the analysis, although it should be evident from Table XII that this will not be an important problem in our calculation. To test this we have performed continuum extrapolations using $m_{eff}(3a)$ whenever a blind application of our criterion for identifying mass plateaux so dictated. We found it makes no significant difference although the fits are often worse. The reason for the latter fact is that we discount any *rise* in $m_{eff}(t)$ with t simply because we know from positivity that the effective masses must decrease monotonically with t. From the statistical point of view, this is a bias in the procedure which undermines the statistical analysis.

It is apparent from Table XII that as we go to heavier states, the evidence for effective mass plateaux becomes less significant simply because the statistical errors will overwhelm the signal at smaller values of t. As we go to smaller β, and so larger a, this becomes very much worse and we will often not have a useful effective mass beyond $t = 2a$. In these cases we simply assume that $m_{eff}(2a)$ provides a good mass estimate. This is reasonable. If at a high value of β a particular operator gives us a mass plateau from $t = 2a$, then at a larger lattice spacing, e.g. $a' = 2a$, an operator that is one blocking level down, and hence half the size, should surely give us a mass plateau from $t = 2a' = 4a$.

While the above argument is plausible, it cannot replace a direct demonstration. This can be provided by allowing the spacelike, a_s, and timelike, a_t, lattice spacings to differ. We then choose a_t small enough that the correlation functions fall slowly enough over several (temporal) lattice spacings for us to obtain several accurate effective masses. This is an old idea that was used precisely for this purpose [41] in the early days of glueball calculations. More recently it has been used very successfully [42] as part of the action improvement program. Since this is a somewhat different type of calculation to the one in this paper, we leave its discussion to Appendix D. The reader will find there an explicit demonstration that even for a coarse spatial discretization, using effective masses at distances between a_s and $2a_s$ is an accurate way to estimate the masses.

In summary, we have taken all the masses that we use in the spectrum calculations of this paper from $m_{eff}(t = 2a)$. We have checked that using $m_{eff}(t = 3a)$ in the few cases that are ambiguous makes no significant difference.

B. Finite volume effects

In a theory with a mass gap, m, and on a periodic spatial volume that is L lattice units across, the leading finite size corrections to masses are typically $O(e^{-camL})$ where the constant $c = O(1)$ will depend on the details of the theory being considered [43]. Of course this correction will only be relevant once aL is significantly larger than the typical hadronic length scale, ξ. In that case amL will be large, since hadron Compton wavelengths are usually $\ll \xi$, and so the correction will be small: usually too small to be observed

with the kind of accuracy we possess. This means that we cannot expect to obtain a reliable estimate of the coefficient of this correction term. This correction is interesting because it is proportional to a triple-glueball effective coupling. However, if what we are interested in is controlling finite-volume corrections, then the known functional form of this correction has a very useful consequence. Essentially it tells us that if we calculate a mass on volumes aL_1 and aL_2 which are both significantly larger than ξ, and if we find that the change in mass is small when we go from L_1 to L_2, then we can be confident that any mass shift in going from $L=L_2$ to $L=\infty$ will be small compared to the observed change in the mass [as long as $a(L_2-L_1)\sim\xi$]. This is important: if the leading correction were power-like rather than exponential, then this would not be true and controlling finite-volume corrections would be appreciably more difficult.

So our strategy to control finite volume corrections is as follows. We calculate masses on a range of lattice volumes. We include volumes that satisfy the conditions of the previous paragraph. And once we observe very small changes on our larger volumes, we can be confident that the mass calculated on the very largest volume is identical, within errors, to the $L=\infty$ mass.

In practice it would be wasteful to perform such an analysis at each value of β. Instead we choose a couple of values of β where we perform an extensive analysis, including very large volumes in order to make sure there are no unpleasant surprises. This allows us to establish what volumes are large enough that any change in mass becomes invisible within the typical statistical errors of our calculations. We then use scaling to infer how this translates to other values of β.

We perform these calculations in SU(2), simply because that consumes much less computer time. Having determined how large the volume has to be in, say, units of $1/a\sqrt{\sigma}$ we can take this criterion over to SU(3) etc. Of course there is some danger in doing this and so we perform at least a modest finite-volume check for each of our non-Abelian groups.

As a first step, we show in Fig. 5 how some of the lightest masses vary with the size, L, of the spatial volume, in the case of SU(2) and at a coupling of $\beta=9.0$. This, as we see from Table V, corresponds to quite a small lattice spacing. Our spatial length varies from $L=6$ to $L=32$ which corresponds to a variation from ~1 to ~5 in units of $1/a\sqrt{\sigma}$ (about 0.5–2.5 fm if we were in QCD), a range of sizes that satisfies the conditions laid out above. Note that since this is SU(2), we have no $C=-$ states; these shall appear in our (less extensive) SU(3) study. So what we show in Fig. 5 are the masses of the lightest 0^{++}, 0^{-+}, 2^{++}, 2^{-+}, 1^{++}, and 1^{-+} glueballs. We also show twice the mass of the periodic flux loop, $2am_P$, for reasons that shall soon be apparent.

There are several observations we can make from Fig. 5 and the calculations on which it is based.

(i) As we decrease L we do indeed observe the onset of substantial finite size effects.

(ii) The parity doubling that we see at large volumes is badly broken by these finite-volume corrections. This is not unexpected: the toroidal boundary conditions break the effective rotational symmetry from the (dynamically restored) continuous one down to rotations of $\pi/2$. As discussed ear-
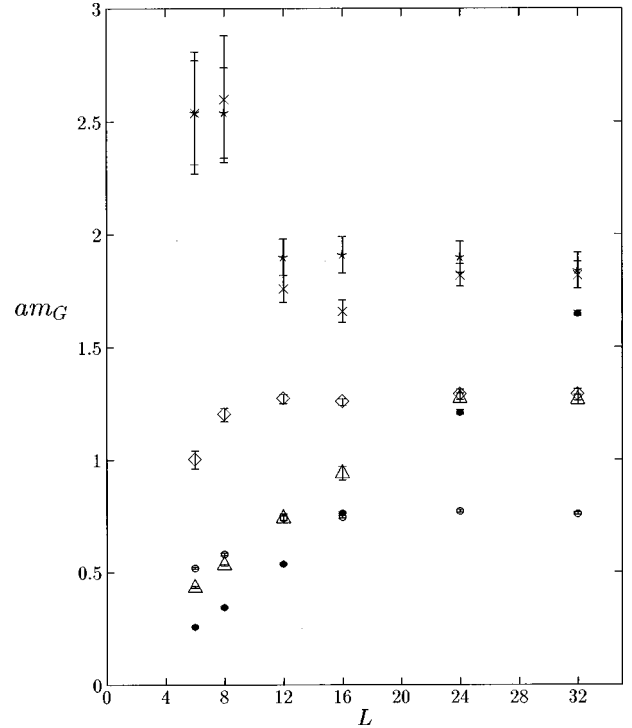

FIG. 5. How the lightest SU(2) masses vary with the spatial volume, L^2, at $\beta=9$. States are the $0^{++}(\bigcirc)$, the $2^{++}(\triangle)$, the $2^{-+}(\diamond)$, the $1^{++}(\times)$ and the $1^{-+}(\star)$. Also shown is twice the mass of the periodic flux loop ($\bullet$).

lier, this undermines the argument for $2^{\pm}$ degeneracy although not $1^{\pm}$ degeneracy. This is precisely what we observe in Fig. 5. Thus the observed degeneracy of the $2^{\pm}$ states can serve as a criterion for the lack of finite volume effects.

(iii) We observe that the value of L at which the 2^+ begins to show finite-volume corrections is roughly where the asymptotic glueball mass equals twice the flux loop mass:

$$2am_P(L)\simeq am_{2^+}/_{L=\infty}. \qquad (48)$$

The same is true for the 0^+. Since the latter is lighter, and since $m_P\uparrow$ as $L\uparrow$, the scalar becomes volume-independent at smaller volumes than the tensor.

This correspondence with $2m_P$ is easy to understand. Suppose we denote by l_x the $\vec{p}=0$ smeared Polyakov loop in the x-direction which has the best overlap onto the x-periodic flux tube. Typically this overlap will be ~90–100%. Consider now the operator $l_x l_x^\dagger$. This will also be $\vec{p}=0$ and color singlet, but it falls into the sector of contractible loops and so can couple to glueball states. If the transverse spatial size, L_y, were very large, then this operator would mainly couple to a state that consists of two periodic flux loops whose energy would be $2m_P(L)$. We shall refer to such states as "torelons." On our lattices $L_x=L_y=L$ and as L becomes small these flux loops will necessarily interact; thus the lowest energy will deviate somewhat from $2m_P$. We can form 0^{++} and 2^{++} combinations, $l_x l_x^\dagger+l_y l_y^\dagger$ and $l_x l_x^\dagger-l_y l_y^\dagger$, respectively. Again, on large volumes these will mainly couple to states with two flux tubes and mass $2m_P(L)$. On smaller

volumes, $aL \lesssim \xi$, the interaction between the flux tubes will split these states away from each other and from this mass. While we cannot predict the precise variation of these masses with L, one would expect them to decrease, at least until $aL \ll \xi$. Thus the fact that the 2^{++} mass begins to decrease with decreasing L, just when Eq. (48) is satisfied, would seem to simply reflect the fact that for smaller L than this the 2^{++} state which is composed of a pair of flux loops becomes the lightest state in that sector. And the same for the 0^{++}.

We have explicitly confirmed this scenario. For large L at least one of our usual glueball operators has a large, ~ 90–100%, overlap onto the lightest 0^{++} or 2^{++} state. By contrast the double flux loop operators have poor overlaps. The value of L at which the lightest mass begins to decrease as L decreases marks the point at which things reverse. For smaller L it is one of the double flux loop operators that has a very high overlap onto the lightest state and the usual operators all become poor.

We remark that similar finite volume effects are observed in $D = 3 + 1$ gauge theories [44], but because $m_G / \sqrt{\sigma}$ is slightly higher in $D = 2 + 1$, the effects occur on somewhat larger volumes, and so their interpretation is that much less ambiguous.

(i) Naively we would expect the spatial size at which we begin to encounter large finite size effects to be related to the size of the glueball. However, in the case of the 0^{++} and 2^{++} glueballs, we have seen that the onset of finite size effects is simply determined by the (infinite volume) mass and the string tension. Thus the fact that we can go to smaller spatial volumes for the scalar than for the tensor, before encountering large finite size effects, is not telling us that the size of the scalar is less than that of the tensor. The same holds true in the case of four dimensions.

(ii) In addition to the above, there are finite size effects, visible in the $0^-, 2^-, 1^\pm$ states, whose onset appears at much smaller values of L, and which does not appear to be linked to mixing with torelon states. (There are no simple torelon states with these quantum numbers.)

(iii) We infer from Fig. 5 that at $\beta = 9$ a spatial size of $L = 24$ is large enough for the lightest glueballs to be free of finite size effects within our statistical errors. Assuming scaling and $\beta = 4/ag^2$ this implies that at a general value of β a safe size is $L \geq 24\beta/9$. One can do better by using the calculated value of $a\sqrt{\sigma}$ to set the scale. Doing so, one can then extend the criterion to SU(3) etc.

In practice we are more cautious than this and have performed an extensive finite volume analysis at $\beta = 6$ as well. This is for a larger value of a, and we include larger lattices, up to more than 8 in units of $1/a\sqrt{\sigma}$. These masses are shown in Table XIII. We also have a more limited study, on $L = 32$ and $L = 48$ lattices, at $\beta = 12$ where a is smaller. These masses will be displayed later, in Table XVII, where we display our ''$V = \infty$'' SU(2) mass values. All these results confirm our criterion for what constitutes a safe volume.

In Table XIV we show our SU(3) study. The presentation here is slightly different to that in Table XIII in that we show estimates of the 0^{++} and 2^{++} torelon masses using the op-

TABLE XIII. How the lightest SU(2) glueball masses depend on the spatial volume. Twice the mass of the periodic flux loop is also shown.

State	SU(2),$\beta=6$					
	$L=6$	$L=8$	$L=12$	$L=16$	$L=24$	$L=32$
0^{++}	0.99(2)	1.12(2)	1.21(2)	1.19(2)	1.20(2)	1.18(2)
2^{++}	0.92(2)	1.17(2)	1.71(5)	1.80(8)	1.99(12)	1.87(10)
2^{-+}	2.20(13)	2.17(15)	2.15(21)	1.81(14)	2.01(16)	1.91(11)
$2 \times l_P$	0.62(1)	0.90(1)	1.43(1)	2.00(2)	3.12(6)	4.11(15)

erators described earlier on in this section. The glueball masses have been obtained from the usual glueball operators based on contractible loops. (Of course, the torelon and glueball operators do mix and at $t \to \infty$ we would always find the same effective mass. But if the mixing is small, one will, in general, find different effective mass plateau at small values of t.) Just as we saw in the case of SU(2), it is clear that the onset of large finite size effects for the scalar and tensor glueball masses is linked to the mass of the corresponding torelon state. We are also now able to see what happens to the $C = -$ states and we show the 0^{--} which is the lightest of these. Since our a is not small, we do not have accurate values of $m_{eff}(t=2a)$ for the heavier states. (As usual our quoted masses are extracted at $t \geq 2a$.) We can of course look at $m_{eff}(t=a)$ which has the disadvantage of having some excited state component, but which is accurately calculated even for the heaviest states. Although we do not show the values here, we remark that they show no sign of any finite size effects that violate our above criterion, either for the $C = +$ or for the $C = -$ states. The same is true for our modest SU(4) and SU(5) finite volume studies, which appear in Table XV.

This establishes the level of our control of finite volume effects. There is one further important point. In the case of the 2^{++} the torelon appears to exist as a bound state in the mass spectrum for larger L. This makes it difficult to extract a consistent picture of the excited 2^{++} states. Since there is no such difficulty for the excited 2^{-+} states, and since these states should be degenerate with the non-torelon 2^{++} excitations, we do not try to overcome this difficulty. So the reader should not be surprised to find no masses being

TABLE XIV. How the lightest SU(3) masses depend on the spatial volume.

State	SU(3),$\beta=15$			
	$L=8$	$L=12$	$L=16$	$L=24$
0^{++}	0.99(4)	1.09(2)	1.15(2)	1.10(2)
0_{ll}^{++}	0.98(2)	1.49(4)	1.92(9)	2.0(4)
0^{++*}	1.24(4)	1.59(4)	1.66(6)	1.65(5)
0^{--}	1.72(7)	1.65(5)	1.57(6)	1.57(4)
2^{++}	0.95(5)	1.69(6)	1.81(7)	1.86(11)
2_{ll}^{++}	0.95(2)	1.58(4)	2.08(15)	
2^{-+}	1.87(10)	1.83(7)	1.79(8)	1.76(6)

TABLE XV. How the lightest SU(4) and SU(5) masses depend on the spatial volume.

State	SU(4), $\beta=28$		SU(5), $\beta=44$	
	$L=12$	$L=16$	$L=12$	$L=16$
0^{++}	1.08(2)	1.08(2)	1.09(3)	1.05(2)
0^{++*}	1.53(6)	1.62(4)	1.64(6)	1.65(3)
0^{--}	1.60(8)	1.60(4)	1.52(7)	1.58(5)
2^{++}	1.80(10)	1.76(4)	1.74(11)	1.69(7)
2^{-+}	1.80(12)	1.79(5)	1.78(9)	1.60(6)

quoted for the excited 2^{++} states later on. As an addendum to this, we remark that this "difficulty" appears to disappear for larger values of N_c. We assume that this is a manifestation of the suppression of all mixings at large N_c.

C. Lattice mass spectra

In the previous two subsections we discussed our criteria first for minimizing the systematic error associated with the extraction of masses on a given lattice, and second for controlling the finite volume corrections to such masses. We now use those criteria to extract our "infinite volume" lattice mass spectra.

In Tables XVI, XVII, XVIII, XIX, and XX we list some of the masses that we have extracted in the SU(2), SU(3), SU(4) and SU(5) calculations respectively. All are in lattice units. In addition, all these masses have been extracted from $am_{eff}(t=2a)$. There are a few exceptions to this. It sometimes occurs, particularly at the smaller values of β, that $am_{eff}(t=a)<am_{eff}(t=2a)$. On the other hand, we know from positivity that $am_{eff}(t)$ must decrease as t increases. Since the error at $t=a$ is smaller than at $t=2a$, it is clear that the $t=a$ effective mass is the better mass estimate in these cases, and that is the value we list. However, the error quoted is the larger one which is associated with $t=2a$. In principle when we come to extrapolating to the continuum limit we should use the $t=2a$ effective masses in these cases since otherwise there is a systematic downward bias in the statistical analysis. [That is, we correct some large upward statistical fluctuations in $am_{eff}(t=2a)$, but none of the ones

that are large and downwards.] However, so few values are affected, and these are usually at the lowest values of β, that we choose not to complicate the analysis by doing so. We also note that the volumes used here are always at least as large as the minimum necessary, as indicated by our earlier finite volume studies.

We begin with a brief technical aside. Our calculations, at each value of β and L, typically involved between 80000 and 200000 Monte Carlo sweeps with calculations of glueball correlators being made every 5 sweeps. Typically we would have 3 or 5 over-relaxed sweeps for each heat bath sweep. By comparing the values of $a\sqrt{\sigma}$ the reader can see that the SU(4) and SU(5) β values are more or less equivalent. They are also nearly equivalent to some of the SU(3) and SU(2) β values.

We make some comments now, starting with the SU(5) masses listed in Table XX. Here we focus on features that might affect the reliability of the calculations; we leave a discussion of the physics until later. We first note that the lightest $J=1$ and $J=2$ states display parity doubling within errors, in contrast to the marked lack of doubling in the $J=0$ sector. This confirms that we have made our ultraviolet cutoff small enough and our infrared cutoff large enough. The same is true of the $J=2$ excited states. However, it is less clear what is going on among the excited states in the $J=1$ sector; there appears to be a near-degeneracy between the ground and excited states in some cases. And the expected degeneracy between the 1^{++*} and the 1^{-+*} appears to be broken. This may indicate the presence of a $J=3$ state which is nearly degenerate with the $J=1$ state, it may be that some of these states are multiglueball scattering states, or there may be finite volume corrections. We are not well placed to distinguish among these possibilities in our present calculations. For example to investigate the last possibility, we need to do a finite volume study for a small value of a where these very heavy masses can be accurately calculated. The only calculation of this kind is in SU(2) at $\beta=12$ (see Table XVII). We do not see any trend for the 1^{++*} and 1^{-+*} masses to converge as we increase L from $L=32$ to $L=48$. So it does not seem to be a finite volume effect. If we compare different β values, there appears to be no trend for this effect to decrease; so it would not seem to be a finite-a

TABLE XVI. The lightest SU(2) masses at lower values of β.

State	$\beta=3.75$ $L=8$	$\beta=4.5$ $L=12$	$\beta=5$ $L=16$	$\beta=6$ $L=16$	$\beta=6$ $L=24$	$\beta=6$ $L=32$
0^{++}	2.07(9)	1.642(43)	1.478(24)	1.193(18)	1.191(18)	1.170(23)
0^{++*}	2.7(3)	2.12(19)	2.11(11)		1.67(6)	1.60(6)
0^{++**}			2.6(4)		2.07(12)	2.10(13)
0^{-+}				2.10(33)	2.41(35)	2.59(29)
2^{++}			2.26(17)	1.80(8)	1.94(11)	1.87(11)
2^{++*}					2.00(14)	1.94(12)
2^{-+}			2.20(15)	1.81(14)	1.77(11)	1.91(9)
2^{-+*}					2.28(27)	2.26(16)
1^{++}				2.43(31)	2.35(38)	2.64(27)
1^{-+}				2.9(7)	2.4(5)	3.0(7)

TABLE XVII. The lightest SU(2) masses at higher values of β.

State	$\beta=9$ $L=24$	$\beta=9$ $L=32$	$\beta=12$ $L=32$	$\beta=12$ $L=48$	$\beta=14.5$ $L=40$
0^{++}	0.7643(60)	0.7552(67)	0.5572(36)	0.5628(46)	0.4562(23)
$0^{++}*$	1.082(16)	1.087(14)	0.8072(53)	0.8047(74)	0.6532(33)
$0^{++}**$	1.271(21)	1.340(22)	0.949(8)	0.982(14)	0.790(4)
0^{-+}	1.629(44)	1.60(4)	1.187(18)	1.188(18)	0.965(8)
$0^{-+}*$	1.95(9)	1.75(7)	1.302(20)	1.350(28)	1.178(13)
2^{++}	1.259(13)	1.249(15)	0.913(7)	0.920(13)	0.7557(35)
$2^{++}*$	1.396(22)	1.484(27)	0.971(8)	1.055(11)	0.846(7)
2^{-+}	1.276(24)	1.286(23)	0.928(9)	0.910(10)	0.7626(51)
$2^{-+}*$	1.532(32)	1.480(31)	1.089(13)	1.094(18)	0.958(10)
1^{++}	1.814(54)	1.82(6)	1.258(17)	1.295(20)	1.042(9)
$1^{++}*$	2.04(10)	1.94(8)	1.493(24)	1.491(31)	1.240(15)
1^{-+}	1.892(54)	1.81(8)	1.356(18)	1.317(20)	1.096(10)
$1^{-+}*$	1.83(6)	1.73(6)	1.331(17)	1.320(19)	1.092(12)

effect. This is a puzzle. As far as the $1^{\pm-}$ states are concerned, we have even less to go on, because we have no $C = -$ in our SU(2) studies. These oddities need to be resolved but they afflict the very heaviest of the states we study and so we shall not attempt to resolve the issue here.

Although we have carefully chosen the volumes so that the ground state $J=0$ and $J=2$ masses are essentially infinite volume, this is not necessarily the case for the $J=2$ excited states. Indeed we observe in Table XVII that the mass of the $2^{++}*$ is volume dependent and is only degen-

TABLE XVIII. The lightest SU(3) masses.

State	$\beta=11$ $L=12$	$\beta=15$ $L=16$	$\beta=15$ $L=24$	$\beta=21$ $L=24$	$\beta=28$ $L=32$	$\beta=34$ $L=40$
0^{++}	1.626(36)	1.123(16)	1.095(14)	0.7561(62)	0.5517(38)	0.4482(36)
$0^{++}*$	2.19(14)	1.66(6)	1.652(44)	1.124(15)	0.823(6)	0.6737(45)
$0^{++}**$		2.06(9)	2.04(11)	1.411(23)	1.034(9)	0.8512(67)
0^{--}	2.30(15)	1.568(53)	1.569(38)	1.101(14)	0.8133(57)	0.6682(48)
$0^{--}*$		2.05(16)	2.00(10)	1.385(21)	1.025(10)	0.8386(49)
$0^{--}**$		2.44(41)	2.40(30)	1.596(39)	1.191(16)	0.9969(85)
0^{-+}			2.32(24)	1.627(41)	1.206(15)	0.9634(81)
$0^{-+}*$				1.835(73)	1.322(17)	1.194(14)
0^{+-}			2.08(23)	1.826(59)	1.330(15)	1.088(10)
$0^{+-}*$				1.98(11)	1.582(31)	1.315(16)
2^{++}	2.31(21)	1.81(7)	1.86(11)	1.218(16)	0.9123(70)	0.7354(43)
$2^{++}*$		2.15(14)	2.18(15)	1.520(27)	1.057(10)	0.9134(79)
2^{-+}	2.64(29)	1.786(82)	1.758(58)	1.257(18)	0.937(8)	0.7526(48)
$2^{-+}*$		2.10(16)	2.19(15)	1.618(43)	1.109(10)	0.9142(65)
2^{--}		2.05(15)	1.95(14)	1.475(23)	1.0928(86)	0.8913(63)
$2^{--}*$		2.21(19)	2.35(26)	1.705(42)	1.254(15)	1.0452(85)
2^{+-}		2.04(16)	1.89(11)	1.539(27)	1.114(11)	0.8867(59)
$2^{+-}*$				1.813(54)	1.325(15)	1.085(11)
1^{++}				1.738(40)	1.298(11)	1.0513(70)
$1^{++}*$				1.933(61)	1.481(19)	1.212(10)
1^{-+}				1.881(51)	1.350(12)	1.082(8)
$1^{-+}*$				1.902(48)	1.352(13)	1.096(9)
1^{--}				1.780(34)	1.269(11)	1.036(7)
$1^{--}*$				1.877(51)	1.371(15)	1.075(9)
1^{+-}				1.788(37)	1.297(11)	1.074(9)
$1^{+-}*$				1.996(56)	1.404(16)	1.103(7)

TABLE XIX. The lightest SU(4) masses.

State	$\beta=21$ $L=12$	$\beta=28$ $L=16$	$\beta=40$ $L=24$	$\beta=51$ $L=32$
0^{++}	1.525(36)	1.083(14)	0.7109(52)	0.5466(40)
$0^{++}*$	2.31(22)	1.616(39)	1.080(10)	0.821(6)
$0^{++}**$		1.99(8)	1.364(21)	1.032(9)
0^{--}	2.10(13)	1.599(36)	1.039(13)	0.8040(46)
$0^{--}*$		2.00(7)	1.301(18)	1.010(8)
$0^{--}**$		2.38(17)	1.544(24)	1.186(10)
0^{-+}		2.35(16)	1.575(27)	1.200(10)
$0^{-+}*$			1.80(6)	1.325(14)
0^{+-}		2.66(32)	1.76(6)	1.340(14)
$0^{+-}*$			1.85(6)	1.564(22)
2^{++}	2.08(18)	1.76(4)	1.168(14)	0.9122(56)
$2^{++}*$		2.09(10)	1.408(17)	1.085(10)
2^{-+}	2.15(19)	1.79(5)	1.205(18)	0.8936(67)
$2^{-+}*$		1.99(10)	1.429(23)	1.095(12)
2^{--}		2.08(12)	1.430(23)	1.067(12)
$2^{--}*$		2.38(18)	1.57(4)	1.244(13)
2^{+-}		2.17(10)	1.394(24)	1.077(9)
$2^{+-}*$		2.53(29)	1.59(4)	1.296(13)
1^{++}		2.66(28)	1.720(31)	1.300(11)
$1^{++}*$			2.05(4)	1.454(15)
1^{-+}		2.68(26)	1.67(3)	1.340(13)
$1^{-+}*$			1.76(3)	1.344(10)
1^{--}		2.48(13)	1.70(3)	1.251(9)
$1^{--}*$			1.74(5)	1.320(13)
1^{+-}		2.42(18)	1.73(5)	1.264(10)
$1^{+-}*$			1.79(4)	1.313(16)

TABLE XX. The lightest SU(5) masses.

State	$\beta=33$ $L=12$	$\beta=44$ $L=16$	$\beta=64$ $L=24$	$\beta=82$ $L=32$
0^{++}	1.550(47)	1.054(15)	0.695(5)	0.5325(48)
$0^{++}*$	2.4(3)	1.654(30)	1.053(11)	0.798(7)
$0^{++}**$		2.06(11)	1.342(27)	1.009(10)
0^{--}	2.29(24)	1.581(44)	1.041(11)	0.765(10)
$0^{--}*$		2.05(11)	1.278(20)	0.997(8)
$0^{--}**$		2.27(19)	1.555(34)	1.19(2)
0^{-+}		2.32(14)	1.478(23)	1.155(11)
$0^{-+}*$			1.80(4)	1.347(18)
0^{+-}		2.54(32)	1.78(7)	1.256(14)
$0^{+-}*$			1.81(5)	1.580(33)
2^{++}		1.69(7)	1.08(5)	0.8914(69)
$2^{++}*$		2.05(9)	1.39(3)	1.072(9)
2^{-+}		1.60(6)	1.07(5)	0.8785(69)
$2^{-+}*$		2.06(14)	1.37(3)	1.075(9)
2^{--}		2.14(11)	1.390(25)	1.054(10)
$2^{--}*$		2.57(28)	1.559(31)	1.225(16)
2^{+-}		2.08(12)	1.430(21)	1.043(9)
$2^{+-}*$		2.51(36)	1.557(34)	1.230(17)
1^{++}		2.38(22)	1.718(30)	1.294(14)
$1^{++}*$			1.93(8)	1.421(14)
1^{-+}		2.57(23)	1.697(31)	1.300(10)
$1^{-+}*$			1.78(5)	1.331(15)
1^{--}		2.29(10)	1.654(32)	1.212(9)
$1^{--}*$			1.66(4)	1.27(2)
1^{+-}		2.41(16)	1.71(5)	1.255(14)
$1^{+-}*$			1.73(4)	1.29(2)

erate with the $2^{-+}*$ on the largest volume, and then only in those cases, $\beta=9$ and 12, where this is exceptionally large. Explicit calculations with the double Polyakov loop operators described in the previous subsection indicate that this is an artifact of the presence of a corresponding scattering (or bound?) state whose mass increases approximately linearly with L. So as $L\uparrow$ the mass moves out of the range of masses we probe. We remark that we have no clear evidence of a corresponding $J=0$ state. (It would, in any case, not interfere with the lowest 0^{++} excitations because these are so light.) It is interesting that this problem appears to disappear for the larger SU(N) groups. A possibility is that, as expected, the mixing between the double flux loops and our ordinary ''local'' glueballs is suppressed by powers of $1/N$. To investigate this properly one needs to include both double flux loops and our normal contractible loops within a single basis for our cross-correlation matrix (as has been done in [45] for precisely this purpose). We have not been able to do this here because of the very large storage costs this would have entailed. Since we cannot resolve the states unambiguously, we shall not attempt a continuum extrapolation of the SU(2) $2^{++}*$. For larger groups it seems that this problem is not there and so we shall attempt to obtain the corresponding continuum masses.

D. Continuum mass spectrum

A lattice spectrum is only interesting insofar as it can lead us to the spectrum of the corresponding continuum theory. To obtain the continuum spectrum we need to extrapolate our lattice masses to $a=0$. The first step is to take ratios of masses so that the scale, a, in which they are expressed cancels. We choose to take ratios of the glueball masses, am_G, to $a\sqrt{\sigma}$ since the string tension is our most accurately calculated quantity.

The second step is motivated by the observation [46] that in pure lattice gauge theories the leading lattice correction to dimensionless ratios of physical quantities, such as $m_G/\sqrt{\sigma}$, is $O(a^2)$. So for small enough a we expect the a-dependence to be given, just as in four dimensions, by

$$\frac{m_G(a)}{\sqrt{\sigma(a)}} = \frac{m_G(a=0)}{\sqrt{\sigma(a=0)}} + ca^2\sigma. \qquad (49)$$

Of course, instead of using the correction term $ca^2\sigma$ we could use $\tilde{c}a^2\tilde{m}_G^2$ where $a\tilde{m}_G$ is any calculated glueball mass. The difference is formally $O(a^4)$. The reason for choosing σ is simply that it is so accurately determined. An alternative way of extrapolating such a mass ratio to $a=0$ is
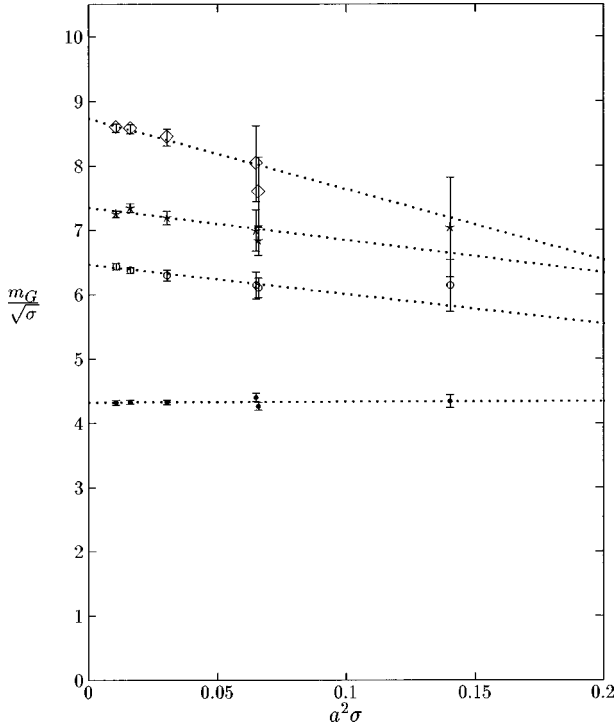
FIG. 6. The ratio of some SU(3) masses to $a\sqrt{\sigma}$, plotted against $a^2\sigma$ to show how they vary with a: the $0^{++}(\bullet)$, the $0^{--}(\circ)$, the $2^{-+}(\star)$ and the $2^{--}(\diamond)$. Extrapolations to the continuum limit are shown as straight lines.

to use the fact that g^2 has dimensions of mass and that $\lim_{\beta\to\infty}\beta=2N_c/ag^2$. Thus, for small enough a,

$$\frac{m_G(a)}{\sqrt{\sigma}(a)}=\frac{m_G(a=0)}{\sqrt{\sigma}(a=0)}+\frac{c}{\beta^2}. \tag{50}$$

What we do in practice is to choose one of the above forms and attempt to fit all the mass values of some state with it. If a good fit is not possible, we assume that this is because the largest value of a used is too large for the $O(a^2)$ correction to be adequate. So we drop the mass corresponding to the largest value of a and try again. We keep doing this until we get a good fit.

In Fig. 6 we show some examples drawn from the SU(3) calculation. Since the mass ratios are plotted against $a^2\sigma$, the continuum extrapolations, in Eq. (49), are simple straight lines. The really striking feature of this plot is how little variation with a there is. This will make for unambiguous and very accurate continuum extrapolations.

Our continuum extrapolations for our various theories are displayed in Table XXI. They have been obtained by fitting the form in Eq. (50) to the masses listed in Tables XVI, XVII, XVIII, XIX, and XX and the string tensions listed in Tables V, VI, and VII. The quality of each fit, as given by the confidence level, is given in Table XXII. We have also performed extrapolations using Eq. (49); these give essentially identical results, with any differences being much smaller than our quoted errors.

TABLE XXI. Glueball masses in units of the string tension: in the continuum limit.

| State | $m_G/\sqrt{\sigma}$ | | | |
	SU(2)	SU(3)	SU(4)	SU(5)
0^{++}	4.718(43)	4.329(41)	4.236(50)	4.184(55)
$0^{++}*$	6.83(10)	6.52(9)	6.38(13)	6.20(13)
$0^{++}**$	8.15(15)	8.23(17)	8.05(22)	7.85(22)
0^{--}		6.48(9)	6.271(95)	6.03(18)
$0^{--}*$		8.15(16)	7.86(20)	7.87(25)
$0^{--}**$		9.81(26)	9.21(30)	9.51(41)
0^{-+}	9.95(32)	9.30(25)	9.31(28)	9.19(29)
0^{+-}		10.52(28)	10.35(50)	9.43(75)
2^{++}	7.82(14)	7.13(12)	7.15(13)	7.19(20)
$2^{++}*$			8.51(20)	8.59(18)
2^{-+}	7.86(14)	7.36(11)	6.86(18)	7.18(16)
$2^{-+}*$		8.80(20)	8.75(28)	8.67(24)
2^{--}		8.75(17)	8.22(32)	8.24(21)
$2^{--}*$		10.31(27)	9.91(41)	9.79(45)
2^{+-}		8.38(21)	8.33(25)	8.02(40)
$2^{+-}*$		10.51(30)	10.64(60)	9.97(55)
1^{++}	10.42(34)	10.22(24)	9.91(36)	10.26(50)
1^{-+}	11.13(42)	10.19(27)	10.85(55)	10.28(34)
1^{--}		9.86(23)	9.50(35)	9.65(40)
1^{+-}		10.41(36)	9.70(45)	9.93(44)

The reader will note that the mass of the $2^{++}*$ is missing from the SU(2) and SU(3) columns. This is because we could find no acceptable fits. We believe this is related to mixing with torelons, as discussed previously. The mass of the latter depends sensitively on the volume and so will not provide a consistent set of masses at different values of β (since the volumes are not exactly the same). This is no longer a problem with SU(4) and SU(5) and we assume that this is because any such mixing becomes suppressed at large N_c. A calculation including overlaps between torelon and glueball operators would resolve this question, but we have not carried this out. Why we cannot get an acceptable fit for the SU(2) $2^{-+}*$ is less clear. The reason might be that our SU(2) calculations in the 2^{-+} channel had a smaller basis (4 operators) than in the later calculations with larger groups. This meant a very small basis for the excited states.

In addition to these spectra we have performed in Appendix D some calculations with a very asymmetric lattice action, $a_t\simeq a_s/4$. This may be thought of as being close to the "Hamiltonian" limit, and it is interesting, as a test of universality, to confront this spectrum with the SU(2) spectrum that we have obtained in this section. This we do in Table XXIII and we observe good agreement within errors. For a detailed discussion of our calculations with the asymmetric lattice action we refer the reader to Appendix D.

We now have all our continuum spectra and can turn to their dependence on N_c.

E. N_c dependence of the mass spectrum

We can already see from Table XXI that the variation of our mass ratios with N_c is weak and that it appears to become weaker with increasing N_c.

TABLE XXII. Confidence levels of the best fits in Table XXI; in brackets those of the fits that provide the errors.

State	Best fit confidence level (%)			
	SU(2)	SU(3)	SU(4)	SU(5)
0^{++}	85(25)	70(20)	70(20)	60(20)
$0^{++}*$	25(5)	80(25)	90(25)	100(25)
$0^{++}**$	15(3)	90(25)	40(10)	60(20)
0^{--}		95(25)	35(10)	15(3)
$0^{--}*$		90(25)	35(10)	23(5)
$0^{--}**$		65(20)	70(20)	70(20)
0^{-+}	90(25)	45(15)	85(25)	35(10)
0^{+-}		85(25)	95(25)	13(2)
2^{++}	95(25)	40(10)	25(6)	17(3)
$2^{++}*$			90(25)	90(25)
2^{-+}	60(20)	50(15)	15(3)	30(8)
$2^{-+}*$		12(3)	14(10)	65(20)
2^{--}		80(25)	25(6)	85(25)
$2^{--}*$		70(20)	40(10)	30(10)
2^{+-}		25(5)	45(10)	3(0.3)
$2^{+-}*$		80(25)	12(3)	40(10)
1^{++}	60(20)	40(10)	100(25)	22(4)
1^{-+}	60(20)	60(15)	10(2)	100(25)
1^{--}		45(10)	10(2)	2(0.1)
1^{+-}		25(5)	12(3)	15(3)

To illustrate this we plot in Fig. 7 and Fig. 8 the quantity $m_G/g^2 N_c$, which is obtained from the ratios in Table XXI and the string tensions in Eq. (38). We choose to plot against $1/N_c^2$ because the usual diagrammatic analysis predicts that at large enough N_c we should expect

$$\frac{m_G}{g^2 N_c} = R_\infty + \frac{R_1}{N_c^2} \tag{51}$$

where $R_\infty = \lim_{N_c \to \infty} m_G/g^2 N_c$. So on our plot this will be a simple straight line. We observe that the dependence of our

TABLE XXIII. Comparison between the continuum mass ratios, $m_G/\sqrt{\sigma}$, obtained with the asymmetric $r=0.25$ SU(2) action, and our previous $r=1$ SU(2) results. Also shown is $\sqrt{\sigma}/g^2$ for both cases.

State	SU(2), $r=1.0$	SU(2), $r=0.25$
0^{++}	4.718(43)	4.65(10)
$0^{++}*$	6.83(10)	6.83(20)
$0^{++}**$	8.15(15)	8.39(33)
0^{-+}	9.95(32)	9.23(38)
2^{++}	7.82(14)	7.81(20)
$2^{++}*$		8.86(30)
2^{-+}	7.86(14)	7.54(20)
$2^{-+}*$		8.94(27)
1^{++}	10.42(34)	10.51(24)
1^{-+}	11.13(42)	11.03(30)
		[10.38(44)]
$\sqrt{\sigma}/g^2$	0.3353(18)	0.3375(130)
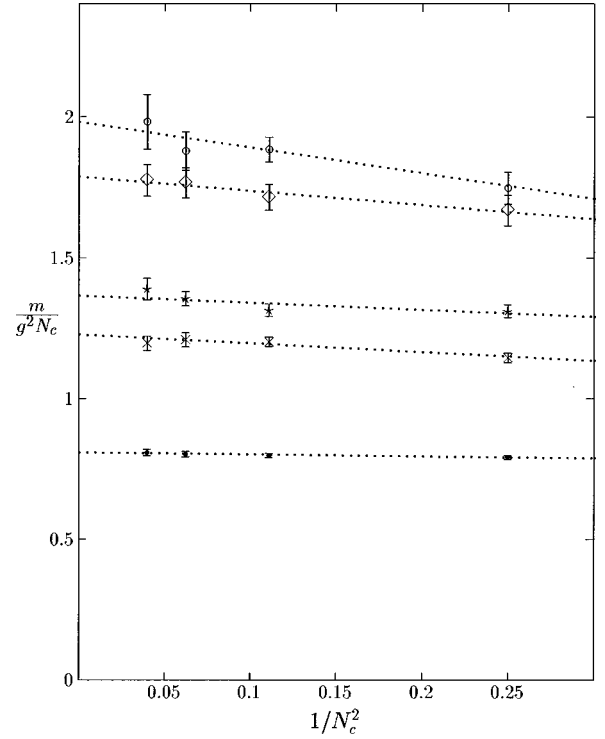
FIG. 7. Some of the $C=+$ glueball masses for 2, 3, 4, and 5 colors, in units of $g^2 N_c$ and plotted against $1/N_c^2$: $0^{++}(\bullet)$, $0^{++}*(\times)$, $2^{++}(\star)$, $0^{-+}(\diamond)$, $1^{++}(\bigcirc)$. The best linear extrapolations to the $N_c=\infty$ limit are also shown.

masses on N_c is really very weak indeed, all the way down to $N_c=2$. This indicates once again that the mass scale of the SU(N_c) theory is $\propto g^2 N_c$, as expected from the diagrammatic analysis.

In Table XXIV we list the $N_c \to \infty$ limits and the slopes, R_1, that result from fitting our continuum masses with Eq. (51). We can, of course, perform a similar analysis using $m_G/\sqrt{\sigma}$ instead. The results of the corresponding extrapolations are presented in Table XXV.

Is there anything we can add to our previous result, in Eq. (43), on the power of the leading correction? The only mass that is accurate enough to be potentially useful is $m_{0^{++}}/g^2 N_c$. However, as we see from Fig. 7, this varies almost not at all with N_c and so provides us with no useful information on the power of this correction. (The stronger variation in $m_{0^{++}}/\sqrt{\sigma}$ simply reflects the variation of $\sqrt{\sigma}$ which we have already studied.)

For purposes of comparison, it would be interesting to provide an example of a mass spectrum that is quite different to the one we have calculated here and yet comes from a theory with a dynamics that is not so dissimilar as to make the comparison meaningless. A natural possibility is to consider the U(1) theory. Since the leading-order large-N_c arguments are in fact for U(N_c), this theory belongs naturally to the sequence of theories we have considered. And yet it is so far from $N_c=\infty$ that we would not expect it to fit into the pattern we have observed so far. As far as dynamics goes, it is a lattice gauge theory which is linearly confining and free at short distances. We discuss our results for the U(1) mass
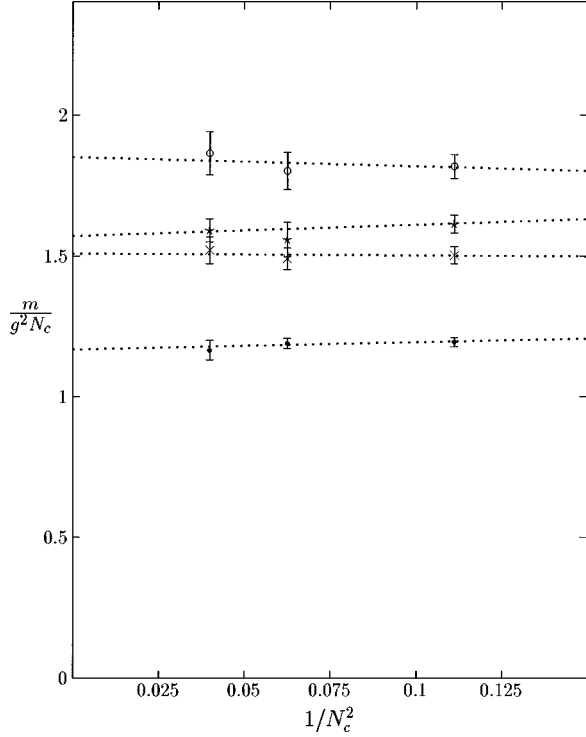
FIG. 8. Some of the $C=-$ glueball masses for 3, 4, and 5 colors, in units of $g^2 N_c$ and plotted against $1/N_c^2$: 0^{--} (●), $0^{--}*$ (×), 2^{--} (⋆), 1^{--} (○). The best linear extrapolations to the $N_c = \infty$ limit are also shown.

spectrum (listed in Table XXVI) and some peculiarities of the theory, in Appendix E. Here we merely note that in the

TABLE XXIV. The large N_c limit of the mass spectrum in units of $g^2 N_c$, with the slope of the linear fit when plotted against $1/N_c^2$. Also the range of colors fitted and the confidence level of the fits.

State	$\lim_{N_c \to \infty} m/g^2 N_c$	Slope	$N_c \geq$	C.L. (%)
0^{++}	0.808(11)	-0.070(79)	2	90(25)
$0^{++}*$	1.227(25)	-0.31(18)	2	65(20)
$0^{++}**$	1.581(42)	-0.84(28)	2	50(15)
0^{-+}	1.787(60)	-0.50(51)	2	85(25)
2^{++}	1.365(33)	-0.25(28)	2	35(10)
2^{-+}	1.369(36)	-0.20(27)	2	15(4)
$2^{-+}*$	1.704(70)	-0.74(88)	3	95(25)
1^{++}	1.98(8)	-0.90(57)	2	80(25)
1^{-+}	1.99(8)	-0.61(70)	2	35(10)
0^{--}	1.167(42)	0.26(50)	3	65(20)
$0^{--}*$	1.508(72)	-0.07(87)	3	65(20)
$0^{--}**$	1.77(13)	0.24(161)	3	30(8)
0^{+-}	1.87(23)	0.63(245)	3	45(10)
2^{--}	1.57(8)	0.40(93)	3	55(15)
$2^{--}*$	1.87(12)	0.23(143)	3	90(25)
2^{+-}	1.59(10)	-0.37(117)	3	65(20)
$2^{+-}*$	1.97(17)	-0.28(188)	3	50(15)
1^{--}	1.85(13)	-0.33(149)	3	55(15)
1^{+-}	1.87(16)	0.37(200)	3	45(10)

TABLE XXV. The large N_c limit of the mass spectrum in units of the string tension, with the slope of the linear fit when plotted against $1/N_c^2$. Also the range of colors fitted and the confidence level of the fits.

State	$\lim_{N_c \to \infty} m/\sqrt{\sigma}$	Slope	$N_c \geq$	C.L. (%)
0^{++}	4.065(55)	2.58(42)	2	80(25)
$0^{++}*$	6.18(13)	2.68(100)	2	70(20)
$0^{++}**$	7.99(22)	0.79(160)	2	50(15)
0^{-+}	9.02(30)	3.52(275)	2	85(25)
2^{++}	6.88(16)	3.50(134)	2	30(10)
2^{-+}	6.89(21)	3.13(162)	2	20(5)
$2^{-+}*$	8.62(38)	1.69(165)	3	90(25)
1^{++}	9.98(25)	1.78(203)	2	80(25)
1^{-+}	10.06(40)	3.58(365)	2	30(8)
0^{--}	5.91(25)	5.24(300)	3	55(15)
$0^{--}*$	7.63(37)	4.61(460)	3	70(20)
$0^{--}**$	8.96(65)	7.2(80)	3	35(10)
0^{+-}	9.47(116)	9.7(12.4)	3	40(10)
2^{--}	7.89(35)	7.6(44)	3	60(20)
$2^{--}*$	9.46(66)	7.6(77)	3	95(25)
2^{+-}	8.04(50)	3.2(60)	3	60(20)
$2^{+-}*$	9.97(91)	5.1(10.0)	3	50(15)
1^{--}	9.36(60)	4.4(70)	3	60(20)
1^{+-}	9.43(75)	8.4(98)	3	50(15)

U(1) theory the 0^{++} is no longer the lightest state; the 0^{--} is about half its mass. We also note that the mass ratio $m_{0^{++}}/\sqrt{\sigma}$ is much lower than in SU(2) [or in SU(∞) for that matter]. So this spectrum is indeed quite different, and the comparison enhances, by contrast, our claim that SU(2) $\simeq$ SU(∞).

The lack of any visible N_c dependence in our most accurately calculated mass, $m_{0^{++}}/g^2 N_c$, is quite striking and provides strong evidence that there is a smooth nontrivial

TABLE XXVI. The U(1) mass spectrum in units of the string tension, at several values of β. In the last row is the string tension in lattice units.

	$m_G/\sqrt{\sigma}$, U(1)		
State	$\beta = 2.0$	$\beta = 2.2$	$\beta = 2.3$
0^{++}	3.54(9)	3.29(23)	3.36(17)
0^{--}	1.97(7)	1.52(5)	1.50(5)
0^{-+}	7.1(9)	8.1(4)	8.8(3)
0^{+-}		8.5(4)	10.4(5)
2^{++}	5.2(7)	4.64(30)	5.12(27)
2^{-+}	4.8(11)	4.9(9)	5.45(40)
2^{--}	6.1(4)	7.0(3)	6.3(4)
2^{+-}	7.0(5)	6.7(3)	6.7(6)
1^{++}		9.6(6)	11.0(6)
1^{-+}		9.7(6)	11.6(6)
1^{--}	7.8(8)	7.9(3)	8.7(3)
1^{+-}	8.2(5)	8.0(3)	8.6(3)
$a\sqrt{\sigma}$	0.2251(18)	0.1734(16)	0.1505(15)

large-N_c limit, with a physical mass scale $\propto g^2 N_c$. Coupled with our previous analysis of the string tension, this also tells us that the $N_c = \infty$ limit possesses linear confinement. (As we see immediately from the behavior of $m_G/\sqrt{\sigma}$.) From the intercepts and slopes listed in Tables XXIV and XXV and from Eq. (44), we can obtain the mass spectrum for any value of N_c. In this very concrete sense we can say that SU(N_c) theories are close to SU(∞) all the way down to SU(2). Thus the large-N_c analysis unifies our understanding of all SU(N_c) theories in a compact and elegant fashion.

F. Features of the mass spectrum

The purpose of this paper is to calculate the mass spectrum. Extracting interesting physics from the detailed features of that spectrum is something that belongs elsewhere. However, it would be churlish of us not to make a few comments. These will be brief and incomplete.

(i) There is clear evidence for the expected parity doubling in the cases of the $2^{\pm+}$, $2^{\pm-}$, $2^{\pm-*}$, $1^{\pm+}$, and $1^{\pm-}$. In contrast, for the $J=0$ states, where we do not expect parity doubling, the splitting between the $P=+$ and $P=-$ states is huge.

(ii) Our lightest glueball state is the 0^{++}, just as it is in $D=3+1$ gauge theories. Moreover, its mass, in units of $\sqrt{\sigma}$, is not that different. If we take the SU(3) continuum extrapolation in [25], which uses the $D=3+1$ lattice glueball mass calculations in [32,49], and if we perform a corresponding SU(2) continuum extrapolation using the $D=3+1$ lattice calculations in [47,50], then we find

$$\frac{m_{0^{++}}}{\sqrt{\sigma}} = \begin{cases} 3.87(12) & \text{SU(2)}, D=3+1, \\ 3.65(11) & \text{SU(3)}, D=3+1. \end{cases} \qquad (52)$$

The fact that the $D=3+1$ mass ratio is smaller than the one in $D=2+1$ follows naturally [10,11] in flux tube models of gluonic states [9]. (It does so from the fact that the closed flux loop has more transverse dimensions in which to oscillate; this increases the corresponding ''Casimir energy,'' and so decreases the mass of the loop, for a given loop length.) We also note from Eq. (52) that the $D=3+1$ N_c dependence has the same sign as in $D=2+1$.

(iii) Just as in $D=3+1$ [25,32,49], the next heaviest state in the $C=+$ sector is the 2^{++} (ignoring excitations of the 0^{++} since these have not been calculated in 4 dimensions). The scalar-tensor mass splitting is not dissimilar: e.g.

$$\frac{m_{2^{++}}}{m_{0^{++}}} = \begin{cases} 1.65(3) & \text{SU(3)}, D=2+1, \\ 1.41(7) & \text{SU(3)}, D=3+1. \end{cases} \qquad (53)$$

(iv) Unlike the $C=+$ sector, the $C=-$ sector is very different from its $D=3+1$ counterpart. For example, we have a light 0^{--}, while there are no light $C=-$ states in 4 dimensions. This may arise from the fact that in 3 space dimensions there is an interplay between C and J that does not exist in 2 space dimensions. Consider, for example, a circular flux string. It will have an arrow on it, for $N_c \geq 3$. Under C the direction of the arrow flips. In 3 (but not 2) space dimensions we can rotate the circle by π around a

diameter and this also flips the direction of the arrow. Note that this means that a rotationally symmetric linear combination of such circular loops cannot be $C=-$. One needs a fluctuation away from a circle to allow $J=0$ and $C=-$ and this raises the energy. Of course we have gradually incorporated some dynamical assumptions as we moved through the last few sentences. One needs to make the argument within a specific model framework and that belongs elsewhere [9–11].

(v) We observe that whatever splits the $C=+$ and $C=-$ states is weakly dependent on N_c and survives the $N_c \rightarrow \infty$ limit. On the other hand, in SU(2), where we have no $C=-$, the spectrum is clearly a smooth continuation of the $N_c \geq 3$ $C=+$ spectrum (since our simple mass fit encompasses $2 \leq N_c \leq 5$). This provides a constraint on dynamical mechanisms for the $C=\pm$ splitting.

(vi) There are some striking approximate degeneracies in the spectrum. The typical pattern is $m_{0^{++*}} \simeq m_{0^{--}}$, $m_{0^{++**}} \simeq m_{0^{--*}}$ and similarly for the $J=2$ states. Again, if this is not an accident, it does suggest some simplicity in the dynamics.

To go further requires confronting specific models with the spectrum we have calculated here. That goes well beyond the scope of this paper.

VI. CONCLUSIONS

In this paper we presented our calculations of the mass spectra and string tensions in three dimensional SU(2), SU(3), SU(4) and SU(5) lattice gauge theories. From these we obtained the corresponding continuum spectra. The accuracy of these continuum results reflects the large range in the lattice spacing, a, over which we performed our lattice calculations. We can compare this range to that in the more familiar $D=4$ SU(3) gauge theory by using the calculated values of the string tension, $a^2\sigma$. Doing so we observe that the (useful) range of our $D=3$ calculations would correspond to $5.50 \leq \beta \leq 6.55$ for the case of SU(2), $5.50 \leq \beta \leq 6.50$ for SU(3), and $5.70 \leq \beta \leq 6.35$ for both SU(4) and SU(5). This range, and the statistics of our calculations, is the primary reason why our $D=3$ calculations are so much more accurate than what is available in four dimensions. We also gain something from the fact that our best operators are slightly better in three than in four dimensions.

We noted some strong similarities, in the $C=+$ sector, between the 2+1 and 3+1 dimensional spectra. This should provide an interesting test for models of glueballs. Indeed one of the main motivations for our calculations is to provide a detailed spectrum against which models and analytic approaches can test themselves.

At the more technical lattice level, we studied, during the course of our calculations, the effectiveness of over-relaxation, the use of asymmetric lattice actions, how good are operators with baryonic vertices, the efficiency of our ''blocking'' algorithm, and the extent to which the mean-field–tadpole improvement of the coupling really represents an improvement. In this last case we were aided by the super-renormalizability of the theory; this allowed us to compare directly extrapolations using the improved and bare

lattice couplings, in a way which is not at present possible in four dimensions.

The primary purpose of our calculations was to study the large-N_c limit of SU(N_c) gauge theories in 2+1 dimensions and to compare the results of our fully non-perturbative calculations with the standard expectations obtained from all-order perturbation theory. We found that there does appear to be a smooth $N_c \to \infty$ limit and that it is obtained, as expected, by varying $g^2 \propto 1/N_c$. The leading correction is $O(1/N_c^2)$, again as expected. We found that confinement—the crucial ingredient for the usual phenomenology—does indeed survive the large-N_c limit. And we obtained the detailed mass spectrum in that limit. Finally, we observed that even SU(2) is close to SU(∞), in the sense that the difference between the mass spectra can be described by just the leading $O(1/N_c^2)$ correction.

Thus all $D=2+1$ SU(N_c) gauge theories can be described by the SU(∞) theory with a modest $O(1/N_c^2)$ correction. This provides a very elegant way to unify and understand all these potentially quite different theories.

There is a wealth of large-N_c expectations that we have not explored. For example those involving decays, $G \to GG$, and, more generally, the N_c-dependence of matrix elements involving various products of singlet operators, as well as their factorization properties. Neither have we attempted to expose the existence of Witten's master field [51] or to determine its properties. All these topics should be readily accessible in three dimensional calculations of the kind presented in this paper. The reason we have not addressed them in this paper is not because we find them less interesting than the questions we have addressed, but because the SU(2) and SU(3) calculations were completed before we realized that we might have something interesting to contribute concerning the large-N_c limit.

These calculations also need to be extended by the inclusion of matter fields in the fundamental representation. In this case the leading corrections are expected to be larger, $O(1/N_c)$, and so it is an interesting open question whether SU(2) or even SU(3) will remain close to SU(∞). Needless to say, all the above questions need to be addressed in four dimensions, and what we can say there is that the first indications [8] are quite promising.

ACKNOWLEDGMENTS

APPENDIX A: TESTING THE BENEFITS OF MONTE CARLO OVER-RELAXATION

Although there is no systematic procedure known for reducing the exponents associated with critical slowing down in $D=4$, or $D=3$, non-Abelian gauge theories, a method that appears to have some effectiveness, and which is now in common use, is to mix heat bath and over-relaxation [26,27] sweeps during the update (for reviews see [28]). As far as testing the efficiency of this method is concerned, what is available are studies of the decorrelation of blocked Wilson loops in SU(2) and SU(3) [29] which show that there is a strong reduction in fluctuations when most heat bath sweeps are replaced with over-relaxation. This has helped to motivate the widespread use of overrelaxation.

However, useful as these tests are, what one would like to see is how the statistical errors on the physical quantities of interest (glueball masses, string tension, etc.) are reduced when some fraction of the heat bath sweeps are replaced with over relaxation sweeps. In $D=3+1$ such an exercise would be prohibitively expensive for the small lattice spacings where the answer is interesting, and so, as far as we know, no study of this kind has been published. In $D=2+1$, such a study becomes possible and this is what we shall present in this appendix. Because the $D=2+1$ and $D=3+1$ theories have so much in common—in particular they both become free at short distances—we can hope that what we find has some relevance to four dimensions as well.

Our heat bath and over-relaxation algorithms have been described in Sec. III A. We note that in both SU(2) and SU(3) the over-relaxation algorithm explores phase space at a constant value of the total action. We shall characterize the update pattern by the ratio, R_o, of the number of over-relaxation sweeps to the number of heat bath sweeps. Since we use a pipelined CPU, all our sweeps employ a variation of a checkerboard update.

Our study of SU(3) is the more extensive of the two and so this is where we shall begin. We have performed comparisons at three values of β: at $\beta = 11$ and 15 on $12^2 16$ lattices, and at $\beta = 21$ on a 24^3 lattice. If we use the calculated string tension to set the scale of the lattice spacing, then these three values of β correspond to $\beta \simeq 5.7, 5.9, 6.15$, respectively in the $D=4$ theory with which the reader is probably more familiar. The lattices at $\beta = 11$ and $\beta = 21.0$ are effectively of infinite physical volume for the quantities we shall be considering here. The lattice volume at $\beta = 15$ is of an intermediate size, which mainly effects the nature of the 2^{++} glueball. At $\beta = 11$ we performed calculations for $R_o = 0$ (pure heat bath) and for $R_o = 5$. Each calculation involved 80000 sweeps with the data split into 40 bins of 2000 sweeps each for the error analysis. At $\beta = 15$ we performed 25000 sweeps at each of $R_o = 0, 2, 5, 10, 20$, with the data divided into 20 bins in each case. At $\beta = 21$ we performed 20000 sweeps at each of $R_o = 0, 3, 5, 7, 10$, with 20 bins in each case.

The quantities we use in our comparison are, first, the masses of the lightest glueballs: the $0^{++}, 0^{--}, 2^{++}$ and, where available, the 2^{-+} (which should be degenerate with the 2^{++} in large volumes and for small lattice spacings). We also use the mass of the lightest flux loop that closes through a periodic boundary. This provides us with our estimate of the string tension, σ, since the mass of this loop is $a^2 \sigma L$, up to $O(1/L)$ finite size corrections, where L is the minimal length of the loop (in lattice units). In addition to these masses we also calculate expectation values of the simplest

TABLE XXVII. Errors on SU(3) masses on a $12^2 16$ lattice at $\beta = 11$; R_o is the number of over-relaxed sweeps for every heat bath sweep.

State	$R_o = 0$	$R_o = 5$
Flux loop	0.0054	0.0050
	0.024	0.030
0^{++}	0.0098	0.0097
	0.056	0.051
0^{--}	0.019	0.024
	0.22	0.20
2^{++}	0.036	0.031
	0.29	0.32

TABLE XXVIII. Errors on SU(3) masses on a $12^2 16$ lattice at $\beta = 15$. R_o is the number of over-relaxed sweeps for every heat bath sweep.

State	$R_o = 0$	$R_o = 2$	$R_o = 5$	$R_o = 10$	$R_o = 20$
Flux loop	0.0036	0.0053	0.0033	0.0044	0.0043
	0.0085	0.0123	0.0078	0.0074	0.0094
0^{++}	0.0086	0.0132	0.0075	0.0139	0.0085
	0.034	0.040	0.037	0.038	0.033
0^{--}	0.017	0.026	0.020	0.018	0.022
	0.081	0.113	0.086	0.082	0.125
2^{++}	0.025	0.015	0.015	0.024	0.021
	0.090	0.092	0.092	0.079	0.070

closed loops made out of our ''blocked'' links. At a ''blocking'' level of unity, $B_l = 1$, we have the simple plaquette. More generally these ''superplaquettes'' consist of a square that is length $2^{B_l - 1}$ in lattice units. The simple plaquette is dominated by ultraviolet fluctuations and is of relatively little physical interest. At higher smearing levels, the expectation value is dominated by fluctuations closer to physical length scales and how the accuracy of these is affected by over-relaxation is a more interesting question.

We compare the errors on these quantities in the different runs characterized by different values of R_o. The reference run is the one with $R_o = 0$, i.e., pure heat bath. If the $R_o = 0$ error is changed by a factor of, say, γ in the mixed run, then the latter is as good as a pure heat bath run whose length is $1/\gamma^2$ times that of the mixed run. This of course assumes that our bins are large enough to be essentially independent. We have performed a variety of checks to convince ourselves that this is the case for the results we present here. For example, for the $\beta = 15$ pure heat bath run we checked that the bins could be made a factor of 10 smaller and still be negligibly correlated. (With a factor of 20 the independence began to break down.) In order to keep our bin sizes sufficiently large so that we could be confident of their mutual independence, the number of bins for each calculation could not be made very large. Hence there will be substantial fluctuations on our error estimates. For this reason the reader should be cautious about drawing conclusions from any one error ratio, and in practice we will average the error comparisons over several quantities.

In Tables XXVII, XXVIII, and XXIX we show the statistical errors for the flux loop and glueball masses at the three different values of β. There are 2 rows of numbers for each mass. The second row contains the actual mass estimates. The first row is the error on the effective mass extracted from the same correlation function but from one time step earlier. This contains an admixture (typically only a few percent) of excited states. (See Sec. III B for a discussion of effective masses.) We display both because the individual error estimates contain quite large fluctuations which appear to be largely independent and so can be averaged to obtain more reliable error ratio estimates. Because we are equally interested in all these physical quantities, it makes sense to construct a global average of these error ratios. We attach to this average an ''error'' obtained by treating the variations of the

individual error ratios around the global average as though they were statistical fluctuations. This is intended to do no more than provide an *indication* of the significance of the value of the average error ratio. The reader can manipulate the numbers in the tables in other ways if he so prefers.

Consider first $\beta = 11.0$ (Table XXVII) and the ratio of errors in the run with over-relaxation to the errors in the pure heat bath run. Taking the ratio of corresponding errors in the two columns we obtain an overall average error ratio of 1.02(6). So in this case there is no improvement in incorporating over-relaxation. At $\beta = 15.0$ (Table XXVIII) we obtain average ratios 1.27(12), 0.96(7), 1.09(9), 1.09(10) for $R_o = 2,5,10,20$, respectively. Again there is no sign of a significant improvement for any over-relaxation mix. The global error ratio average, 1.10(5), confirms this.

We turn now to our calculation at the weakest coupling, $\beta = 21.0$ (Table XXIX). We obtain average ratios of 0.91(8), 0.81(6), 0.88(7), 0.94(7) for $R_o = 3,5,7,10$, respectively. We observe a clear reduction in the errors of the runs with over-relaxation: the global error ratio average is 0.885(33). Although we cannot be certain which mix is best, there is evidence that a ratio of around 5:1 to 7:1 is as good as any at this value of β and that this leads to an error ratio of around 0.84. To this improvement we should add the fact that an over-relaxed sweep, for SU(3) in $D = 2 + 1$, takes about 77% of the time for a heat bath sweep. Thus the gain in using

TABLE XXIX. Errors on SU(3) masses on a 24^3 lattice at $\beta = 21$. R_o is the number of over-relaxed sweeps for every heat bath sweep.

State	$R_o = 0$	$R_o = 3$	$R_o = 5$	$R_o = 7$	$R_o = 10$
Flux loop	0.0053	0.0044	0.0040	0.0038	0.0030
	0.0089	0.0075	0.0070	0.0057	0.0069
0^{++}	0.0085	0.0072	0.0058	0.0056	0.0095
	0.0170	0.0172	0.0138	0.0132	0.0142
0^{--}	0.0123	0.0072	0.0090	0.0150	0.0103
	0.030	0.035	0.035	0.030	0.034
2^{++}	0.0148	0.0106	0.0103	0.0119	0.0120
	0.044	0.029	0.032	0.041	0.045
2^{-+}	0.0094	0.0132	0.0103	0.0102	0.0094
	0.043	0.044	0.026	0.044	0.054

TABLE XXX. Errors on SU(2) masses on a $12^2 24$ lattice at $\beta = 9$. R_o is the number of over-relaxed sweeps for every heat bath sweep.

State	$R_o=0$	$R_o=5$	$R_o=9$	$R_o=49$
Flux loop	0.004	0.003	0.002	0.002
	0.006	0.004	0.003	0.004
0^+	0.007	0.004	0.006	0.007
	0.015	0.014	0.009	0.009
2^+	0.011	0.007	0.010	0.010
	0.019	0.019	0.017	0.021

over-relaxation is about 40% in the update time. Although the gain in the total time will be reduced by the inclusion of measurements (typically tuned to be about half of the total time), there is no doubt that this is a worthwhile gain.

We turn now to the case of SU(2) where our tests are much more limited. The lightest masses here are of the flux loop and of the 0^+ and 2^+ glueballs. We performed comparisons at $\beta=6.0$ and $\beta=9.0$. Using the calculated string tension to set the physical scale, these values of β correspond to $\beta \simeq 2.4$ and 2.55, respectively, in the $D=4$ SU(2) theory. At $\beta=6.0$ we see no sign of any benefit from over-relaxation, albeit in a calculation of limited statistics. Our calculations at $\beta=9.0$ (Table XXX) are with R_o $=0,5,9,49,249,\infty$ and have much better statistics: 25000 sweeps, split into 25 bins, for each value of R_o. The lattice is $12^2 24$ which is of small, but not very small, physical size: there are certainly some finite size effects involving the 2^+. We see from Table XXX that there is a significant benefit to using over-relaxation. We do not show our results for R_o $=249$ and $R_o=\infty$ (all sweeps over-relaxed) which, while amusing for various reasons, are not really relevant to this study. We obtain average error ratios of 0.76(8), 0.71(9), 0.80(11) for $R_o=5,9,49$ respectively. The global error ratio average is 0.76(5). For SU(2) over-relaxation is a simple operation and is much faster than the heat bath; a run with $R_o=5$ or 9 is about twice as fast as a run with only heat bath sweeps. Thus the overall saving is a factor of $2 \times 1/0.76^2 \sim 4$. This is a large reduction. Again, the inclusion of measurements will reduce the gain somewhat.

We turn now to the smeared superplaquettes. The average error ratios, for the runs described above, are summarized in Table XXXI. We note that, not surprisingly, the simple plaquette acquires a larger error if we include over-relaxation. (These global averages mask the fact that for

TABLE XXXI. Ratio of errors with and without over-relaxation, for "plaquettes" at blocking level B_l.

B_l	SU(3),$\beta=21$	SU(3),$\beta=15$	SU(3),$\beta=11$	SU(2),$\beta=9$
1	1.28(15)	1.00(13)	1.29	1.01(14)
2	0.92(5)	0.63(6)	0.88	1.02(5)
3	0.64(5)	0.63(4)	0.81	0.78(3)
4	0.75(4)	0.69(4)	0.79	0.71(6)
5	1.01(10)			

small R_o the error is often reduced, which *is* surprising.) On the other hand we observe that the errors on large superplaquettes are reduced and that, in contrast to what we saw for masses, this effect is present at smaller couplings. This is similar to what has been found in 4 dimensions [29] for large and blocked Wilson loops.

In conclusion, we have seen that for sufficiently small couplings—equivalent to $D=4$ values of $\beta \sim 6.15$ for SU(3) and $\beta \sim 2.55$ for SU(2)—there is a substantial increase in efficiency through mixing heat-bath and over-relaxation sweeps. The CPU saving is about 40% for SU(3) and about 75% for SU(2). The difference is largely due to the fact that SU(2) over-relaxation is a very simple and fast operation. In $D=4$ the operation of calculating "staples" is a little lengthier and so this effect will be somewhat weaker there.

APPENDIX B: TESTING THE EFFICIENCY OF THE OPERATORS

In constructing a "good" basis of operators for our various mass calculations, the use of spatial blocking is crucial. The general motivation is that if one wants a good overlap onto the lightest physical states, then one needs to employ (combinations of) large smooth operators. There are obviously many possible variants on the particular recipe we have used in this paper (which is the one that has been used successfully in earlier $D=3+1$ mass calculations). In the first part of this appendix we will consider some variation in the blocking procedure and we shall see that our choice is indeed an efficient one.

The range of operators we have used has been limited not only in the type of blocking employed but also in the variety of ways we put the blocked loops together to form color singlet operators. In practice we limited ourselves to simple closed loops. However, once we go beyond SU(2) there is a whole new class of operators that we can construct, and which take advantage of the fact that one can tie together N_c indices with a totally anti-symmetric tensor. We refer to this, for obvious reasons, as a baryonic vertex. Such operators have not been used in previous lattice glueball calculations as far as we are aware. Our attention was drawn to them by their possible role in splitting the $C=\pm$ sectors, as pointed out in [11]. For this reason we have carried out a small calculation to check whether they encode some interesting new information. This is described in the second part of this appendix.

1. Variations on the blocking procedure

In our construction of "blocked" link matrices the most obvious parameter is the weighting of the direct path as compared to the staple-like paths. The choice we made was to take an equal weighting for all the paths. So, for say the x-direction, we would take $xx+yxxy^\dagger+y^\dagger xxy$ using the notation in Sec. III B 1. In this section we shall perform some calculations using a variable weighting γ_d. That is to say, we use a blocking

$$\bar{U}_x^B = \gamma_d U_x U_x + U_y U_x U_x U_y^\dagger + U_y^\dagger U_x U_x U_y \qquad \text{(B1)}$$

where we have suppressed some obvious arguments etc. The blocked link, U_x^B, is then obtained by projecting $\bar{U}_x^B$ back into the group. We then see which value of γ_d is most efficient in the sense of producing the best operators.

Before doing so we briefly comment on the projection back into the group and the resulting gauge transformation properties of the U^B. We begin by noting that if we perform a local gauge transformation on the fields, then $\bar{U}^B \to g_n \bar{U}^B g_{n'}^\dagger$, where g_n is the gauge transformation at site n and the paths making up $\bar{U}^B$ start at the site n and end at the site n'. If the group is SU(2), we obtain U^B by dividing $\bar{U}^B$ by $\det\{\bar{U}^B\}$. Since the matrices g are unitary, we have $\det g_n = 1$ and so $\det\{\bar{U}^B\}$ is gauge invariant. Thus, in the case of SU(2), U^B has the gauge transformation properties of a product of links from n to n' and we can form color singlet operators out of closed loops in the usual way. For SU(N_c) $\neq 2$) the situation is different: $\bar{U}^B$ is not proportional to an SU(N_c) matrix, and if we want U^B to be in the group, we need to define it some other way. The method we use is to define U^B as equal to the value of the SU(N_c) matrix U that maximizes $\text{Tr}\{\bar{U}^B U^\dagger\}$. It is easy to see that for SU(2) this reduces to the method we use there. It is also trivial to see (using the cyclic property of the trace) that if $\bar{U}^B \to g_n \bar{U}^B g_{n'}^\dagger$, then, just as in SU(2), $U^B \to g_n U^B g_{n'}^\dagger$, and we can form color singlet closed loops in the usual way. However, in practice we maximize the trace by a simple iterative procedure which we stop before complete convergence in order to save computer time. This procedure requires, as its starting point, some first guess, U_s, for the blocked matrix. In practice we construct U_s from $\bar{U}^B$ in such a way that it does not transform as $U_s \to g_n U_s g_{n'}^\dagger$ under a gauge transformation g. This means that when we stop the algorithm prior to complete convergence, the resulting U^B only transforms approximately as $U^B \to g_n U^B g_{n'}^\dagger$. In principle this does not matter; averaging over all field configurations in the Monte Carlo calculation will lead to a cancellation of the non-gauge invariant pieces in the correlation functions. However, again in practice, this means we generate extra noise and this will increase our statistical errors—something to be avoided if possible.

We see from the discussion in the previous paragraph that there is more to ''blocking'' than choosing a sum of paths and a relative weighting. One can ask if projecting back to the group produces better operators than not doing so (and perhaps using some other form of normalization). Studies in $D=3+1$ of several alternative strategies in SU(2) [30] and SU(3) [32] suggested that this was more or less so. Some tests then showed that approximating the maximization of the trace by one or two iterations did not significantly worsen the operators or increase the errors. However, there has been no demonstration that this continues to be the case as we increase the size of the group or that all this continues to hold in $D=2+1$. These are studies that still need to be carried out.

We return now to our study of how the operators vary with the choice of γ_d in Eq. (B1). Our calculations are in

TABLE XXXII. Effective masses at $t=a$ from the ''best'' operators in different blocking schemes, as described in Appendix B.

| State | $\min_\phi \{am_{\text{eff}}(t=a)\}$ | | | | |
	$\gamma_d=0.25$	$\gamma_d=0.50$	$\gamma_d=1.0$	$\gamma_d=2.0$	$\gamma_d=4.0$
Flux loop	0.622(11)	0.612(10)	0.603(10)	0.601(9)	0.630(8)
0^{++}	0.979(15)	0.967(13)	0.963(12)	0.969(11)	1.008(11)
2^{++}	1.53(4)	1.55(4)	1.56(3)	1.56(5)	1.63(3)
2^{-+}	1.71(4)	1.61(3)	1.58(3)	1.58(3)	1.63(3)
0^{-+}	2.51(6)	2.13(4)	1.99(3)	2.01(4)	2.12(5)
1^{++}	2.80(6)	2.32(7)	2.19(5)	2.20(4)	2.34(4)
1^{-+}	3.01(19)	2.43(8)	2.27(8)	2.30(6)	2.48(6)

SU(2) and are performed on a 16^3 lattice at $\beta=7.5$ in a run consisting of 10000 sweeps. On these configurations we performed separate mass calculations, using our usual basis of operators, for the 5 different blocking schemes that used $\gamma_d = 0.25$, 0.50, 1.0, 2.0, and 4.0.

What we want to know is how efficient are the different schemes, and in particular how efficient is our usual choice, $\gamma_d = 1$. We shall confine ourselves to the lightest states in each J^{PC} channel. In that case our usual variational criterion, as discussed in Sec. III B 3, provides us with a simple criterion for comparing operators of the same quantum numbers: one calculates the effective mass at $t=a$ and the ''best'' operator is the one that gives the smallest value of this effective mass. So what we have done here is to find the best operator in our basis for each type of blocking. The best form of blocking will then be the one that produces the minimal value of the effective mass.

In Table XXXII we present the value of $am_{eff}(t=a)$ for the best operator for each of the 5 kinds of blocking we consider and for the various J^{PC} quantum numbers. We observe that $\gamma_d \in [1,2]$ seems to work best overall, although $\gamma_d = 0.5$ is virtually just as good if we ignore the $1^\pm$ states. Note that since the different calculations are performed on exactly the same sequence of field configurations, the errors will be highly correlated.

We have therefore seen that with respect to variations in this particular parameter, our choice of $\gamma_d = 1$ is about as good as any. Of course one can vary the algorithm in many other ways, for example by including other paths than just the direct path and the ''staples.'' A systematic study would be useful.

2. Operators with ''baryonic'' vertices

We will consider the specific case of SU(3). Suppose we have three curves C_1, C_2, C_3 each of which starts at some point n and finish at some point n'. Let us denote by U^1, U^2, U^3 the corresponding path ordered products of (blocked) link matrices along these three curves, running from n to n'. We can form singlet operators out of pairs of these in the usual way, e.g.

$$\phi = \text{Tr} U^1 U^{2\dagger}. \tag{B2}$$

But in the case of SU(3) we also can form a color singlet out of all three of them:

TABLE XXXIII. Effective masses at $t=a$ obtained from bases with and without the operator, ϕ_Y, which contains two ''baryonic'' vertices. From a 16^3 lattice at $\beta=15$ in SU(3).

State	$am_{\mathrm{eff}}(t=a)$ With ϕ_Y	Without ϕ_Y
0^{++}	1.08(2)	1.08(2)
$0^{++}{*}$	1.67(5)	1.67(5)
$0^{++}{**}$	2.03(4)	2.05(3)
$0^{++}{***}$	2.26(6)	2.26(5)
2^{++}	1.78(2)	1.78(2)
$2^{++}{*}$	2.15(6)	2.15(6)
$2^{++}{**}$	2.33(7)	2.34(7)
$2^{++}{***}$	2.56(7)	2.61(7)
1^{--}	2.60(6)	2.60(6)
$1^{--}{*}$	2.62(5)	2.63(5)
$1^{--}{**}$	2.74(8)	2.78(9)
$1^{--}{***}$	2.92(10)	3.02(7)

$$\phi_Y = \epsilon_{ijk} U^1_{ii'} U^2_{jj'} U^3_{kk'} \epsilon_{i'j'k'} \tag{B3}$$

where we have exposed the matrix indices and ϵ_{ijk} is the usual totally anti-symmetric tensor. This extends to $N_c > 3$ in the obvious way; we have $U^1, \ldots, U^{N_c}$ paths joined by the appropriate N_c-component ϵ tensor.

Since the operators in Eq. (B2) and Eq. (B3) have the same quantum numbers, they will have non-zero overlaps and there is no *a priori* reason to think that we have lost anything by excluding the latter. However, it might be that they constitute more efficient operators for some states, and if that is the case for one of the heavier states, where in practice we cannot calculate correlators beyond small t, it might be that, in using them, we will expose a state that we have not been able to see with operators of the type in Eq. (B2).

In this appendix we will describe a small exploratory calculation designed to see if including such operators might make a serious difference to our calculations. We shall consider an operator, ϕ_Y, of the form in Eq. (B3) with

$$U^1 = U_x U_y U_x^\dagger$$

$$U^2 = U_y$$

$$U^3 = U_x^\dagger U_y U_x, \tag{B4}$$

suppressing obvious arguments and indices. This is a rectangle with a central link crossing the rectangle. The path ordering is out from the same vertex for all three curves. Under C such an operator reverses all three arrows on the curves, which for this particular operator is equivalent to a rotation of π. So one can easily see that from this operator (and the one we obtain by $x \leftrightarrow y$) we can obtain 0^{++}, 2^{++}, and 1^{--} quantum numbers.

We have performed a calculation on a 16^3 lattice at $\beta=15$ with this operator. In Table XXXIII we list the effective 0^{++}, 2^{++} and 1^{--} masses obtained at $t=a$ using a basis that includes the best two blocking levels of this operator. We compare it with what we obtain (on the same set of field configurations) if we do not include ϕ_Y. We observe that there seems to be nothing new in these channels when we include ϕ_Y, at least not as far as the ground state and the first few excitations are concerned. There is a slight improvement in some of the overlaps, as indicated by a decrease in $m_{eff}(t=a)$, but one would expect that just from an increase in the size of the basis.

This, albeit minimal, study leads us to believe that the inclusion of operators incorporating baryonic vertices will not alter our conclusions in any significant way. However, such operators can be convenient in providing a simple means for constructing $J=1$ operators, and they may well be important in investigating some physics, e.g. the $C = \pm$ splittings, lower order in $1/N_c$ corrections, etc., so a more detailed investigation would be useful.

APPENDIX C: TESTING THE BENEFITS OF MEAN-FIELD IMPROVEMENT

In this appendix we shall show that the mean-field–tadpole improved inverse coupling [40]

$$\beta_I = \beta \times \left\langle \frac{1}{N_c} \mathrm{Tr}(U_p) \right\rangle \tag{C1}$$

provides a much better expansion parameter than β in our $D=2+1$ calculations. This both complements the available $D=3+1$ evidence [40] and provides us with a more accurate way to determine $\lim_{a \to 0} \sqrt{\sigma}/g^2$.

Our strategy will be to compare directly various extrapolations to $a=0$ using either $1/\beta$ or $1/\beta_I$ as expansion parameters. We shall perform these comparisons using our calculations in the SU(2) and SU(3) theories, since these cover large ranges in β. Having found which extrapolation works best, we shall take that information over to the SU(4) and SU(5) theories where the range of our calculations is much more limited and where the use of a good expansion parameter pays significant dividends.

We have focussed upon the string tension because in practice this is the quantity that we calculate most accurately on the lattice. Since $\lim_{a \to 0} \beta = 2N_c/ag^2$, we know that

$$\lim_{\beta \to \infty} \beta a \sqrt{\sigma} = \lim_{a \to 0} 2N_c \sqrt{\sigma}/g^2. \tag{C2}$$

The approach to the continuum limit will involve higher order corrections that are inverse powers of β and hence vanish as powers of a. We thus expect that the approach to the continuum limit will be under much better control than in 4 dimensions, where the analogous quantity that one would be calculating is $\lim_{a \to 0} \sqrt{\sigma}/\Lambda_{mom}$ and where the corrections would be inverse powers of $\log a$. This will allow us to make a much more explicit and direct comparison than is possible in $D=3+1$.
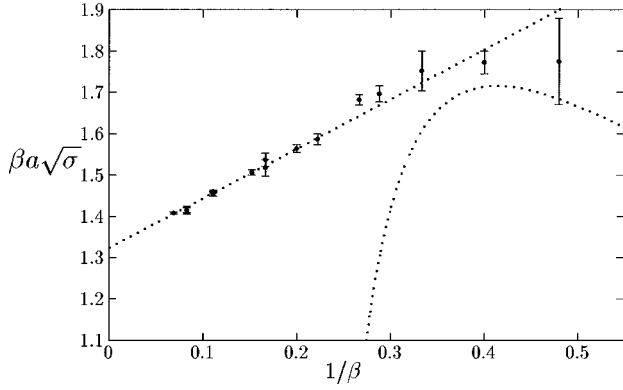
Since we expect

FIG. 9. The values of $\beta a \sqrt{\sigma}$ plotted against $1/\beta$ for SU(2). Also shown is the leading-order strong coupling prediction at low β and a leading-order continuum extrapolation at high β.

$$\beta a \sqrt{\sigma} = c_0 + \frac{c_1}{\beta} + \frac{c_2}{\beta^2} + \cdots \qquad \text{(C3)}$$

for large β, it is useful to plot the values of $\beta a \sqrt{\sigma}$ against $1/\beta$; we do this in Fig. 9 for SU(2) and in Fig. 10 for SU(3). For large enough β the first two terms in Eq. (C3) will dominate and so the values should fall on a straight line as we approach the continuum limit. This we observe to be the case. For orientation we also show in Fig. 9 and Fig. 10 the strong coupling predictions for the string tension up to $O(\beta)$:

$$a^2\sigma = -\log\left(\frac{\beta}{4}\right) + O(\beta^2) \qquad \text{(C4)}$$

for SU(2) and

$$a^2\sigma = -\log\left(\frac{\beta}{18}\right) - \frac{\beta}{12} + O(\beta^2) \qquad \text{(C5)}$$

in the case of SU(3). [The extra $O(\beta)$ term in the case of SU(3) arises because in that case a product of two plaquettes can be used just as well as a single plaquette in tiling the minimal surface spanning the Wilson loop.] We see that our calculated values of the string tension extend well into the
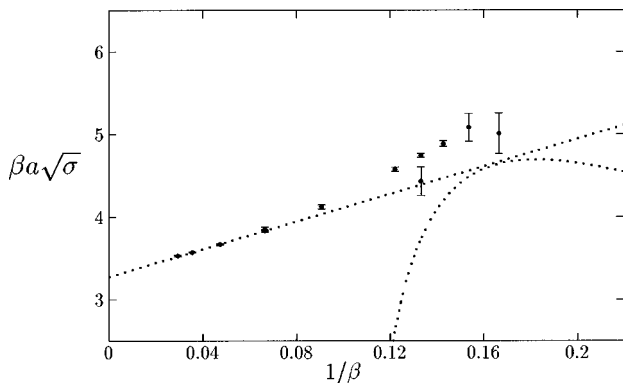

FIG. 10. The values of $\beta a \sqrt{\sigma}$ plotted against $1/\beta$ for SU(3). Also shown is the strong coupling prediction to $O(\beta)$ at low β and a leading-order continuum extrapolation at high β.

strong-coupling regime. In this region an expansion in $1/\beta$, such as in Eq. (C3), should no longer be valid.

The maximum range, more or less, over which we can perform linear fits with acceptable χ^2, turns out to be $\beta \geqslant 4.5$ in the case of SU(2) and $\beta \geqslant 15.0$ for the case of SU(3). These fits are given by

$$\beta a \sqrt{\sigma} = 1.324(12) + \frac{1.20(11)}{\beta}, \quad \text{SU(2)}, \qquad \text{(C6)}$$

and

$$\beta a \sqrt{\sigma} = 3.275(24) + \frac{8.35(61)}{\beta}, \quad \text{SU(3)}. \qquad \text{(C7)}$$

(Note that the errors on the intercept and slope are anti-correlated.)

While such a linear extrapolation is a perfectly acceptable procedure for extracting the continuum value of the string tension, it must suffer from some systematic bias due to the neglect of higher order terms. These, it is clear from the figures, are certainly not negligible at intermediate values of β. If we include $O(1/\beta^2)$ terms in our fits, we naturally find larger acceptable ranges for the fits: $\beta \geqslant 3.0$ for SU(2) and $\beta \geqslant 6.5$ for SU(3). The fits are

$$\beta a \sqrt{\sigma} = 1.337(23) + \frac{0.95(38)}{\beta} + \frac{1.1(1.3)}{\beta^2}, \quad \text{SU(2)},$$
$$\text{(C8)}$$

and

$$\beta a \sqrt{\sigma} = 3.367(50) + \frac{4.1(1.7)}{\beta} + \frac{46.5(11.0)}{\beta^2}, \quad \text{SU(3)}.$$
$$\text{(C9)}$$

We observe that in both cases the inclusion of the extra $O(1/\beta^2)$ term has increased the value of the continuum limit by an amount that, while small in absolute units, is uncomfortably large when compared to the claimed errors, especially so in the case of SU(3). Moreover, in the case of SU(3) the coefficient of the $1/\beta^2$ correction is so large that the value of this correction is comparable to that of the $1/\beta$ correction over much of our range. Under such circumstances one cannot motivate the neglect of the next, $O(1/\beta^3)$, correction. However, it is clear, from the large errors in Eq. (C9), that our SU(3) data will not be able to resolve these higher order terms with any useful accuracy. Moreover, there is also the danger that the $O(1/\beta^2)$ correction is being overly biased by the values of $a\sqrt{\sigma}$ in the transition region between weak and strong coupling, where the very validity of an expansion in $1/\beta$ is breaking down. This leaves us with an intrinsic systematic error on the SU(3) continuum limit that may well be larger than the quoted statistical error.

The lattice corrections in Eq. (C3) are precisely what the use of a better coupling should improve—by reducing their coefficients. How well does that work here? If we use Eq. (C2) to define β_I, we can plot $\beta_I a \sqrt{\sigma}$ against $1/\beta_I$ as in Fig. 11 and Fig. 12. It is immediately apparent from a comparison
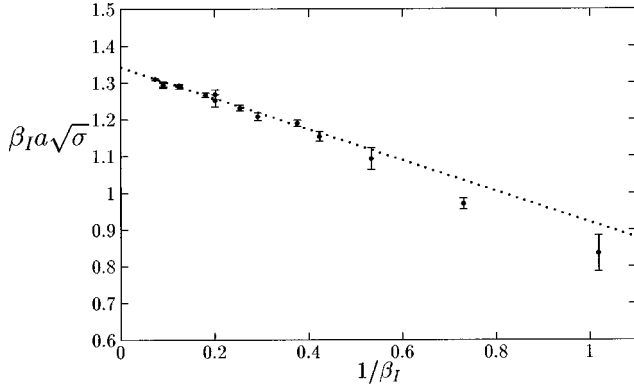
FIG. 11. As in Fig. 9 but using the mean-field improved coupling, β_I, in place of β.

with Fig. 9 and Fig. 10. that in terms of the "improved" coupling the higher order lattice corrections are dramatically reduced. More quantitatively, if we perform fits as before but with β_I replacing β, we obtain the following results. In the case of SU(2) we obtain good fits with just the leading $O(1/\beta_I)$ correction for the much larger range $\beta \geqslant 3.0$ while for SU(3) excellent fits are possible for $\beta \geqslant 8.175$ (and reasonable ones all the way down to $\beta = 6.0$). Moreover, these fits

$$\beta_I a \sqrt{\sigma} = 1.341(7) - \frac{0.421(50)}{\beta_I}, \quad \text{SU}(2), \quad \text{(C10)}$$

$$\beta_I a \sqrt{\sigma} = 3.318(12) - \frac{2.43(22)}{\beta_I}, \quad \text{SU}(3),$$

$$\text{(C11)}$$

display much smaller corrections to the leading asymptotic terms than was the case in Eqs. (C6) and (C7). Since these fits are so good, there is no real reason to include higher order corrections. However, if we do so, then we obtain

$$\beta_I a \sqrt{\sigma} = 1.336(9) - \frac{0.35(9)}{\beta_I} - \frac{0.18(15)}{\beta_I^2}, \quad \text{SU}(2),$$
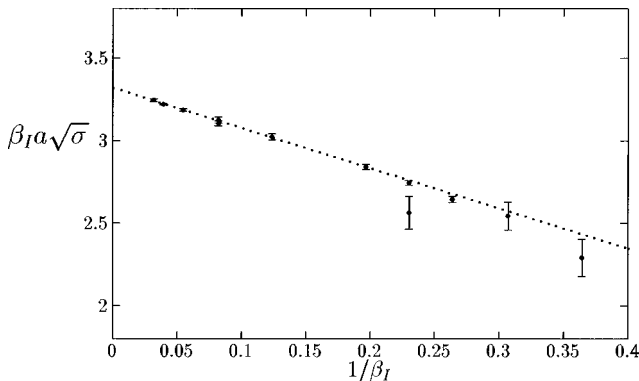
$$\text{(C12)}$$

FIG. 12. As in Fig. 10 but using the mean-field improved coupling, β_I, in place of β.

$$\beta_I a \sqrt{\sigma} = 3.323(28) - \frac{2.57(80)}{\beta_I} + \frac{0.7(3.7)}{\beta_I^2}, \quad \text{SU}(3).$$

$$\text{(C13)}$$

We observe that the coefficients of the higher order terms are small: so there is no reason to worry about the next correction. A second and related observation is that the asymptotic values are little changed with the inclusion of the $O(1/\beta_I^2)$ correction—in contrast to what happened when we used β as our expansion parameter. Indeed even the coefficients of the $1/\beta_I$ terms are insensitive to the inclusion of a higher order term. All this represents a substantial improvement in the perturbative control of the continuum limit.

The fact that we can extrapolate $\beta_I a \sqrt{\sigma}$ with fits involving just two parameters means that we do not need to perform calculations at more than four values of β in the case of SU(4) and SU(5). This represents a substantial saving in computational effort.

From fits such as the above we can extract the continuum mass ratios shown in Eq. (38). We remark that it is both because we are in 3 dimensions, where the bare coupling decreases linearly with the scale a rather than just logarithmically, and because of the extent and accuracy of our lattice calculations, that it is possible to perform reasonably accurate extrapolations to the continuum limit even with the "bad" lattice bare coupling. This has enabled us to quantify, in a way that is not yet possible in 4 dimensions, how much the mean-field improved coupling actually improves the approach to the continuum limit of the lattice spacing, a.

APPENDIX D: CALCULATIONS WITH AN ASYMMETRIC LATTICE ACTION

In this appendix we present an SU(2) calculation of the mass spectrum on lattices with timelike and spacelike lattice spacings related by $a_t \simeq a_s/4$. As discussed in Sec. V A the primary purpose of this study is to check explicitly that our criteria for which effective masses adequately reflect the actual masses are in fact accurate. A second reason is that this, being a calculation with a different action to the one we have used so far, will provide us with some test of universality. We shall first discuss some of the features that are peculiar to such calculations. We then present our results.

1. Preliminaries

To allow different spatial and temporal lattice spacings we use the action in Eq. (8). What is the relation between our choice of β_s, β_t and the lattice asymmetry? Suppose we are aiming for a particular ratio

$$r = \frac{a_t}{a_s}. \quad \text{(D1)}$$

In the limit $a_s, a_t \to 0$ we have

$$\left\{ 1 - \frac{1}{N_c} \mathrm{ReTr}\, U_{p_s} \right\} \to a_s^4 \frac{1}{2N_c} \mathrm{Tr} F^2$$

$$\left\{ 1 - \frac{1}{N_c} \mathrm{ReTr}\, U_{p_t} \right\} \to a_s^2 a_t^2 \frac{1}{2N_c} \mathrm{Tr} F^2$$

$$\beta S \to \frac{1}{g^2} \int d^2 x dt \frac{1}{2} \mathrm{Tr} F^2 \tag{D2}$$

where F^2 is the continuum field strength squared. Since the integration measure gives a factor $a_s^2 a_t$ when discretized, we see that the choice

$$\beta_s = r\beta, \quad \beta_t = \frac{1}{r}\beta, \quad \beta = \frac{2N_c}{a_s g^2} \tag{D3}$$

is what is needed, at least at the *classical* level, to achieve the asymmetry, r, defined in Eq. (D1).

In practice there will be quantum corrections to these classical relations. Three related questions immediately arise. (a) What do we need to know about a_s and a_t? (b) In a given simulation, how can we calculate a_s and a_t directly? (c) Can we easily ''improve'' upon the relations in Eq. (D3)?

Before considering each of these questions in turn, we need to remark that the classical relations in Eq. (D3) should remain a roughly reliable guide in the full theory. This is because our theory is super-renormalizable and this is in contrast to the situation in 4 dimensions. Nonetheless, we do expect significant corrections, as we saw when considering the β dependence of $\beta a\sqrt{\sigma}$. We saw there (see Appendix C) that the corrections to the classical relation $\beta = 2N_c/ag^2$ are quite large and can be drastically decreased by the use of a mean-field improved coupling.

In the rest of this Appendix we shall assume that the asymmetric lattice has been chosen so that $a_t \ll a_s$. This means that we shall systematically ignore any $O(a_t^2)$ corrections as compared to ones that are $O(a_s^2)$.

a. How well do we need to know a_s and a_t?

The first thing we need to establish is whether we actually need to know a_s and a_t any more accurately than we already know them through using Eq. (D3).

If we just wanted to calculate some lattice mass ratios, m_i/m_0, then these could be obtained without knowing the lattice spacing at all: our usual procedure would give us estimates of $a_t m_i$ and the lattice spacing then cancels in the ratio. However, if we want to extrapolate to the continuum limit, then the leading correction will be $O(a_s^2)$, assuming $a_t \ll a_s$ as will be the case here, and so we need to know $a_s m$ for some mass m in order to provide the correction term in the analogue of Eq. (49). This can, however, be finessed by using Eq. (50) instead; although $1/\beta^2 \simeq a^2 g^4/4N_c^2 + O(a^3)$, the correction has a small enough coefficient that it should not significantly degrade the accuracy of our extrapolations.

Of course, we also need to control finite volume effects in an efficient way—that is to say, more efficient than doing a detailed finite volume study at each coupling. So we need to

be able to compare the lattice size, $L \equiv a_s L_s$, at different couplings. For this we need to know a_s to a reasonable approximation; great accuracy is not needed because we usually include a margin of safety in our choice of the volume.

There is however at least one place where we do need accurate values for the lattice spacings. This is in our calculation of the string tension. Our usual procedure is to calculate the mass, $a_t m_P(L)$, of a flux loop of length $L = a_s L_s$ that winds around the spatial torus. This mass, $a_t m_P(L)$, can be written, using Eq. (32), as

$$a_t m_P(L) = a_t \times L\sigma(L)$$

$$= a_t L\left(\sigma(\infty) - \frac{\pi}{6L^2} \right) = a_t a_s L_s \sigma - \frac{\pi}{6L_s} \frac{a_t}{a_s}. \tag{D4}$$

Clearly we need to know $r = a_t/a_s$ very accurately if we are to be able to calculate $a_t\sqrt{\sigma}$ with the accuracy we are used to. A similar situation arises if we calculate potentials using Wilson loops.

b. How do we calculate a_t/a_s directly?

There are two obvious methods that we can use to calculate $r = a_t/a_s$. The first involves calculating the energies of states with non-zero momenta. Suppose we have a particle of mass m. The allowed momenta are $a_s \vec{p} = (2\pi n_x/L_s, 2\pi n_y/L_s)$ and the corresponding energies that we obtain from our correlators may be written as $a_t E(p)$. For small momenta we expect the continuum dispersion relation, $E^2 = p^2 + m^2$, to be accurately satisfied. (We have explicitly seen that this is so on the symmetric lattices that we have used in our main calculations in this paper.) So we expect to have

$$a_t^2 E^2(p) = a_t^2(p^2 + m^2) = \left(\frac{a_t}{a_s}\right)^2 \left(\frac{2\pi}{L_s}\right)^2 (n_x^2 + n_y^2) + (a_t m)^2. \tag{D5}$$

Therefore, from our calculated values of $a_t E(p)$ and $a_t m$ we can obtain, using Eq. (D5), a value for a_t/a_s.

Our second method is even more direct. Normally we calculate correlators in the t-direction. We could instead calculate our correlators in, say, the x-direction. In that case our space would be (y,t) in place of (x,y). As long as $a_t L_t$ is large, as it will always be, this new spatial volume will also be large and we can assume there are no finite volume effects. Thus we obtain the same mass in both calculations, up to lattice spacing corrections. That is to say, we obtain $a_t m$ from our t-correlators and $a_s m$ from our x-correlators. Equating the two we obtain a_t/a_s.

We can combine the above two methods by calculating glueball correlation functions in the x-direction with non-zero momenta in either the y or t directions. Comparing the energies of such states gives us another direct estimate of a_t/a_s. If we include a range of momenta one can attempt to tune this ratio so that the dispersion relations in p_t and p_y coincide. This allows us to fix the asymmetry without assuming the continuum dispersion relation.

In practice, we shall not use this last method, and we shall only consider the lowest two momenta in applying our first method. While this reduces the precision with which we can estimate the ratio a_t/a_s, it suffices for our purposes.

Both of the above methods will suffer from lattice spacing corrections. The continuum dispersion relation will only be valid up to corrections of order $(a_s p)^2$ and the eigenstates of the transfer matrices defined on the x,y and y,t spatial tori will differ by order a_s^2 corrections because the latter torus has a lattice spacing a_t rather than a_s in one of the two directions. However, as long as we are consistent in the method used to estimate a_t/a_s we can absorb this correction into the correction term used in taking the continuum limit.

Before turning to some explicit calculations of the above kind it is worth pointing out that although the second method described above seems more direct, it is in practice more awkward to implement. The reason is that we need to produce blocked link matrices in order to have useful operators, and this has to be carefully tailored in the case where one spatial lattice spacing is very different from the other. And this is in addition to the fact that using two different spatial planes means producing two sets of blocked links. For these reasons our calculations using the second method will be on only a subset of our lattices.

c. Can we ''improve'' upon the estimate of r?

We have seen in our previous calculations that we get much smaller corrections to the limit $\beta a \sqrt{\sigma} \rightarrow 2 N_c \sqrt{\sigma}/g^2$ as $a \rightarrow 0$, if we use a mean-field improved inverse coupling, β_I, in place of β. One might hope that a similar approach with an asymmetric lattice action would improve our control over the value of r. The straightforward implementation of this idea in the context of the action in Eq. (8) would be to define ''improved'' values of r and β by

$$r_I \beta_I = r \beta \left\langle \frac{1}{N_c} \mathrm{Tr} U_{p_s} \right\rangle$$

$$\frac{1}{r_I} \beta_I = \frac{1}{r} \beta \left\langle \frac{1}{N_c} \mathrm{Tr} U_{p_t} \right\rangle. \tag{D6}$$

This is in the spirit of the approach suggested in [42] although there one effectively replaces $(1/N_c)\langle \mathrm{Tr} U_{p_t} \rangle$ by unity. We shall calculate r_I below and explicitly check how much of an improvement one really obtains.

2. Calculation

We perform calculations at $\beta = 4.0$, 5.3, and 8.0. In all three cases we choose $r = 0.25$ in the action, as given in Eq. (8). The lattice sizes are $12^2 60$, $16^2 64$ and $24^2 96$. If the classical relations in Eq. (D3) were valid, then the value of a_s would be exactly what we obtained at the corresponding values of β on symmetric lattices. The reader will note that our lattice sizes are somewhat larger than would be necessary if this were the case; this is to give us some margin in case the quantum corrections to these relations are significant.
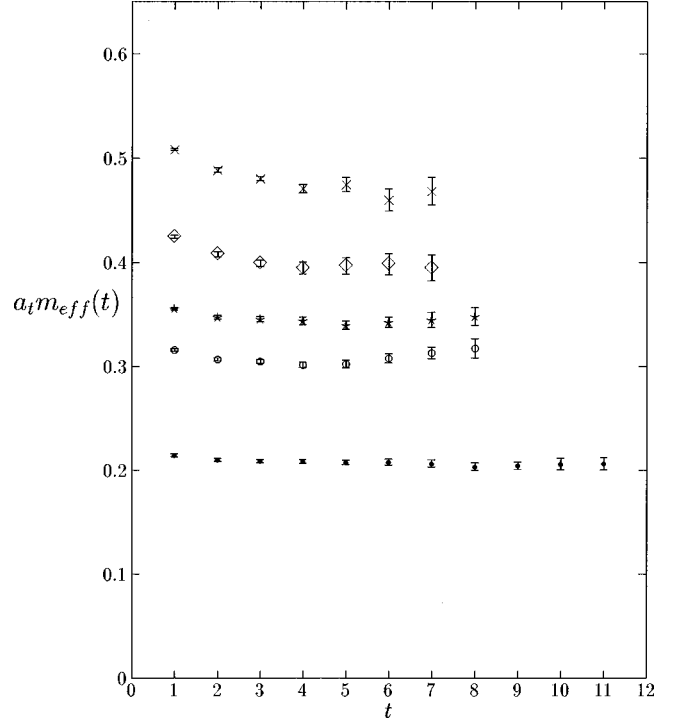

FIG. 13. The effective masses obtained on a $24^2 96$ lattice at $\beta = 8$ in SU(2), with a very small temporal lattice spacing: $a_t \sim 0.25 a_s$. States are the $0^{++}(\bullet)$, the $0^{++*}(\bigcirc)$, the $2^{++}(\star)$, the $2^{++*}(\Diamond)$ and the $1^{++}(\times)$.

In addition to these calculations we also perform calculations on somewhat smaller lattices, $8^2 60$, $12^2 64$, and $16^2 96$, respectively. It is on these lattices that we calculate correlators in both t and x directions. We shall only calculate the mass of the periodic flux loop, $m_P(L)$, on these lattices. Smaller lattices are preferable for this purpose because $m_P(L)$ will be smaller and so we will have more accurate values. (Obviously this is only important for the correlators in the x-direction where $a_s m_P$ will not be small.)

Our original motivation for performing such calculations was to have a finer resolution on the effective mass plot, so as to see whether the typical heavier mass could really be extracted from its effective masses between $t=a$ to $t=2a$. Since we have $a_t \sim a_s/4$, this question becomes, have the effective masses in the region $4a_t \leq t \leq 8a_t$ already reached their asymptotic plateau? So without further ado we plot the effective masses from the $24^2 96$ lattice in Fig. 13. Note that if we wished to obtain such a small lattice spacing in our usual symmetric lattice calculation, we would have had to do it on a 96^3 lattice at $\beta \sim 30$: a daunting prospect. We see from Fig. 13 that there is reasonably good evidence in all cases that an effective mass extracted over the interval $4a_t \leq t \leq 8a_t$ provides an unbiased estimate of the asymptotic mass. We infer from this that extracting masses from the range $t=a$ to $t=2a$ on symmetric lattices in the neighborhood of $\beta=8$, where the heavier states are in the noise for $t>2a$, is in fact justified. Our $\beta=5.3$ calculations also support this way of calculating masses (although with less precision), thus reassuring us that the estimates we have used in

TABLE XXXIV. Masses with asymmetric SU(2) action; r = 0.25 in Eq. (8). Also shown are the average timelike and spacelike plaquettes.

State	$a_t m$ with $a_t \approx 0.25 a_s$		
	$\beta = 4.0$ $12^2 60$	$\beta = 5.3$ $16^2 64$	$\beta = 8.0$ $24^2 96$
Flux loop	0.431(7)	0.305(5)	0.185(2)
0^{++}	0.443(5)	0.321(4)	0.207(2)
$0^{++}*$	0.63(1)	0.448(12)	0.302(3)
$0^{++}**$	0.77(2)	0.582(7)	0.368(7)
0^{-+}	1.01(3)	0.68(3)	0.427(9)
$0^{-+}*$	1.14(3)	0.73(3)	0.527(5)
2^{++}	0.717(10)	0.532(8)	0.344(4)
$2^{++}*$	0.86(2)	0.636(9)	0.395(6)
2^{-+}	0.750(13)	0.538(5)	0.339(4)
$2^{-+}*$	0.93(3)	0.647(8)	0.407(5)
1^{++}	1.03(3)	0.75(5)	0.471(4)
$1^{++}*$	1.3(1)	0.76(6)	0.551(7)
1^{-+}	1.12(4)	0.80(6)	0.499(6)
$1^{-+}*$	1.22(5)	0.80(5)	0.477(12)
$\langle \text{Tr} U_{p_s}/N_c \rangle$	0.64060(7)	0.73195(3)	0.82418(1)
$\langle \text{Tr} U_{p_t}/N_c \rangle$	0.91436(2)	0.93597(1)	0.95795(1)

TABLE XXXV. Various estimates of a_t/a_s as described in Appendix D. Also shown is r_I, the mean-field improved value of r.

β	L_s	r	r_I	$p=0,1$	$p=0,2$	$a_t m_l/a_s m_l$
8.0	24	0.25	0.232	0.249(11)	0.252(5)	
	16	0.25	0.232	0.244(9)	0.241(4)	0.235(8)
5.3	16	0.25	0.221	0.239(25)	0.235(7)	
	12	0.25	0.221	0.235(10)	0.238(4)	0.241(6)
4.0	12	0.25	0.209	0.236(28)	0.241(8)	
	8	0.25	0.209	0.223(7)	0.219(5)	0.241(12)

tematic errors although larger statistical errors. The values thus obtained are listed in Table XXXV. We also show there the values we get for $a_t m_P/a_s m_P$; these have only been calculated for the smaller lattices. From these results we infer the following values of the asymmetry:

$$\frac{a_t}{a_s} = \begin{cases} 0.245(5), & \beta = 8.0, \\ 0.237(6), & \beta = 5.3, \\ 0.230(10), & \beta = 4.0. \end{cases} \quad (D7)$$

The deviation from the classical value, $a_t/a_s = r = 0.25$, is not large. We also note that although the ''improved'' value, r_I, is shifted in the right direction, it overshoots so that it is no closer to the ''true'' value than is r. This is even more so if one replaces the time-like plaquettes by unity in Eq. (D6). Thus it seems that the most naive mean-field ''improvement'' is not an improvement here.

Using in Eq. (D4) the values of a_t/a_s in Eq. (D7) and the values of $a_t m_P$ in Table XXXIV, we obtain

$$a_t \sqrt{\sigma} = \begin{cases} 0.04408(56), & \beta = 8.0, \\ 0.06806(102), & \beta = 5.3, \\ 0.0919(21), & \beta = 4.0. \end{cases} \quad (D8)$$

The uncertainty in a_t/a_s has roughly doubled the error on $a_t \sqrt{\sigma}$; thus it is no longer the most accurately calculated quantity (as it was in case of the symmetric action), and if we were to calculate mass ratios from scratch, we might prefer to use the scalar glueball mass as our basic scale. We now extrapolate these values (multiplied by β) to the continuum limit, using a $1/\beta$ correction just as in Eq. (35). The fit has a very good confidence level and gives us the continuum value of $4 a_t \sqrt{\sigma}/a_s g^2$. In the continuum limit $a_t/a_s = r = 0.25$ and so we finally obtain

$$\frac{\sqrt{\sigma}}{g^2} = 0.3375(130). \quad (D9)$$

this paper are indeed unbiased over the whole range of β relevant to our continuum extrapolations.

Since these lattice actions are different from the symmetric ones that we have used in the body of the paper—indeed, as we have already remarked, one may regard them as being close to the Hamiltonian limit—it is interesting to extract a continuum mass spectrum from them, so testing universality, to some extent.

In Table XXXIV we list the masses we have extracted at our three value of β. They are all in units of a_t. In addition to the glueball masses we also list the mass of the flux loop that winds around the spatial torus. As discussed above, we need to know the value of a_t/a_s in order to extract $a_t \sqrt{\sigma}$ (or $a_s \sqrt{\sigma}$). And we need to know $a_t \sqrt{\sigma}$ if we are to calculate $m_G/\sqrt{\sigma}$ for comparison with our previous calculations. We therefore turn to this next.

In order not to confuse different quantities, we shall continue to use r for the parameter in the action, and we shall choose $r = 0.25$ here. Classically, but only classically, we know that $r = a_t/a_s$. The ''true'' value of a_t/a_s is the one that we explicitly calculate using the methods described earlier in this appendix: this we shall either label r_{meas} or simply refer to as a_t/a_s. Finally there is r_I as defined by Eq. (D6).

We calculate a_t/a_s by comparing the flux loop energy as calculated from two momenta, p_1 and p_2, and then using Eq. (D5). We do so using the lowest three momenta which we shall refer to as $p_i = 0,1,2$ for convenience. This we shall do on both our larger and smaller lattices at each value of β. Note that the smaller p, the more reliable will be the continuum energy-momentum dispersion relation. Since the lowest momenta decrease as the lattice size increases, the values obtained on the larger lattices will have smaller sys-

This is certainly consistent with the value of 0.3353(18) in Eq. (38) which was obtained with $r=1$, but the error is much larger. In large part this is just because the present calculation is a much smaller one. But in some part it is due to our uncertainty in the value of a_t/a_s. Without this uncertainty our error in Eq. (D9) would have been smaller by about a factor of 1.5. We have performed other continuum extrapolations as well. If we use the classical value $a_t/a_s=r=0.25$ in our calculations, then we again obtain a good fit, this time with a continuum value of

$$\frac{\sqrt{\sigma}}{g^2} = 0.3288(50). \tag{D10}$$

This is consistent with our previous values, as it should be because the corrections to r can be absorbed into the $1/\beta$ correction. Indeed we find that the coefficient of the $1/\beta$ term is larger in the latter case, $\simeq 0.22(3)$ versus $\simeq 0.12(8)$, when we use the values in Eq. (D7). We have performed other extrapolations as well: the errors vary but the values are consistent with each other. It is worth remarking that the fit leading to Eq. (D9) has a much smaller correction than one finds in the symmetric case when using β; indeed it is about the same size as one obtains using the improved coupling, β_I. This suggests that lattice corrections are smaller on very asymmetric lattices, and perhaps explains why we did not gain anything from using the mean-field recipe.

We can now take the values of $a_t m_G$ in Table XXXIV, the values of $a_t\sqrt{\sigma}$ in Eq. (D8), form ratios, and extrapolate to the continuum limit using Eq. (50). We obtain the continuum mass ratios shown in Table XXIII. We also show there the symmetric lattice values that have been obtained elsewhere in this paper. We observe that they are consistent within errors. We note that if we extrapolate with an $O(a^2\sigma)$ correction as in Eq. (49), we obtain almost identical results. This is also the case if we use string tensions calculated using $a_t/a_s=0.25$, except that the fits tend to be significantly worse—as one would expect if this involved an error that was really $O(1/\beta)$ rather than $O(1/\beta^2)$.

We observe in Table XXIII that the errors on the lighter masses are larger in the asymmetric case. This is no surprise since our symmetric calculations are *very* much larger. What is striking is that for the heaviest masses, such as the $1^{\pm+}$, the asymmetric errors are actually smaller. This displays the power of such calculations for determining the masses of heavier states.

Two final asides on the spectrum. For reasons we do not entirely understand, we seem to have no problem in obtaining a set of excited $2^{\pm+}$ masses that continue well to $a=0$ and, indeed, are consistent with what one finds for higher groups—see Table XXI. This is in contrast to the case of a symmetric lattice action. We also note in Table XXXIV that the mass of the 1^{-+} is larger than that of the 1^{-+*}. Our ordering of the states is determined by the effective mass at $t=a$, which in this case seems to be unreliable. This is undoubtedly related to the peculiarities in the $J=1$ sector that we have previously noted during our symmetric action calculations. Obviously it is hard to argue with using the lower

mass for the ground state 1^{-+}, and if we do so we obtain the value in square brackets in Table XXIII. It is amusing that this value fits better with parity doubling and with the values obtained for the higher groups.

APPENDIX E: THE U(1) MASS SPECTRUM

In this appendix we calculate the mass spectrum in the $D=2+1$ U(1) theory. U(1) is as far as one can get from U(∞); so this should provide us with a useful contrast to the SU(N_c) mass spectra which we have calculated in this paper.

Calculating the U(1) spectrum might seem pointless; the continuum limit should be a theory of free, non-interacting photons. While this would certainly provide a contrast to our SU(N_c) spectra, it would hardly be very illuminating.

Although the continuum limit is indeed trivial, in the sense that there will be no bound state whose mass is finite in units of the mass scale g^2, there is nonetheless interesting dynamics at finite values of the lattice spacing, a. This arises from the presence of magnetic monopoles in the theory. (To be more precise, in $D=3+1$ these would be magnetic monopoles. Here they are pointlike instantons whose fields are identical to the spatial fields of a static Dirac monopole. Hence we shall follow the usual custom and refer to them as magnetic monopoles, even in $D=2+1$.) These monopoles clearly have an action that is $\simeq c_M/ag^2$ where c_M is a constant that depends on the particular lattice action being used. Thus a monopole has a weighting $\sim\exp\{-c_M/ag^2\}$ and hence the average distance between monopoles will be $d_M \sim a\exp\{c_M/3ag^2\}$ (up to weakly varying factors that come from integrating small fluctuations around the monopoles). This provides a scale for the theory that is different from g^2. This scale is interesting because the monopoles change the physics in a qualitative fashion. As is well known [48] they produce a linear confining force between external static charges. One could also expect them to produce a nontrivial mass spectrum. At the very least, there will be a massive "photon." Of course, in the continuum limit $d_M\rightarrow\infty$ in units of $1/g^2$ and so on the latter scale the monopoles disappear to $r=\infty$ as we approach the continuum limit.

Actually, the above description represents an over-simplification. There is not just one new scale introduced by the monopoles. There is also a scale associated with the string tension, $l_\sigma\equiv 1/\sqrt{\sigma}$, and a scale associated with the screening mass, $l_s\equiv 1/m_s$. These scales mutually diverge in the continuum limit: $l_s\sim l_\sigma^2\sim d_M^{4/3}$ up to constants and powers of β. The origins of this peculiar situation lie in the fact that the monopoles are singular objects.

For these reasons we will not try to calculate a "continuum" mass spectrum. Rather we shall calculate the spectrum for lattice spacings that are small compared to the obvious dynamical length scale, $a\ll 1/\sqrt{\sigma}$.

The results of our calculation are presented in Table XXVI. How do they compare to the SU(N_c) spectra listed in Tables XXI and XXV? An immediate difference with all of the SU(N_c) spectra is that the 0^{++} is no longer the lightest particle; the 0^{--} is about half the mass. We also note that while the ratio $m_{0^{++}}/\sqrt{\sigma}$ was increasing as N_c decreased,

the U(1) value is about as much below the SU(∞) value as the SU(2) ratio is above. Apart from these striking differences, the rest of the spectrum seems quite similar (albeit within the large errors). This is particularly so if we compare to the 0^{++} mass rather than to $\sqrt{\sigma}$. For example, the 2^{++} to

0^{++} mass ratio is close to its SU(N_c) value. We note also that we have approximate parity doubling for $J \neq 0$, thus confirming that a is indeed small enough for continuum rotational symmetry to have been restored on hadronic length scales.

---

[1] G. 't Hooft, Nucl. Phys. **B72**, 461 (1974).

[2] E. Witten, Nucl. Phys. **B160**, 57 (1979).

[3] S. Coleman, in *Pointlike Structures Inside and Outside Hadrons*, edited by A. Zichichi (Plenum, New York, 1982).

[4] A. Manohar, 1997 Les Houches Lectures, hep-ph/9802419.

[5] T. Eguchi and H. Kawai, Phys. Rev. Lett. **48**, 1063 (1982).

[6] S-J. Rey and J. Yee, hep-th/9803001; J. Maldacena, hep-th/9711200; Phys. Rev. Lett. **80**, 4859 (1998); E. Witten, hep-th/9803131.

[7] S.R. Das, Rev. Mod. Phys. **59**, 235 (1987); S. Chin and M. Karliner, Phys. Rev. Lett. **58**, 1803 (1987).

[8] M. Teper, Phys. Lett. B **397**, 223 (1997); Nucl. Phys. B (Proc. Suppl.) **53**, 626 (1997).

[9] N. Isgur and J. Paton, Phys. Rev. D **31**, 2910 (1985).

[10] T. Moretto and M. Teper, hep-lat/9312035.

[11] R. Johnson and M. Teper, Nucl. Phys. B (Proc. Suppl.) **63**, 197 (1998); and (in preparation).

[12] F. Antonuccio and S. Dalley, Nucl. Phys. **B461**, 275 (1996); B. van de Sande and S. Dalley, Phys. Rev. D **56**, 7917 (1997); hep-th/9707180.

[13] C. Csaki, H. Ooguri, Y. Oz, and J. Terning, hep-th/9806021; H. Ooguri, H. Robins, and J. Tannenhauser, hep-th/9806171.

[14] C. Hamer, M. Sheppeard, Wei-hong Zheng, and D. Schutte, Phys. Rev. D **54**, 2395 (1996); C. Hamer, *ibid*. **53**, 7316 (1996).

[15] Shuo-Hong Guo and Xiang-Qian Luo, hep-lat/9706017; Lian Hu *et al.*, Commun. Theor. Phys. **28**, 327 (1997).

[16] D. Karabali and V.P. Nair, Nucl. Phys. **B464**, 135 (1996); Int. J. Mod. Phys. A **12**, 1161 (1997); D. Karabali, C. Kim, and V.P. Nair, Nucl. Phys. **B524**, 661 (1998); hep-th/9804132.

[17] M. Teper, Phys. Lett. B **289**, 115 (1992).

[18] M. Caselle, M. Hasenbusch, and P. Provero, Nucl. Phys. B (Proc. Suppl.) **63**, 616 (1998).

[19] M. Teper, Phys. Lett. B **311**, 223 (1993).

[20] M. Teper, Phys. Lett. B **313**, 417 (1993); and (unpublished).

[21] M. Billo, M. Caselle, A. D'Adda, and S. Panzeri, Int. J. Mod. Phys. A **12**, 1783 (1997).

[22] A. Kennedy and B. Pendleton, Phys. Lett. **156B**, 393 (1985).

[23] N. Cabibbo and E. Marinari, Phys. Lett. **119B**, 387 (1982).

[24] J. Hoek, M. Teper, and J. Waterhouse, Phys. Lett. B **180**, 112 (1986); Nucl. Phys. **B288**, 589 (1987).

[25] M. Teper, Newton Institute, NATO-ASI School Lectures, hep-lat/9711011, 1997.

[26] S. Adler, Phys. Rev. D **23**, 2901 (1981); **37**, 458 (1988).

[27] M. Creutz, Phys. Rev. D **36**, 515 (1987); F. Brown and T. Woch, Phys. Rev. Lett. **58**, 2394 (1987).

[28] A. Kennedy, Nucl. Phys. B (Proc. Suppl.) **30**, 96 (1993); U. Wolff, *ibid.* **17**, 93 (1990); S. Adler, *ibid.* **9**, 437 (1989).

[29] K. Akemi *et al.*, Nucl. Phys. B (Proc. Suppl.) **34**, 789 (1994); **30**, 253 (1993); Phys. Lett. B **328**, 407 (1994); R. Gupta *et al.*, Mod. Phys. Lett. A **3**, 1367 (1988); K. Decker and Ph. de

Forcrand, Nucl. Phys. B (Proc. Suppl.) **17**, 567 (1990).

[30] M. Teper, Phys. Lett. B **183**, 345 (1987); **185**, 121 (1987); Nucl. Phys. B (Proc. Suppl.) **4**, 41 (1988); B. Carpenter, C. Michael, and M. Teper, Phys. Lett. B **198**, 511 (1987).

[31] M. Albenese *et al.*, Phys. Lett. B **192**, 163 (1987); **197**, 400 (1987).

[32] C. Michael and M. Teper, Phys. Lett. B **199**, 95 (1987); **206**, 299 (1988); Nucl. Phys. **B305**, 453 (1988); **B314**, 347 (1989).

[33] O. Philipsen, M. Teper, and H. Wittig, Nucl. Phys. **B469**, 445 (1996); **B528**, 379 (1998).

[34] D. Perkins, *Introduction to High Energy Physics* (Addison-Wesley, Reading, MA, 1972).

[35] B. Berg and A. Billoire, Nucl. Phys. **B221**, 109 (1983); G.C. Fox, R. Gupta, O. Martin, and S. Otto, *ibid.* **B205**, 188 (1982); M. Lüscher, and U. Wolff, *ibid.* **B339**, 222 (1990); A.S. Kronfeld, Nucl. Phys. B (Proc. Suppl.) **17**, 313 (1990).

[36] Ph. de Forcrand, G. Schierholz, H. Schneider, and M. Teper, Phys. Lett. **160B**, 137 (1985).

[37] M. Luscher, K. Symanzik, and P. Weisz, Nucl. Phys. **B173**, 365 (1980).

[38] R. Johnson and M. Teper, hep-lat/9808012; and (in progress).

[39] S. Aoki *et al.*, Nucl. Phys. B (Proc. Suppl.) **47**, 354 (1996).

[40] G. Parisi, in *High Energy Physics*, edited by Loyal Durand and Lee E. Pondrom, AIP Conf. Proc. No. 68 (AIP, New York, 1981); P. Lepage and P. Mackenzie, Phys. Rev. D **48**, 2250 (1993); P. Lepage, 1996 Schladming lectures, hep-lat/9607076.

[41] K. Ishikawa, G. Schierholz, and M. Teper, Z. Phys. C **19**, 327 (1983).

[42] C. Morningstar and M. Peardon, Phys. Rev. D **56**, 4043 (1997).

[43] M. Luscher, lectures at Cargèse 1983 (unpublished); Commun. Math. Phys. **104**, 177 (1986); G. Munster, Nucl. Phys. **B249**, 659 (1985).

[44] C. Michael, J. Phys. G **13**, 1001 (1987); C. Michael, G. Tickle, and M. Teper, Phys. Lett. B **207**, 313 (1988).

[45] O. Philipsen, M. Teper, and H. Wittig, Nucl. Phys. **B528**, 379 (1998).

[46] K. Symanzik, Nucl. Phys. **B226**, 187 (1983).

[47] M. Teper (unpublished).

[48] A. Polyakov, Nucl. Phys. **B120**, 429 (1977); *Gauge Fields and Strings* (Harwood, Academic, Chur, Switzerland, 1987).

[49] Ph. de Forcrand, G. Schierholz, H. Schneider, and M. Teper, Phys. Lett. **152B**, 107 (1985); UKQCD Collaboration, G. Bali *et al.*, Phys. Lett. B **309**, 378 (1993); H. Chen, J. Sexton, A. Vaccarino, and D. Weingarten, Nucl. Phys. B (Proc. Suppl.) **34**, 357 (1994).

[50] C. Michael and M. Teper, Nucl. Phys. **B305**, 453 (1988); C. Michael and S. Perantonis, J. Phys. G **18**, 1725 (1992); S. Booth *et al.*, Nucl. Phys. **B394**, 509 (1993).

[51] E. Witten, in *Recent Developments in Gauge Theories*, edited by G. 't Hooft (Plenum, New York, 1980).